Department of Chemistry

Lanthanoid Complexes of Tetrazolyl-Functionalised Calix[4]arenes

Daniel Mark D'Alessio

This thesis is presented for the Degree of

Doctor of Philosophy

of

Curtin University

May 2015

Declaration

To the best of my knowledge and belief this thesis contains no material previously published by any other person except where due acknowledgement has been made. This thesis contains no material which has been accepted for the award of any other degree or diploma in any university.

Signature: 

Date: 20/05/2015

Abstract

A tetrazole-substituted calix[4]arene was found to support the formation of unprecedented Ln_{19} or Ln_{12} clusters, depending on the carboxylate co-ligand used.

Lanthanoid complexes of the macrocyclic polyphenol ligands termed 'calixarenes' are well known. Elaboration of the basic calixarene framework with a range of ligating groups has provided excellent control of the properties of the resulting ionophores. To date, however, there have been very few reports of tetrazolyl-functionalised calixarenes, with only one example focused on forming receptors for cations. The aim of this work was to synthesise a range of tetrazolyl-functionalised calixarenes, modified at the phenolic rim, to create metal-binding sites with a combination of O, and N donor atoms.

The most convenient precursor for the tetrazole moiety is a nitrile group. To that end, addition of cyanomethoxy (nitrile) functional groups to the lower rim of *p*-tert-butyl-calix[4]arene was performed. In addition to the known tetra- and 1,3-di-nitrile derivatives, the tri-nitrile substituted calix[4]arene **5** was synthesised and isolated for the first time. Syntheses of the corresponding di-, tri- and tetra-tetrazolato calix[4]arene ligands (**1**, **2** and **3**) were successfully performed *via* the conversion of the cyanomethoxy substituents to the tetrazole moiety. These ligands were characterised by X-ray crystallography and NMR techniques.

Conformational equilibrium between the cone and partial cone conformers of the tetra-nitrile (**6** and **7**) and di-amide di-nitrile (**8** and **9**) substituted calix[4]arenes was examined at 150°C in a d_6-DMSO solution. The distribution between the cone and partial cone conformations isolated from the syntheses, in comparison to the equilibrium experiments was found to be dissimilar for most of the ligands tested. This difference was related to metal templating of the calix[4]arene by the alkali metal present in the synthesis solutions.

Lanthanoid complexes with the tetra-tetrazole calixarene ligand **3** were unable to be isolated, however a sodium adduct was characterised *via* X-ray crystallography. A 1:1 mono-nuclear lanthanoid complex of the tri-tetrazole calixarene **2** was isolated and characterised, but with the calixarene ligand acting only as a unidentate ligand bound to

a singular N atom of the tetrazole ring. In contrast, typical hexadentate mono-nuclear 1:1 lanthanoid complexes with the di-tetrazole calixarene ligand **1** were successfully isolated and characterised, when the ligand and metal were combined in the presence of triethylamine. Replacing the triethylamine with aqueous ammonium acetate resulted in the formation of an unprecedented discrete linear lanthanoid hydroxo cluster, supported by the di-tetrazole calixarene, and acetate co-ligands. This cluster was formulated as $[Ln_{19}(\mathbf{1}\text{-}3H)(\mathbf{1}\text{-}2H)_{11}(CH_3CO_2)_6(OH)_{26}(H_2O)_{30}]$. Formation of the cluster was specific to the heavier lanthanoids, from samarium to lutetium, with the lighter, larger lanthanoids only forming the mono-nuclear species. Replacing ammonium acetate with an aqueous ammonium benzoate solution caused a new discrete cluster to be formed: $[Ln_{12}(\mathbf{1}\text{-}3H)_3(\mathbf{1}\text{-}2H)_3(PhCO_2)6(OH)_{16}(H_2O)_{21}]$. This benzoate capped cluster had an identical trigonal bipyramidal lanthanoid hydroxo cluster motif, with a reduction in length.

Attempts to observe the presence of lanthanoid clusters in solution were made using dynamic light scattering, ^{1}H NMR, and photophysical measurements. In all cases, differences could be observed depending on which solution was added. DLS measurements had a trend towards a higher average size distribution along with an increase in peak width upon addition of ammonium acetate, consistent with the presence of clusters in solution. While both ^{1}H NMR and photophysical measurements could not determine the origin of additional signals within their respective spectra, in each case these signals did not match the 1:1 complex and free ligand/metal.

Acknowledgements

I would like to thank my supervisors, Dr Massimiliano Massi and Professor Mark Ogden, for without their ingenuity and constant reassurance this thesis would not have eventuated. The wisdom, advice, meetings and corrections will always be remembered and appreciated.

To my unofficial supervisors and colleagues at ANSTO I would also like to extend my thanks. Dr Benjamin Fraser, Dr Nigel Lengkeek and Dr Anwen Krause-Heuer you were most welcoming of me as I used your facilities and lived in your lives. You always remained supportive of the project even when it did not go to plan. Without your help this thesis would not contain anywhere near as much useful information as it does.

I cannot thank the crystallographers Dr Brian Skelton and Dr Alexandre Sobolev enough for their tireless efforts in solving my crystal structures, especially the clusters. This thesis would not have made sense without understanding what we actually isolated.

Thanks to Team Lanthanide and all past and present members of the Empire. You all helped me stay sane throughout this work and some of you even gave me good advice. To Jamila Vaughan, thanks for being my lab and desk companion for the past 4 years (even if you did abandon me in the end). To Dr Ching Yong Goh and Dr Matthew McIldowie for teaching me most of what I know on calixarene synthesis and characterisation. Phil Wright and Brendan Ennis thanks for helping me make my ligands when my hands went all Zoidberg. To the synthesis collective, thank you for making the lab that little bit less dreary.

I am grateful of my family's patience and support throughout this whole process. Special thanks to my lovely wife Rene and son James, thank you for putting up with me while completing this work, even on the weekends. You have encouraged and consoled me when required, without you I would never have completed this chapter of my life.

Funding is acknowledged from the Australian Institute of Nuclear Science and Engineering (AINSE), Australian Nuclear Science and Technology Organisation (ANSTO) and the Australian Government (APA).

List of Compounds

Structure	Compound Name	ID Number
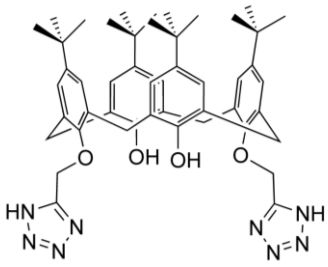	Di-tetrazole calixarene	**1**
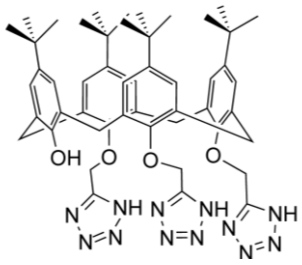	Tri-tetrazole calixarene	**2**
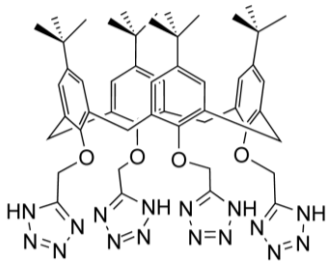	Tetra-tetrazole calixarene	**3**
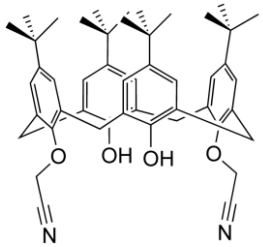	Di-nitrile calixarene	**4**
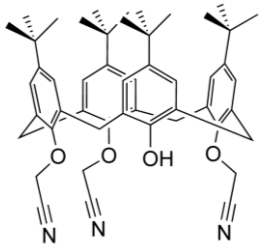	Tri-nitrile calixarene	**5**

Structure	Compound Name	ID Number
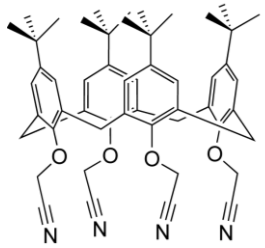	Tetra-nitrile calixarene (cone)	**6**
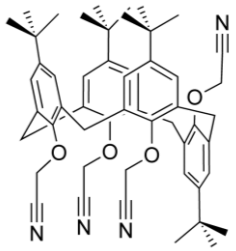	Tetra-nitrile calixarene (partial cone)	**7**
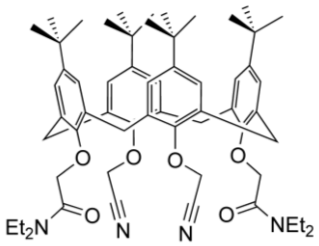	Di-amide di-nitrile calixarene (cone)	**8**
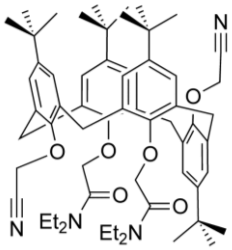	Di-amide di-nitrile calixarene (partial cone)	**9**
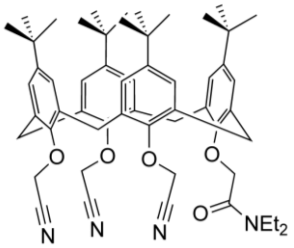	Mono-amide tri-nitrile calixarene	**10**

Contents

1 Introduction

1.1 Calixarenes

Calixarenes were first reported by Zinke in 1941 in his quest for a simplified product of the phenol-formaldehyde condensation process.[1–3] In an attempt to reduce the number of possible cross-linking side-reactions, *para* substituted phenols were employed. It was reported that the reaction yielded a "brown waxy paste" which, when washed and reprecipitated, yielded a crystalline product decomposing above 300°C. Although at that time no structure was proposed, in 1944 Zinke published a paper proposing the cyclic structure known today.[2] In 1956 Hayes developed a rational 10 step synthesis of the cyclic structure reported by Zinke.[3] In a similar manner, this synthesis obtained a "light brown solid that did not melt below 300°C". They named these cyclic structures 'cyclic tetrameric novolaks'. In 1978 Gutsche published a paper coining the term 'calixarene'. He derived this name from the Latin word for chalice or cuplike; calic or calix, with the

arene portion of the name indicating the presence of the aryl rings. Figure 1.1 demonstrates the cup or cone shape of the core calixarene skeleton.[4]

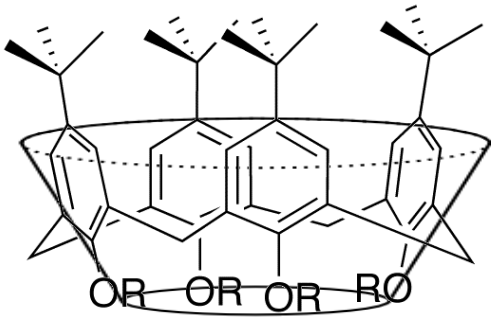

Figure 1.1: The core calixarene structure can be likened to a bowl shape.

The three-dimensional nature of the calixarene structure makes it an ideal pre-organised platform. The range of accessible molecules is virtually endless as both the phenols and *tert*-butyl moieties can be replaced with a variety of substituents. This feature makes the calixarenes a versatile framework, leading to a variety of potential applications.[5–7]

1.1.1 Calixarene nomenclature

Over time, calixarenes have been classified using several different names, ranging from Zinke's mehrkernmethylenephenolverbindungen to Hunter's cyclic tetranuclear *p*-cresol novolak. Broadly, calixarenes are classified as cyclophanes, however, this portion of the name is usually just referred to as 'calixarene'. Initially, official IUPAC nomenclature had not been developed for the macrocyclic structure, therefore much of the literature still uses the original numbering system implemented by Gutsche, which is based on the Chemical Abstract Service (CAS).[8] Gutsche investigated the systematic synthesis of numerous sizes of cyclic calixarene structures.[9] In order to differentiate between these different sizes, the number of aromatic rings is placed in parentheses between the calix and arene *viz* calix[4]arene. The most recent systematic name assigned to the parent calix[4]arene structure by CAS is; pentacyclo[19.3.1.$1^{3,7}$.$1^{9,13}$.$1^{15,19}$]-octacosa-1(25),3,5,7(28),9,11,13(27),15,17,19(26),21,23-dodecaene-25,26,27,28-tetrol,5,11,17,23-tetrakis(1,1-dimethylethyl) (CAS registry number 60705-62-6). One can imagine that using this system for substituted calixarenes becomes significantly more complicated

and difficult to interpret without a pictorial representation. Hence, in an attempt to simplify the nomenclature of these structures, an IUPAC naming system was developed.[10–12] This method gives all rings and methylenes on the calixarene structure a sequential number (red). Where there is a need to allocate a number to a carbon within the ring, the number of the carbon is written in superscript (blue). An example of this is shown in Figure 1.2 with the corresponding name for the basic calix[4]arene structure being simplified to; 1^{5},3^{5},5^{5},7^{5}-tetra-*tert*-butyl-1,3,5,7(1,3)-tetrabenzeneacyclooctaphane -1^{2},3^{2},5^{2},7^{2}-tetrol. The 1,3,5,7(1,3)-tetrabenzeneacyclooctaphane portion of the IUPAC name can be further condensed to just 'calix[4]arene' representing the tetrameric unsubstituted phenolic core structure; 1^{5},3^{5},5^{5},7^{5}-tetra-*tert*-butylcalix[4]arene-1^{2},3^{2},5^{2},7^{2}-tetrol. For the remainder of this thesis, the tetrameric calix[4]arene, consisting of four phenolic units, will simply be referred to as 'calixarene' as the tetramer is used exclusively.

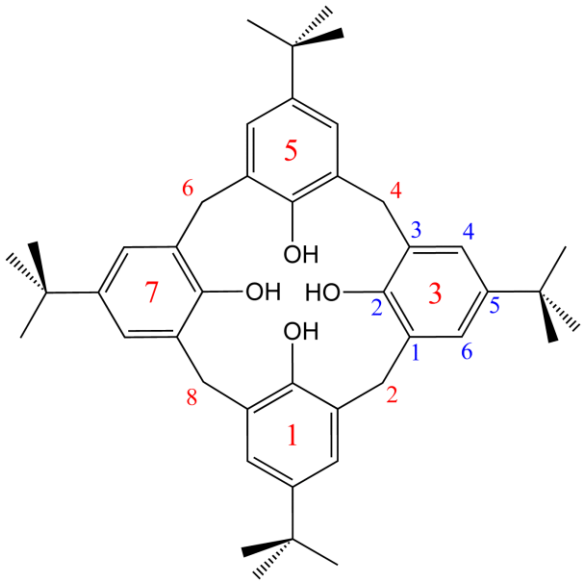

Figure 1.2: Example of the IUPAC numbering scheme for calix[4]arene structures. Sequential numbers for the rings and methylenes (red) and superscript numbers for carbons within each ring (blue).

Substitution of the calixarene is a large portion of the work contained within this thesis. As mentioned previously, the nomenclature of the substituted products can become very long-winded. As all the calixarenes synthesised within this work do not involve substitution of the *tert*-butyl groups on the aryl ring, it can be assumed that within the

naming scheme these are always present. To avoid complicated nomenclature and ensure clarity, all calixarene derivatives have been described using a graphical representation and an associated abbreviation (see List of Compounds).

1.1.2 Graphical representation of calixarenes

There are many different schematic representations of calixarenes in the literature, with Figure 1.3 showing some of the more common forms. The bracketed aryl ring with and without the loop (a,b) are commonly used in older literature and for tetra-substituted calixarenes.[5,13,14] The three-dimensional (c) and 'flattened' (d) structures are generally employed in more recent literature or when describing partial/mixed substitution calixarenes, as well as illustrating intra- and inter-molecular bridged calixarenes.[1,7,15–17] This thesis will primarily use the three-dimensional representation of the calixarene (c), as it is the most effective for identification of partially substituted calixarenes.

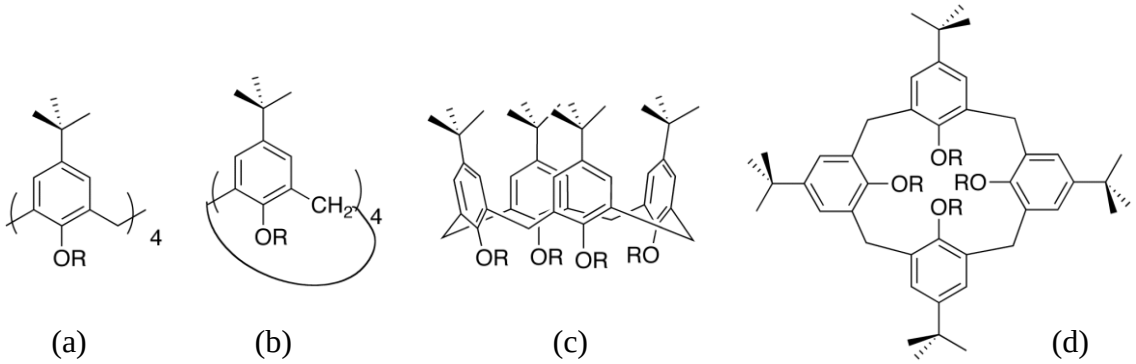

Figure 1.3: Various structural representations of the calixarene used within the literature; a) brackets without loop, b) brackets with loop, c) 3D representation, d) flattened top view.

The pseudo three-dimensional representation of the calixarene bowl structure can be viewed as having a wide rim and a narrow rim, with a cavity in the centre of the molecule.[18] The terminology used to differentiate the two different ends will be; 'upper' and 'lower' rim, with the lower rim being the one with the phenolic oxygens and methylene carbons (Figure 1.4).

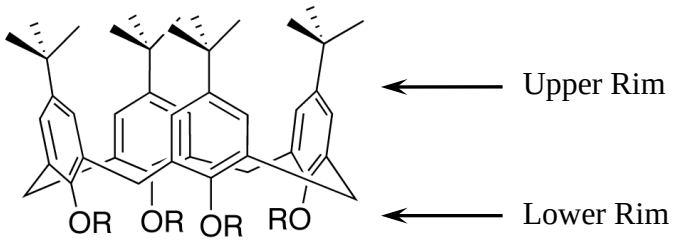

Figure 1.4: The designation of the rims of the calixarene.

1.1.3 Calixarene conformations

One of the distinct features of the calixarenes, is their ability to form complexes with metal ions. This attribute is closely related to the conformational behaviour of the calixarene. There are several literature studies dedicated to the formation and investigation of the different conformational isomers (conformers) each different calixarene can assume.[19–22] For the tetrameric calixarene, it was found that the hydroxyl portion of the phenolic units were free to rotate through the annulus, around the bridging methylene carbons.[9,23,24] Substitution of the lower rim with sufficiently bulky substituents, usually any group larger than ethyl groups, stops the rotation of the phenyl rings. This allows for the isolation of the different conformers, coined by Gutsche as; cone; partial cone; 1,3-alternate and 1,2-alternate conformations, see Figure 1.5.[24]

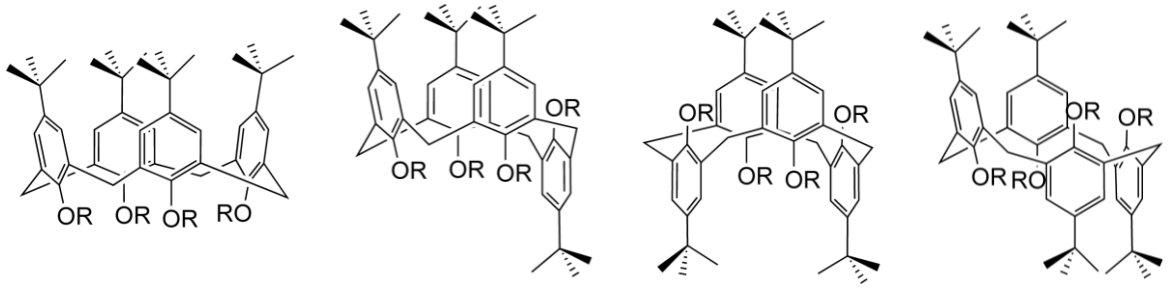

Cone Partial cone 1,3-alternate 1,2-alternate

Figure 1.5: The various conformations that calixarenes can assume.

The most stable conformation of the unsubstituted calixarene has been experimentally determined as the cone conformer. The stability is conferred by the potential for the cone conformer to form more intra-molecular hydrogen bonds on the lower rim of the calixarene than the other conformations.[9,13] This ensures that for an unsubstituted

calixarene, the cone conformation is usually the most populated conformer in solution. As a result, the other conformations are generally only isolated in derivatives where functionalisation of the phenol groups has occurred.[13,15,25] Initial studies by Kammerer showed that at 20°C the ^{1}H NMR of the calixarene has a pair of doublets representing the non-equivalent hydrogens on the methyl bridges between the aryl rings. The spectrum at 60°C showed that these doublets each collapse into a singlet suggesting that at that point, there is enough energy in the system for the interconversion to occur, resulting in increased rate of conformational inversion of the calixarene relative to the timescale of the NMR experiment.[26]

1.2 Tetrazoles

Tetrazoles are aromatic molecules, consisting of a five membered ring of one carbon and four nitrogen atoms. They have the potential to be synthesised as mono- or di-substituted rings with the 5-substituted tetrazole having two tautomeric forms, 1*H* and 2*H* (Figure 1.6).[27–29]

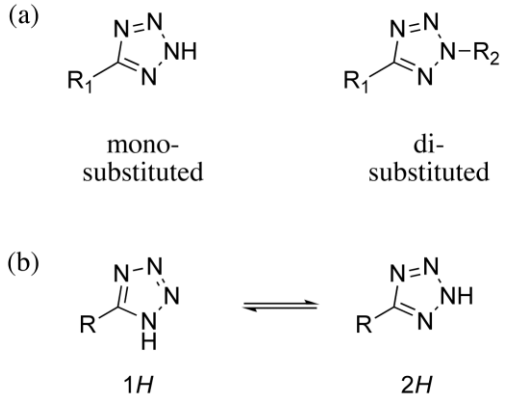

Figure 1.6: (a) Mono- or di-substituted tetrazoles; (b) the two tautomeric products upon protonation.

There are many different substrates from which a tetrazole can be formed, including amides, ketones and carboxylic acids,[30–34] however, the most commonly used is the nitrile functional group.[35-43] Synthesis of a tetrazole moiety from a nitrile substrate could conceivably proceed by either a two-step or a concerted [1,3] dipolar cycloaddition, and is still the source of discussion within the literature (Figure 1.7).[35,36]

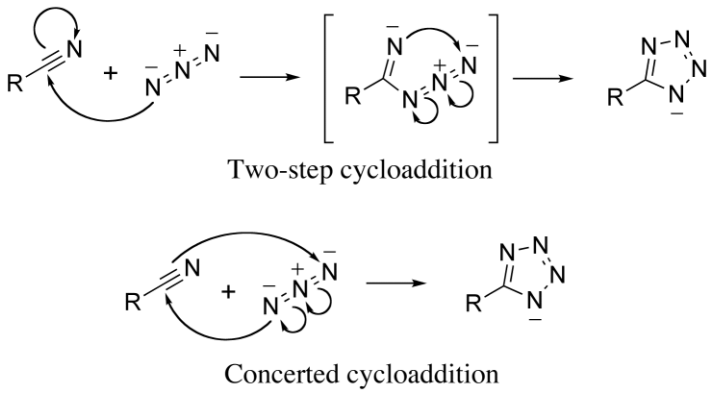

Figure 1.7: Hypothesised mechanisms of tetrazole formation.

The reagents used to perform this cycloaddition have been extensively investigated. Initially, substituted tetrazoles were formed from an organic nitrile and hydrazoic acid, however, this procedure was extremely dangerous due to the use of the highly toxic and explosive hydrazoic acid.[37,38] Subsequent literature from Behringer shows that simple tetrazoles can be synthesised utilising an azide salt which is more stable and less toxic under normal atmospheric conditions.[39] An investigation in the late 1950's by Finnegan showed that the use of sodium azide with ammonium salts in dimethylformamide successfully increased the yield and rate of reaction, however, it also resulted in the formation of numerous by-products with a high risk of the formation of toxic HN_3 gas.[40] Adding ammonium chloride as the salt in dimethylformamide increased the overall yield of the reaction again, while also reducing the possible by-products, however there is the possibility of condensation of the highly explosive ammonium azide. A method developed by Sharpless utilises water as the solvent along with sodium azide and zinc bromide.[41] Employing water as the solvent of the reaction, while environmentally friendly, limits the reaction to water soluble substrates. This becomes particularly pertinent when the molecules are as hydrophobic as *tert*-butyl substituted calixarenes, making this method redundant for this project. The use of organostannane catalysts in aromatic solvents led to increased solubility of larger organic molecules, however, reports state that it was difficult to separate out the stannane compounds from the desired tetrazole.[42] In 1981 Koguro devised a synthesis which employed organic solvents such as toluene to be utilised along with the inorganic azide.[43] This procedure produced no harmful and unnecessary by-products and had simple workup procedures,

resulting in excellent yield and, most importantly, successfully reacts with large organic nitriles such as calixarenes. Consequently, the method implemented for the formation of the tetrazoles in this project is adapted from Koguro's methodology.

1.2.1 Applications of tetrazoles

There are many different applications in which tetrazole-containing molecules are utilised. These include; synthetic drugs, gas generating molecules, antimicrobial/antifungal agents and explosives.[35,38,44,45] The wide variety of applications employ tetrazoles for their chemical properties as a hydrogen bond donor/acceptor, coordinating ligand and/or high nitrogen content. A literature search reveals that the main application for tetrazole-containing molecules is in the pharmaceutical industry. This is mainly due to tetrazoles being metabolically stable isosteres of carboxylic acids. Their low pKa values are similar to corresponding carboxylic acid derivatives in water (4.5-4.9 *vs* 4.2-4.4 respectively).[36,46] This makes them ideal for biological applications as they form stable anions within the physiological pH range.[36,47] Tetrazoles are also a larger substituent than carboxylic acids, allowing the negative charge to be distributed over a higher number of atoms, helping to increase the lipophilicity of the molecule.[46] Tetrazoles are not known to occur within nature, as a result there is a lack of naturally occurring enzymes designed to specifically alter or metabolise the tetrazole functional group. The low number of biologically relevant degradation pathways, increases the metabolic stability of the parent molecule, making tetrazoles an attractive target for synthetic drugs.[48]

1.2.2 Tetrazolyl-functionalised calixarenes

Despite the obvious potential for tetrazole derivatives to be used in metal ion coordination, synthesis of preorganised macrocylic molecules, such as calixarenes, with tetrazoles attached remains relatively unexplored. In fact, the literature on tetrazole functional groups attached to calixarenes in any fashion is very limited. To date there are only six papers reporting the synthesis of tetrazolyl-functionalised calixarenes, with the

majority of examples having the tetrazole(s) on the upper rim of the calixarene (see Figure 1.8).[17, 49–53]

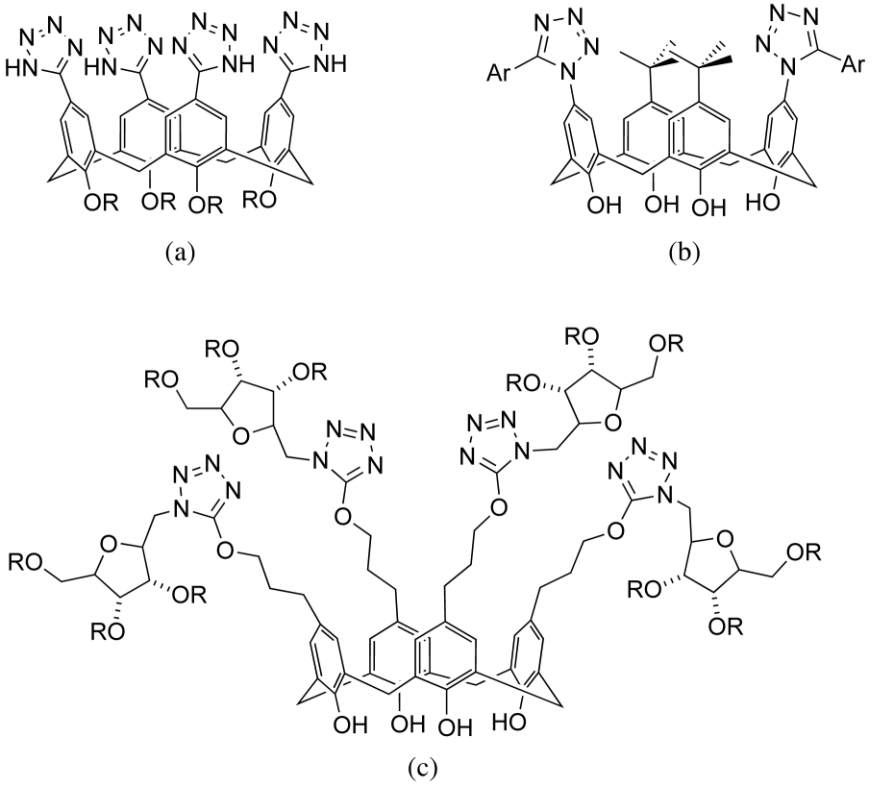

Figure 1.8: Upper rim tetrazoles previously synthesised.[17,49,50]

Each of these tetrazole-containing calixarene molecules were used for a different application. The upper rim tetra-tetrazole calixarene (a) was used as a sensor of anions, specifically chloride ions;[49] the di-*tert*-butyl di-tetrazole calixarene (b) was synthesised to test its coordination ability with palladium, of which it formed a 2:2 complex;[50] while the tetrazoles of the final calixarene molecule (c) were used as a linker for sugar chemistry, substituting a triazole unit.[17] There is one paper which reports a receptor with the tetrazole attached to the lower rim of the calixarene, in a similar fashion to the calixarenes reported in this thesis. The paper by Chen reports the synthesis of a debutylated di-tetrazole calix[4]arene from the nitrile starting material, using the method involving stannous oxide with trimethylsilyl azide, achieving isolation in 87% yield.[51] They used the debutylated calixarene tetrazole as a reference for the chromogenic sensing of Ca^{2+}. Chen hypothesised, through ^{1}H NMR titrations, that the calcium was

binding to the lower rim of the calixarene interacting with the partially deprotonated phenols along with the nitrogen of one tetrazole (see Figure 1.9). Despite the lack of structural determination provided within the paper *via* X-ray crystallography, this finding is consistent with the results obtained in Chapter 4 of this thesis which shows coordination to the lower rim of the calixarene in a similar fashion.

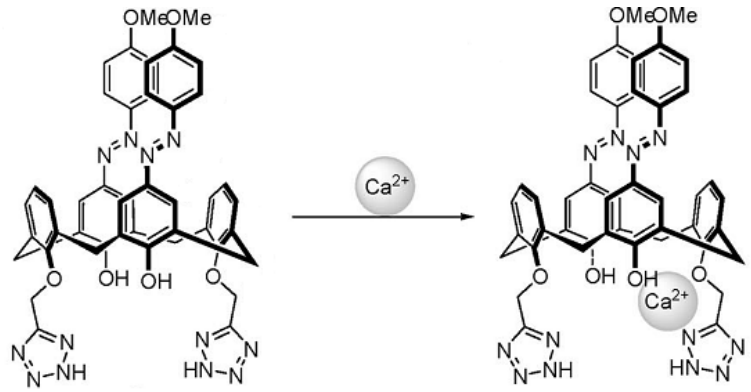

Figure 1.9: Lower rim tetrazole calixarene synthesised for Ca^{2+} sensing applications.[51]

1.2.3 Tetrazole binding modes

The tetrazole ring, consisting of one carbon and four nitrogen atoms, has multiple possible binding modes with metal cations. There are a total of nine different binding modes which can be separated into four distinct categories; $\mu_{1\text{-}4}$, Figure 1.10 details these different groups.[54] Only σ-type bonds involving the lone pairs on the nitrogen atoms are considered, as tetrazole rings bonding to lanthanoid ions *via* π-electrons is unknown.

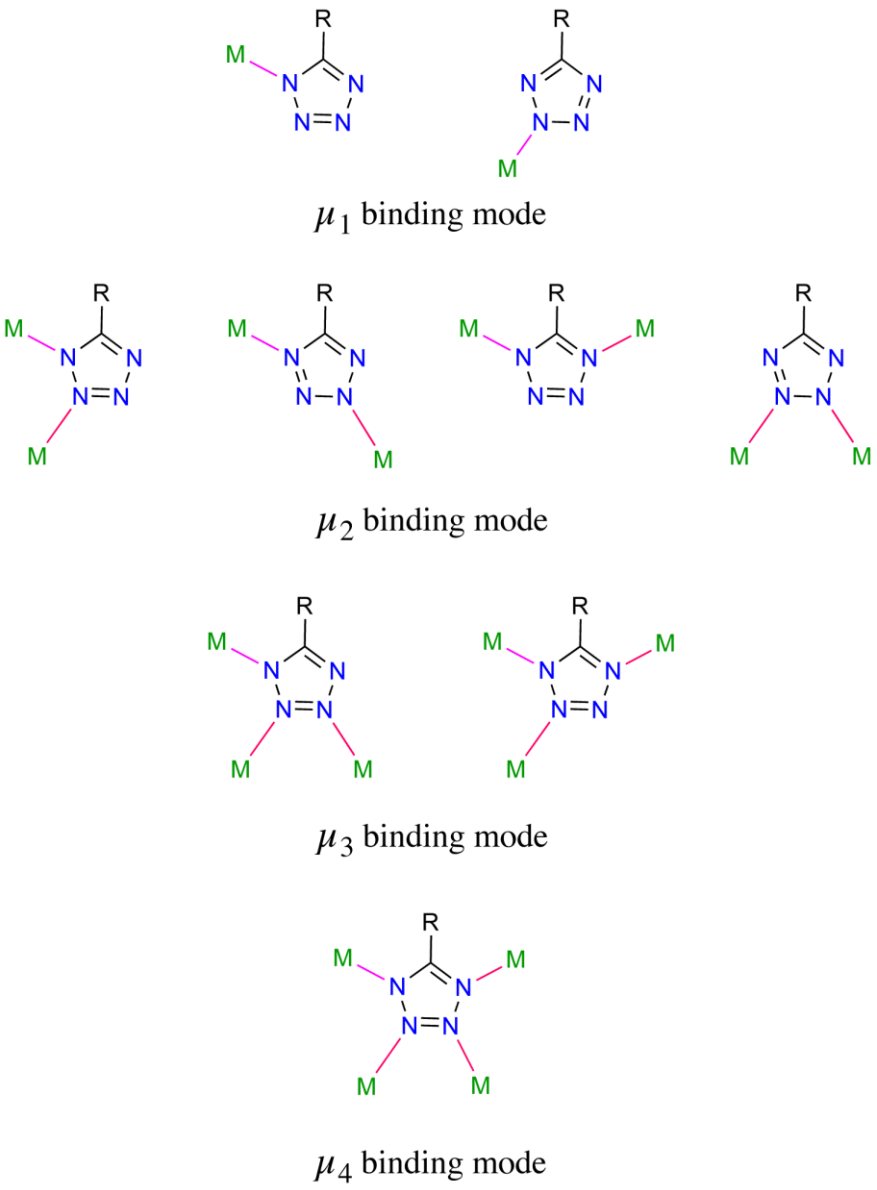

Figure 1.10: Different binding modes of the tetrazole ring.[54]

The different binding modes demonstrate the versatility of the tetrazole to bind as a monodentate ligand[55,56], as part of a di/tri chelating ligand[57–59], or bridging between multiple metals.[60,61] This character can lead to the formation of both mono-nuclear complexes or the construction of coordination polymers[61–63] and discrete clusters.[52] For the formation of mono-nuclear complexes, the ability to bridge between metals can be problematic. Hence, this thesis is focused on the formation of a multidentate ligand combining two to four tetrazoles on the preorganised calixarene scaffold to try and increase the likelihood of forming a monodentate complex.

1.3 Lanthanoids

Despite their name, "rare earth elements" or lanthanoids, are in fact not especially rare, each is more common in the earth's crust than silver, gold or platinum.[64] In 1794, an earth oxide named 'yttria' was obtained from the mineral (gadolinite) by Gadolin. This substance was later separated into what were called erbia, terbia and yttria.[65] Despite this early discovery, it was not until 1839-1843 that the first lanthanoids were isolated in an elemental form, with Mosander successfully separating the oxides of lanthanum and cerium along with a mixture of praseodymium through to gadolinium.[66] In 1907-1915 the work of Bohr and Moseley finalised the number and positioning of the lanthanoid elements, with the last lanthanoid element, radioactive promethium, being isolated and characterised in 1945.[67,68]

1.3.1 Nomenclature and classification

Although the term lanthanides is more commonly used, it can lead to confusion since the suffix –ide is reserved for anionic species. The correct designation following IUPAC nomenclature is lanthanoids, abbreviated as Ln, where the suffix –oid describes the similarity of a group of elements.[69] The lanthanoids are usually defined as the group of elements, lanthanum to lutetium. Lanthanum (Z = 57) is different to the rest of the lanthanoids as it does not have any 4*f* electrons, as a result lanthanum can technically be regarded as part of the group III elements. Yttrium (Z = 39) although technically not contained within the lanthanoid series has a similar ionic radius, which lies close to that of holmium (see Table 1.11). As a result, the physical and chemical behaviour of this group III element is similar to that of the lanthanoids and is sometimes included when describing characteristic traits across the series.[68] A further sub-classification which can be implemented based upon differing chemical properties, divides the lanthanoids into the cerium group (light lanthanoids: lanthanum to europium) and the yttrium group (heavy lanthanoids: gadolinium to lutetium, also including yttrium).[70] This distinction originates from a basis of ionic radius, and has proven to be important for this project.

Table 1.11: List of relevant metals with their electronic configuration, radius and ground term.[65,68]

Z	Name	Symbol	r_{Ln}^{3+}	Configuration		Ground Term
			Å	Ln	Ln^{3+}	Ln^{3+}
39	Yttrium	Y	0.901	$[Kr]4d^15s^2$	[Kr]	$^1S_0$
57	Lanthanum	La	1.032	$[Xe]5d^16s^2$	[Xe]	$^1S_0$
58	Cerium	Ce	1.010	$[Xe]4f^26s^2$	$[Xe]4f^1$	$^7F_{5/2}$
59	Praseodymium	Pr	0.990	$[Xe]4f^36s^2$	$[Xe]4f^2$	$^3H_4$
60	Neodymium	Nd	0.983	$[Xe]4f^46s^2$	$[Xe]4f^3$	$^4I_9$
61	Promethium	Pm	0.970	$[Xe]4f^56s^2$	$[Xe]4f^4$	$^5I_4$
62	Samarium	Sm	0.958	$[Xe]4f^66s^2$	$[Xe]4f^5$	$^6H_{5/2}$
63	Europium	Eu	0.947	$[Xe]4f^76s^2$	$[Xe]4f^6$	$^7F_0$
64	Gadolinium	Gd	0.938	$[Xe]4f^86s^2$	$[Xe]4f^7$	$^8S_{7/2}$
65	Terbium	Tb	0.923	$[Xe]4f^96s^2$	$[Xe]4f^8$	$^7F_6$
66	Dysprosium	Dy	0.912	$[Xe]4f^{10}6s^2$	$[Xe]4f^9$	$^6H_{15/2}$
67	Holmium	Ho	0.901	$[Xe]4f^{11}6s^2$	$[Xe]4f^{10}$	$^5I_8$
68	Erbium	Er	0.890	$[Xe]4f^{12}6s^2$	$[Xe]4f^{11}$	$^4I_{15/2}$
69	Thulium	Tm	0.880	$[Xe]4f^{13}6s^2$	$[Xe]4f^{12}$	$^3H_6$
70	Ytterbium	Yb	0.868	$[Xe]4f^{14}6s^2$	$[Xe]4f^{13}$	$^2F_{7/2}$
71	Lutetium	Lu	0.861	$[Xe]4f^{14}5d^16s^2$	$[Xe]4f^{14}$	$^1S_0$

1.3.2 Properties of the lanthanoids

The low radial extent of the 4*f* shell dictates the vast majority of both the chemical and physical properties of the lanthanoids. The 4*f* electrons are often termed as 'inner core' as they are located inside the 5*s* and 5*p* electron subshells (see Figure 1.12).[71–73] As a result they are shielded from the ligands and take no part in covalent bonding, hence the ionic nature of their interactions. This gives rise to many of the characteristic features of the lanthanoids, including unique spectroscopic and magnetic properties which are largely independent of the coordination environment.[68,74] The lack of interaction with

ligand orbitals causes the coordination geometries of the metal complexes to be determined by ligand steric factors as opposed to crystal field effects. This also extends to the ability of the complexes to have a wide range of coordination numbers (with limits of 2-12), with no preference for a particular geometry. As a result of lanthanoid complexes having predominantly ionic interactions between metal and ligand, the complexes are generally labile, allowing for the ligands to undergo facile exchange.[68,75] One of the most commonly discussed features of the lanthanoids is the steady decrease in the size of the trivalent ions with increasing atomic number, termed the 'lanthanide contraction'.[60,72,75] The contraction in ionic radius is attributed to the imperfect inter-electron shielding of the 4*f* subshell, resulting in an increase in effective nuclear charge experienced by the outer electrons across the series.

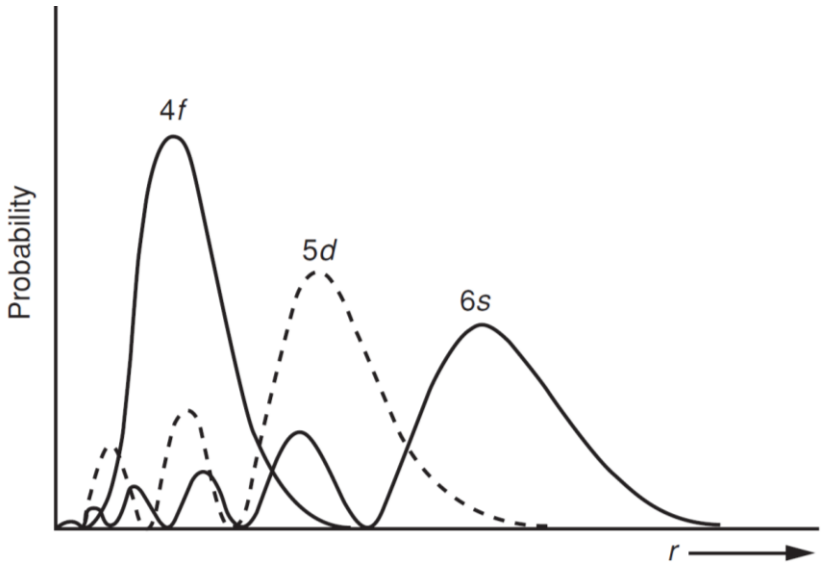

Figure 1.12: The radial part of the hydrogenic wavefunctions.[68]

The inner core nature of the 4*f* electrons can also be invoked to explain several key differences between coordination complexes of the lanthanoids and the *d*-block transition metals.[76,77] The minimal perturbation of the 4*f* electrons reduces the crystal-field splitting, resulting in very sharp electronic spectra in comparison with the *d*-block metals. The lanthanoids behave as hard acids and interact most strongly with anionic, highly electronegative atoms such as oxygen and fluorine. This results in the lanthanoids readily forming hydrated complexes, and precipitating from aqueous solutions as insoluble hydroxides at neutral or basic pH. The chemistry of the

lanthanoids usually involves the (3+) oxidation state, with only cerium, europium and ytterbium having significantly lower ionisation energies for different oxidation states.[68,75]

1.3.3 Tetrazoles and lanthanoids

The lanthanoids high affinity for oxygen atoms, in molecules such as water, can be problematic when trying to replace them with a non-oxygen donor. Traditionally a negatively charged or multidentate ligand is required to remove the oxygen donors from the coordination sphere of the lanthanoid.[59,78] When deprotonated, a ligand containing multiple tetrazoles can fulfill both of these requirements. Despite the increase in favourable interactions, when the lanthanoid is faced with the option of an oxygen donor or a nitrogen based tetrazole, the oxygen donor usually takes precedence. The crystal structures shown in Figure 1.13 demonstrate this preference for oxygen donors, whether it be from a bidentate acid residue or adventitious water molecules. One example, reported by Liang actually has coordination of the tetrazole to a 'softer' *d*-block metal (copper) in preference to the lanthanoid.[56,79]

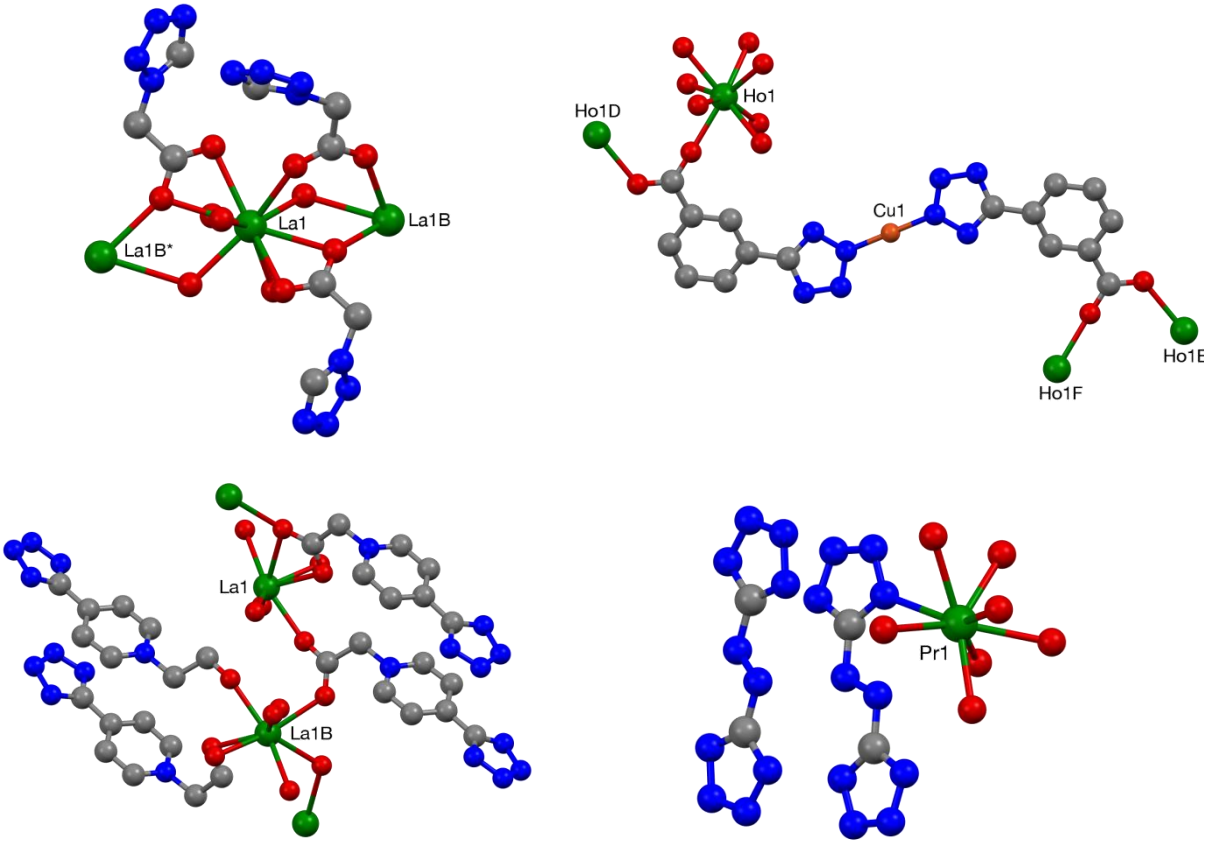

Figure 1.13: A selection of lanthanoid complexes with tetrazole-containing ligands, illustrating the preference of the lanthanoids to bind oxygen donor ligands.[79–82]

The available literature on tetrazole coordinated lanthanoids demonstrates that the majority of complexes only use the tetrazole as a single coordination point of a much larger polydentate ligand. Of the polydentate ligands synthesised, the pyridine tetrazole motif is by far the most commonly used design for the coordination of tetrazoles to lanthanoids.[57,59,83–87] The incorporation of a monodentate tetrazole into a larger bi- or polydentate ligand increases the denticity, enabling stronger interactions with the lanthanoid. This in turn increases the stability of the complex giving the nitrogen donor ligand a higher probability of being included in the coordination sphere over a monodentate oxygen donor. While the majority of these pyridine-tetrazole ligands are "planar" such as the di-tetrazole pyridine and terpyridine-based ligands in Figure 1.14, there have also been examples of three dimensional preorganised ligands. One such example is the triazacyclonane-based tripodal ligand in Figure 1.14, which is more akin to the tetrazole calixarenes synthesised in this thesis.[88–90]

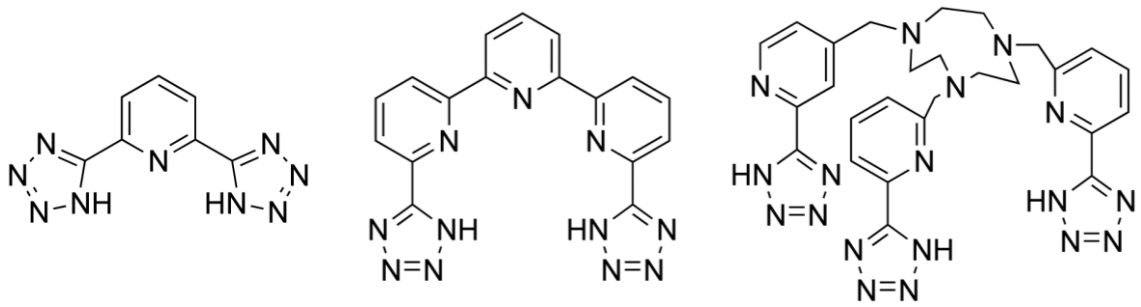

Figure 1.14: Pyridine-tetrazole based polydentate ligands are prevalent in tetrazole lanthanoid literature.[57,59,83–86]

Where tetrazoles were employed as the only coordinating moiety, the complexes formed were usually coordination networks or hydrogen bonded polymeric species, most likely a result of the tendency of tetrazoles to act as bridging ligands.[58,60,91]

1.3.4 Macrocycles and lanthanoids

The coordination chemistry of the lanthanoids with oxygen donor ligands is a broad field, of which only a small portion can be discussed here. The interaction of lanthanoids with aryloxides is of particular interest to the study of calixarene complexes. One example of lanthanoid phenoxides is the chelating diphenol, catechol.[92] Catechols have been reported to form water-soluble mono-nuclear species in basic aqueous solutions with a $[Ln(cat)_4]^{5-}$ stoichiometry.[93] A more sophisticated means of controlling the Ln interactions is the incorporation of the phenolic units into preorganised macrocyclic ligands. There are numerous examples of mono-, bi- and polynuclear lanthanoid complexes with aryl ether macrocyclic ligands such as crown ethers, cryptands and spherands.[66,68,75,94–96] Similarly, within the literature, there are many examples of lanthanoid ions being coordinated by calixarene ligands.[97–100] The calix[4]arene is seen as a versatile platform, as three arms of negative charge can be attached to afford a neutral lanthanoid complex, while possibly substituting the fourth phenol to either complete the coordination sphere or impart an additional characteristic. The first report of a calixarene lanthanoid complex was in 1987 with a di-europium calix[8]arene complex being isolated from a DMF solution.[101] Since then, there have been numerous investigations into the coordination chemistry of the calixarenes, of either the parent or

substituted structure. The majority of literature utilises the calixarene scaffold as a preorganised ligand with the ability to have both the upper rim substituted with a group for specific solubility characteristics or attachment to biopolymers, and the lower rim substituents for strong interaction with the lanthanoid.[100]

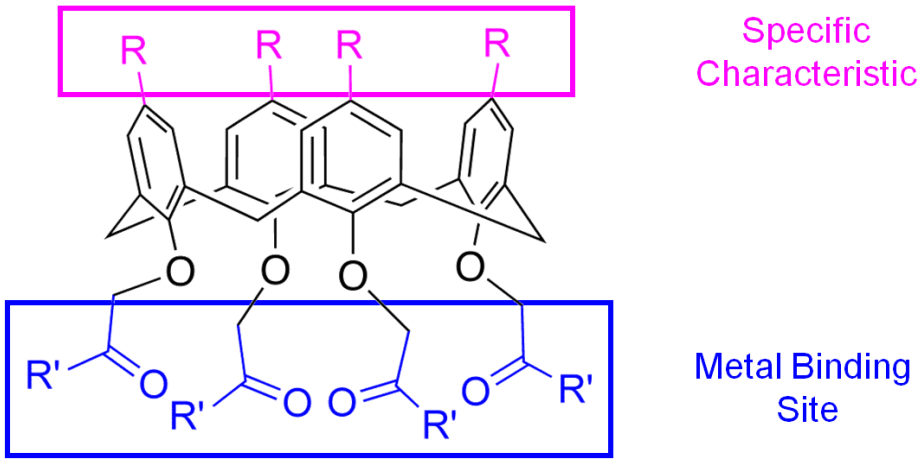

Figure 1.15: Versatility of the calix[4]arene platform.

While the ability to substitute both the upper and lower rims of the calixarene, imparting a specific characteristic to the ligand, is useful, utilisation of the calixarene skeleton itself can often be overlooked. The aromatic rings while providing a very stable core also have the ability to absorb UV radiation, allowing it to be used as an antenna for the excitation of luminescent lanthanoids.[53,102,103] This capability of the calixarene can give useful information on characteristics of the associated metal complex such as the local symmetry of the metal ion, the distance between metal ions (Ln-Ln distance), ligand exchange rates and so on.[75,104] This information is vital to the successful characterisation of the metal complex and provides an additional application, luminescent probe, for the calixarene-lanthanoid complex. Some potential applications of the calixarene luminescent probes include; contrast agents, europium and terbium for fluoroimmunoassays, neodymium and erbium for telecommunications and a range of lanthanoids for light emitting devices.[53,66,105–108] The most common binding motifs on the lower rim of calixarenes unsurprisingly all contain oxygen donors, including functional groups such as acids, esters and amides. The neutral binding diethylamide residues, shown in Figure 1.16, are the most extensively researched lower rim moiety, mainly due to their strong binding affinity, as determined by Ungaro.[109,110]

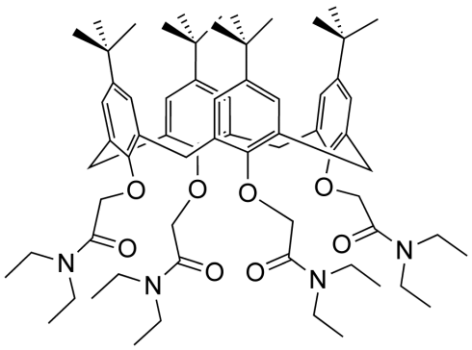

Figure 1.16: The common *N,N*-diethylacetamide binding motif.

1.4 Metal clusters

Clusters are an expanding area of interest within the scientific community for a variety of reasons. One such reason is the use of metal clusters for efficient synthesis of nanoscale materials with regular and consistent structures, while also allowing the modification of specific properties of these nanoscale objects. Metal clusters provide an ideal stepping stone to achieving these goals; as they are a bridge between single mono-nuclear metal complexes and nanoscale objects.[52] Unfortunately, unlike nanoparticles which have been isolated in a plethora of shapes, access to a similar diversity with large ligand-metal nano-sized clusters has been difficult to achieve, with most examples limited to spherical or regular polyhedral (see Figure 1.17).[111,112] Multinuclear lanthanoid clusters generally possess a metal-rich core, while being encapsulated by various organic ligands.[76,111]

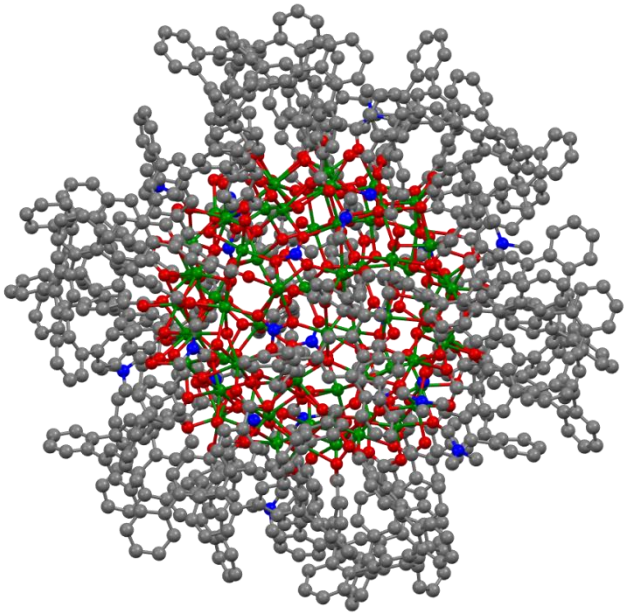

Figure 1.17: A spherical Cd_{66} cluster demonstrating the metal-rich core encapsulated by carboxylate ligands.[111]

The size and shape of the metal core for lanthanoid clusters is sometimes dependent on the lanthanoid cation being incorporated into the cluster, along with the bulkiness of the ligands. This is in contrast to transition metal clusters where the coordination geometry and preferential coordination number are the critical factors.[113,114] Also in contrast to transition metal clusters where metal-metal bonds can be present, the lanthanoids do not have a similar interaction. As a result, there must be atoms bridging two or more lanthanoids to form the cluster motif. These bridging atoms can be anything from halides such as fluoride or chloride to the more common and more extensively researched oxo/hydroxo clusters.[95,114–116]

1.4.1 Lanthanoid-hydroxo clusters

It is unsurprising that lanthanoid ions predominantly form hydroxo clusters, as they have an innate affinity for oxygen (see Section 1.3.3). These clusters are formed through a process termed controlled hydrolysis.[76,117,118] The tendency of the lanthanoids to readily bind water results in the rapid formation of the thermodynamically stable lanthanoid hydroxides in aqueous environments devoid of appropriate ligands. These are insoluble oxo/hydroxo compounds which are not readily defined.[76] The term ‘controlled’ arises

from the fact that the hydroxo clusters are indeed hydrolysis products like the insoluble lanthanoid hydroxides, however the expansion of the network is controlled by the addition of coordinating multidentate ligands. The high denticity of the ligands is the key, as this feature allow the ligands to surround the initial hydroxo core, thereby terminating the growth.[114] This lipophilic barrier prevents additional OH^- ions from attaching and extending the cluster core. Typical ligands are usually bulky and carbon rich, of which a calixarene molecule is ideal. Until recently the isolation of these controlled hydrolysis products was serendipitous with little to no rational design being involved.[114,119] However, recent literature has shown that rational design of ligands allows prediction of different cluster cores.[120–122] There are many different ligands which have been used for either the design or serendipitous discovery of different lanthanoid hydroxo clusters as can be seen in Figure 1.18. As discussed previously, clusters are generally formed through the use of multidentate binding ligands which allow for the bridging of multiple lanthanoid cores as well as encasing the lanthanoid core to prevent hydrolysis. Some of the more common functional groups used to form the clusters include carboxylates[121,123,124], pyridine based units[125,126], alpha amino acids[95,117,127] and beta diketones.[112,114,120,122] However there have also been examples of calixarenes and tetrazoles being used for the formation of these hydroxo clusters.[52,86,128,129]

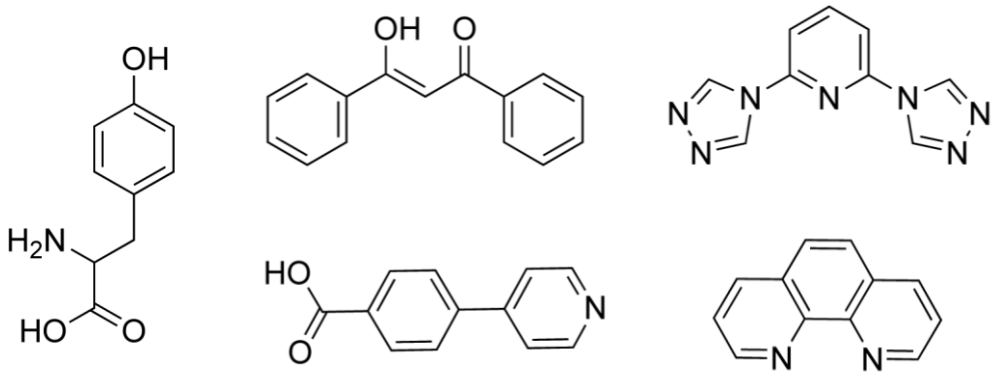

Figure 1.18: Common ligands that are known to form various cluster motifs.

The formation of the lanthanoid hydroxo cluster core tends to occur in specific geometries which repeat themselves in motifs that can extend through either a polymeric matrix or discrete molecule. These motifs are dependent on the number of lanthanoids

present within the cluster sphere. The most common motifs are the cubane, and square based pyramidal structures seen in Figure 1.19.[76] The higher nuclearity lanthanoid hydroxo clusters reported generally have similar motifs, however they are combined to make a larger unit.[52]

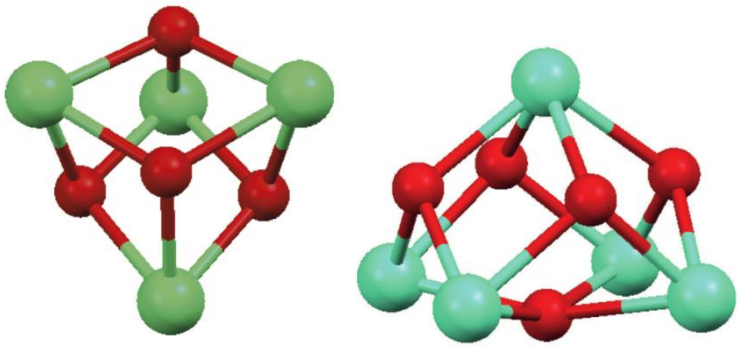

Figure 1.19: Common cluster motifs found forming the cubane (left) and square–based pyramid (right) lanthanoid hydroxo clusters.

1.4.2 Calixarene lanthanoid clusters

Calixarenes are well known for their inclusion properties, and due to their macrocyclic nature allow for either multidentate interaction or simultaneous coordination to numerous metals.[130] These attributes make them an ideal candidate for formation of clusters with both transition metals and lanthanoid ions. Despite the obvious advantages that calixarenes bring to cluster chemistry, in comparison to other ligand systems, there has only been limited literature dedicated to the investigation of these complexes, especially when associated with lanthanoid hydroxo systems. The previously characterised clusters involving a calixarene ligand generally contain the larger calix[8]arene or the more versatile thiacalix[4]arene.[107,131–133] In both these instances, there is a higher chance of additional interactions with the calixarene structure, thereby improving the likelihood of forming a cluster type species. The literature of the calix[4]arene on the other hand typically involves two or more calixarenes surrounding the lanthanoid hydroxo core, in a sandwich-like structure, as demonstrated in Figure 1.20.[130,134–136]

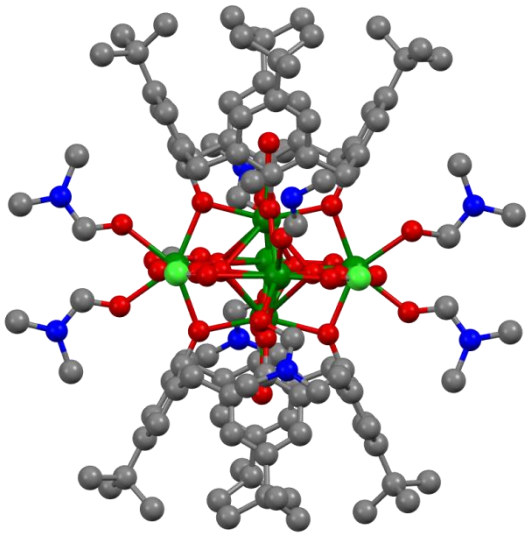

Figure 1.20: The sandwich effect of two calix[4]arene units surrounding the Ln_6 cluster.[134]

The sandwich type effect caused by the two calixarene molecules is similar to the previous examples of the ligand surrounding the cluster core. This suggests that there is a possibility for the synthesis and isolation of even larger clusters using the calixarene core as a ligand. The largest previously reported lanthanoid hydroxo cluster, containing the tetrameric calix[4]arene molecules as the main ligand, is the hexanuclear species shown previously in Figure 1.20.[52]

The majority of the work involving the calix[4]arene has been published by Dalgarno, however the work was only performed with the unsubstituted calixarene structure.[134,135] Interestingly, the structures reported usually have 'co-ligands' which complete the coordination spheres of the lanthanoids (see Figure 1.20). Despite the versatility available for substitution of the calixarene lower rim, there has been no literature to date, of calixarene clusters with lower rim substituents being involved with the cluster core. This is an unexplored area of potential cluster chemistry with the possibility of new cluster motifs owing to the unique binding modes available to calixarenes.

1.5 Project aims

Interest in new ligands for applications such as ionophores with specific tuneable properties leads to the investigation of unconventional donor motifs. There is a significant lack of literature in the area of tetrazoles attached to calixarenes, providing a niche where synthesis of these new ligands allows for the characterisation of new metal complexes, with the potential for varied applications. Upon successful synthesis of a library of tetrazole calixarenes, including the di-, tri- and tetra-substituted receptors (see Figure 1.21), coordination studies to a variety of lanthanoids will be performed.

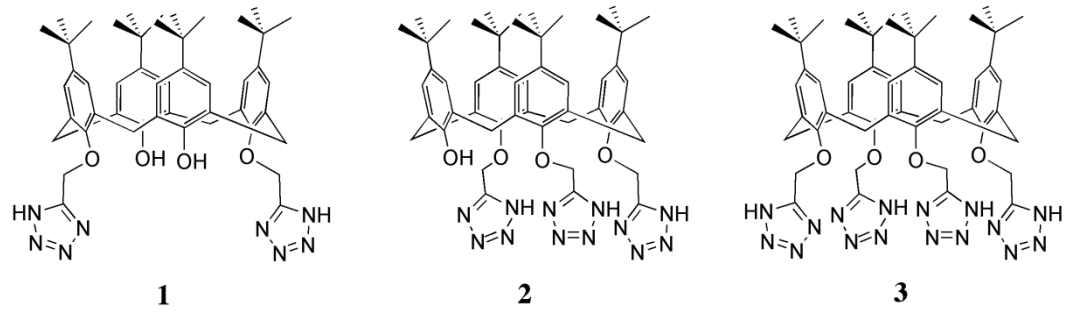

Figure 1.21: Key synthetic targets to be used for lanthanoid complexation. Di-tetrazole calixarene 1, tri-tetrazole calixarene 2 and tetra-tetrazole calixarene 3.

Ideally the deprotonated tri-tetrazole calixarene **2** will form a stable 1:1 metal to ligand complex with the lanthanoids to ensure a neutral complex which is beneficial for particular applications. The free phenolic OH of the tri-tetrazole calixarene can then be substituted with a neutral donor to impart additional characteristics to the molecule. The di-tetrazole calixarene **1** will be a good comparison for the tri- and tetra-tetrazole, while also being a ligand in its own right. The tetra-tetrazole calixarene **3** has the ability to complete the coordination sphere of the lanthanoid, reducing the amount of adventitious water directly attached to the calixarene. This is important for applications where the luminescence of the lanthanoid is being utilised. Synthesis of additional derivatives of both the di- and tri-tetrazole calixarene ligands will be attempted, such as the di-amide di-tetrazole calixarene, allowing a comparative analysis with the tetrazole-only calixarenes to be performed. Characterisation of the lanthanoid complexes will be performed *via* X-ray crystallography and spectroscopic studies.

2 Synthesis of the calixarene ligands

Direct alkylation on the lower rim of the calixarene has been well documented within the literature. Synthetic control of the different substitutions is achieved by altering three different parameters; the base employed for the deprotonation of the calixarene, the number of equivalents of the alkylating agent and the solvent used in the reaction. As stated in the introduction, Section 1.1.3, the lower rim of the unsubstituted calixarene contains hydroxyl groups, which intra-molecular hydrogen bond imparting increased stability for the cone conformer.[9,25] These hydrogen bonds must be broken in order for substitution reactions and subsequent ether linkages to be formed. Literature reports that there are differing pKa values associated with each subsequent deprotonation of the calixarene, allowing for the efficient and selective synthesis of mono-, di-, tri- and tetra-substituted calixarenes. These pKa values have been experimentally determined and confirmed by calculations, showing that each value is markedly different.[137,138]

Table 2.1: Literature pKa values determined for successive deprotonation of calix[4]arene.[137,138]

Deprotonation	pKa value
First	2.9-3.3
Second	10.9-11.8
Third	12.3-12.8
Fourth	＞14

It has been consistently shown that employment of particular bases will produce a higher percentage of one substitution product over another.[6,139,140] The very low pK_a value for the first deprotonation ensures that reaction will occur with addition of only a weak base, most commonly cesium fluoride.[137,140] The increased basicity required for the second deprotonation usually involves the employment of an alkali metal carbonate.[6,141] The tri-substituted product is usually the most difficult to isolate from a one pot reaction in any appreciable yield. Despite this, one pot synthesis of tri-substituted calixarenes has been reported on several occasions.[5,16,141] These papers employ a barium oxide or a mixture of barium oxide/barium hydroxide as the base deprotonating the calixarene. The tetra-alkylated products require a significantly stronger base to ensure complete deprotonation of the phenols, usually sodium or calcium hydride.[5,15,19,142] When the selection of the correct base is combined with adjusting the stoichiometry of the alkylating agent, there is increased control over the distribution of products synthesised.

This chapter of the thesis will mainly focus on the substitution of cyanomethoxy (nitrile) substituents on the lower rim of the calixarene, as organic nitrile moieties, discussed in Section 1.2, are the more traditional substrate used in the formation of tetrazoles.

2.1 Calixarene substitution

Several lower rim nitrile substituted calixarenes have been synthesised, including calixarenes with both pure and mixed substitution. As mentioned in the introduction (Section 1.1.1), the nomenclature of the synthesised calixarenes within this chapter is important. Where a ‘nitrile’ group is mentioned, it is actually in reference to a cyanomethoxy substituent. The scheme below outlines the calixarenes that were synthesised, with the majority using the di-nitrile calixarene **4** as the starting material. Addition of diethylamide substituents to the lower rim produces tetra-substituted, mixed

amide/nitrile substituted calixarenes. The tetra-substitution improves the denticity of the ligand, allowing for comparison to the solely nitrile substituted calixarenes in terms of their coordination to the lanthanoids. The diethylamide functional group was selected, as a literature search identified it to be a neutral functional group well known to form stable complexes with a range of metal ions.[98,99,143]

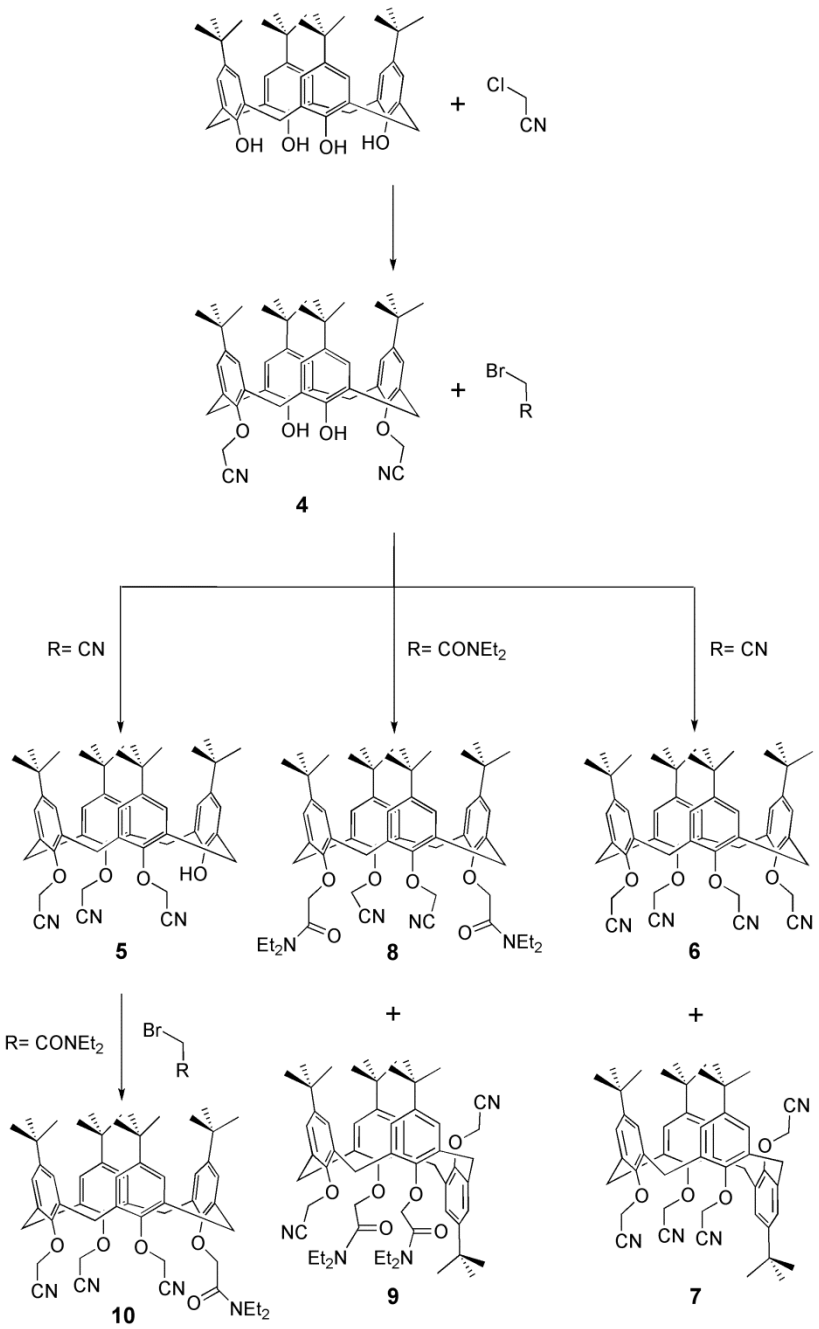

Figure 2.2: Synthetic scheme of the nitrile substituted calixarenes utilised.

The main diagnostic peak within the ^{1}H NMR spectrum suggesting successful formation of an ether linkage on the calixarene is the peak assigned to the methylene hydrogens between the ether oxygen and the nitrile group. This peak generally occurs anywhere between 4-5.5 ppm, which is a region usually devoid of solvent and other interfering signals, making it ideal for determining whether a reaction has occurred.

2.1.1 Di-nitrile calixarene

The di-nitrile calixarene **4** was synthesised according to literature procedure by Collins.[6] The alkylation reaction utilises potassium carbonate (K_2CO_3) as the base to deprotonate the calixarene. This weak inorganic base (pKa of ~10) is known to deprotonate the calixarene twice, resulting in the preferential formation of the 1,3-substituted product.[6,109]

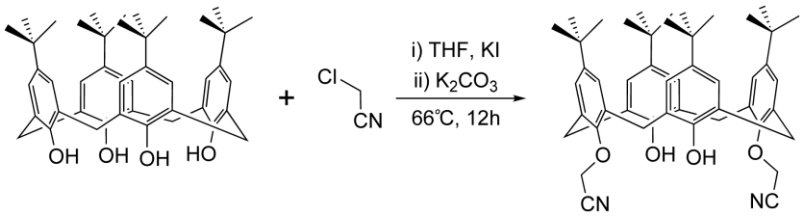

Figure 2.3: K_2CO_3 preferentially forms the 1,3-di-substituted calixarene 4.

The alkylating reagent employed for this reaction is chloroacetonitrile (ClACN). The low reactivity of chloroacetonitrile requires a Finklestein reaction, with potassium iodide, to be performed before successful nucleophilic substitution can take place. This increases the reactivity and thus the reaction rate, allowing this reaction to go to completion over 12 hours. The product was readily purified by recrystallisation, simplifying larger scale reactions (23 g of product). This was important, as calixarene **4** proved to be a useful intermediate for further substitution reactions. Characterisation of **4** was confirmed by both NMR and IR spectroscopy, which was identical to that reported in the literature.[6]

2.1.2 Tetra-nitrile calixarene

Attempts to synthesise the tetra-nitrile calixarene **6** directly *via* conventional calixarene alkylation methods, reaction of *tert*-butyl calix[4]arene with excess bromoacetonitrile (BrACN) and sodium hydride (NaH), were unsuccessful, with starting material isolated from the reaction mixture. This may have been due to failure of the reaction to proceed, however it is more likely to have been caused by the reactivity of the product under these reaction conditions. In an attempt to determine the cause of the alternate reactivity, the previously synthesised di-nitrile substituted calixarene **4** was reacted with bromoacetonitrile (BrACN) and a variety of bases. Table 2.4 demonstrates that the more powerful bases increased the percentage of *tert*-butyl calixarene degradation product isolated, suggesting that the latter hypothesis is more likely to be correct.

Table 2.4: Recovery of t-butylcalixarene after attempted alkylation of di-nitrile calixarene 4.

Alkylating agent	Base	Equivalents	t-butyl calix
BrACN	NaH	6 - 40	80%
BrACN	K_2CO_3	10 - 25	0%
BrACN	$BaO/Ba(OH)_2$	5 - 13	5%
BrACN	CaH_2	4 - 10	35%

One possible reason for this unexpected reactivity is that the stronger bases are reacting with the relatively acidic methylene hydrogen atoms of the ether linkage of any already attached nitrile substituents. This reaction would cause the successfully added nitrile substituents to react further, breaking the ether linkage to the lower rim, thus reverting back to *tert*-butyl calixarene.

Scheerder has shown that when failing to obtain the tetra-substituted calixarene by direct alkylation of *tert*-butyl calixarene, a two-step procedure using the di-substituted product as the intermediate can be employed.[144] Hence, di-nitrile calixarene **4** was reacted with NaH and bromoacetonitrile (BrACN) in dimethylformamide (DMF) at 80°C for 12 hours under an inert atmosphere. Despite the 58% yield reported in the literature, the reaction did not produce the tetra-substituted product as expected.[145]

Instead, degradation to the unsubstituted *tert*-butyl calixarene was again observed, supporting the hypothesis of a reactive product. Various conditions were then tested to optimise this reaction (Table 2.5).

Table 2.5: Varying conditions for formation of tetra-substituted calixarene 6 (B). N.B. NMR ratios quoted.*

Solvent	Base	Reagent	Temperature	Products
Acetone	NaH	ClACN	55°C	A70% S30%
DMF	NaH	ClACN	100°C	A100%
THF	NaH	ClACN	65°C	A70% B25% D5%
THF	NaH	ClACN	r.t.	A5% S95%
DMF	CaH_2	BrACN	150°C	A35% B60% C5%
DMF	NaH	BrACN	r.t.	S45% B10% C15% D30%
THF	NaH	BrACN	65°C	S20% B45% C5% D30%
THF	NaH	BrACN	r.t.	B85% C15%
DCM	NaH	BrACN	40°C	S30% B25% D45%
DMF	NaH	BrACN	50°C	A5% B85% C10%

***Graphical representations of calixarenes produced.**

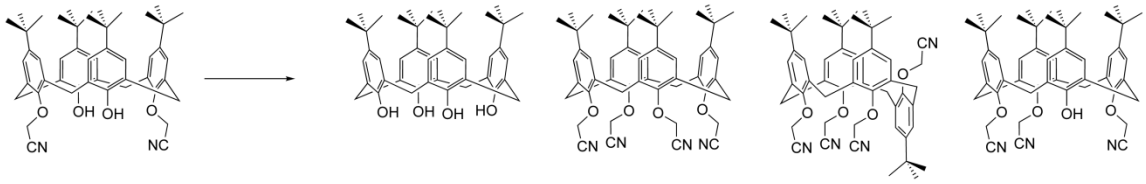

From this data set, bromoacetonitrile (BrACN) can be seen to produce more of the desired cone tetra-substituted product **6** (B) than chloroacetonitrile (ClACN). Initially bromoacetonitrile was added to the reaction solution as a single aliquot, after the di-substituted calixarene **4** had stirred with base for a short period of time. However, it was observed that fast addition of the alkylating agent produced vigorous effervescence, turning the solution from clear to orange and then black. This visual indication of degradation was accompanied by very poor recoveries of products that could be characterised. In subsequent reactions, bromoacetonitrile was diluted with additional

solvent, and added dropwise to the reaction mixture. This measure prolonged the time the black material took to form, however after a few hours formation of the black substance inevitably occurred. Optimisation of the reaction conditions in regards to temperature showed that as the temperature was reduced, there was also a decrease in the amount of degradation. However, unfortunately this was also accompanied with a proportional increase in the amount of partial cone conformer of the tetra-substituted calixarene **7**.

In collecting the data, the reaction was found to give variable outcomes when DMF was used as the solvent, with this traced back to the amount of water present in the solvent. Dry solvent was required for the best outcome, but even then, the conversion was not complete. Other solvents such as dichloromethane (DCM) and tetrahydrofuran (THF) were also tested, and it was found that THF as a reaction solvent was particularly effective, with very little degradation to *tert*-butyl calixarene. As can be seen in Table 2.5, the optimum conditions for the formation of the tetra-nitrile calixarene **6** were mild temperatures, tetrahydrofuran as the solvent with 15 mole equivalents of NaH deprotonating the calixarene. These reaction conditions were consistent in the complete conversion of **4** into mainly tetra-nitrile **6** with a small amount of the partial cone conformer **7**. It must be noted that although these conditions successfully converted the di-substituted starting material, similar attempts at direct synthesis of **6** from *tert*-butyl calixarene were still unsuccessful.

2.1.3 Tri-nitrile calixarene

As reported previously, the formation of the different substitution products are dependent on both hydroxyl acidity and reactant equivalents. The most difficult substitutions to synthesise are the mono- and tri-substituted calixarenes. Although the tri-nitrile calixarene **5** was known to form, as observed with the previous reactions to form **6**, this was only in very limited quantities, typically less than 30%. As a result

optimisation of the reaction was required, with a range of conditions tested (see Table 2.6).

Table 2.6: Varying conditions for formation of tri-substituted calixarene 5 (D). N.B. NMR ratios quoted.*

Solvent	Base	Equivalents	Temperature	Products
THF	$BaO/Ba(OH)_2$	5	r.t.	S80% B5% D15%
DMF	$BaO/Ba(OH)_2$	0.8	r.t.	B50% C5% D45%
DMF	$BaO/Ba(OH)_2$	1	r.t.	B10% D90%
THF	NaH	5	65°C	S50% B50%
DMF	NaH	1.5	r.t.	S10% B75% D15%
DCM	NaH	10	40°C	S90% D10%
DMF	CaH_2	6	r.t.	S45% B20% D35%
DMSO	$BaO/Ba(OH)_2$	1	r.t.	C85% B15%

***Graphical representations of calixarenes produced.**

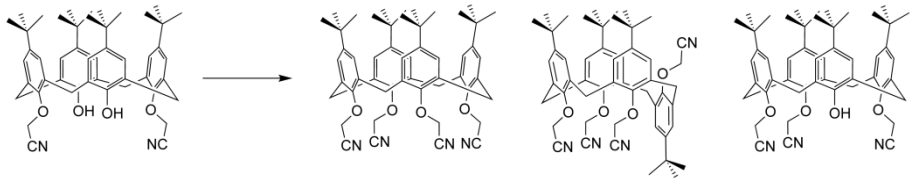

The mixture of barium oxides has been shown in literature to successfully convert, in a one pot reaction, the unsubstituted *tert*-butyl calixarene to the tri-substituted product.[5,99,141] Using DMF as the solvent, accompanied with the alkylating agent bromoacetonitrile, resulted in the production of the tri-nitrile calixarene **5** in approximately 45% yield by ^{1}H NMR observation. This improvement in the proportion of tri-substituted product **5**, was also accompanied by an increase in the percentage of starting material converted. A slight increase in the number of equivalents of alkylating agent increased the ^{1}H NMR ratio of **5**, which corresponded to an isolated yield of 69%, and only 3% being the tetra-substituted product. While this is a useful outcome, it was found that the tetra- and tri-substituted products were virtually inseparable using simple separation techniques. As a result different reaction conditions were tested to produce **5** without any tetra-substituted calixarenes present within the reaction mixture. Unfortunately all efforts to optimise the reaction failed, with either low yields of

tri-nitrile calixarene **5**, or some tetra-nitrile substituted calixarene **6** still produced in the reaction. As optimisation of the reaction conditions to produce **5** failed to exclude the synthesis of **6**, the use of HPLC to separate out these two products was attempted. Unfortunately, in a similar manner to column chromatography, the HPLC conditions also showed very poor separation. As a result, it was hoped that further reaction of the mixture with either another alkylating agent or conversion of the nitrile moiety to a different functional group would transfer a greater difference in polarity between each molecule. The addition of another group on the lower rim *via* nucleophilic substitution would only react with a free phenol, hence the tri-nitrile calixarene **5** would be the only reactant affected. This should then create a substantial difference in polarity between **6** and the newly tetra-substituted tri-nitrile calixarene derivative.

2.2 Synthesis of amide/nitrile calixarenes

The additional group substituted on the lower rim of the calixarene had to fulfill two requirements; be a neutral functional group so that the charge of the ligand remains consistent and also be a moiety with high affinity for the lanthanoids. A literature search quickly identified that the diethylamide moiety was a neutral functional group well known to form stable complexes with a range of metal ions.[98,99,143] As a result, both the di-amide di-nitrile (**8** and **9**) and the mono-amide tri-nitrile (**10**) derivatives were synthesised. In addition, the amide-substituted calixarenes could also be used to compare with the solely nitrile substituted calixarenes in terms of their coordination with lanthanoid ions.

2.2.1 Mono-amide tri-nitrile calixarene

Reaction of 2-chloro-*N*,*N*-diethylacetamide with the mixture of nitrile calixarenes **5** and **6** results in the formation of the mono-amide tri-nitrile calixarene **10**. The synthesis of **10** served the dual purpose of allowing separation of the tri-nitrile **5** from the tetra-nitrile calixarene **6**, while also producing the possibly useful pre-ligand mono-amide tri-nitrile calixarene **10**.

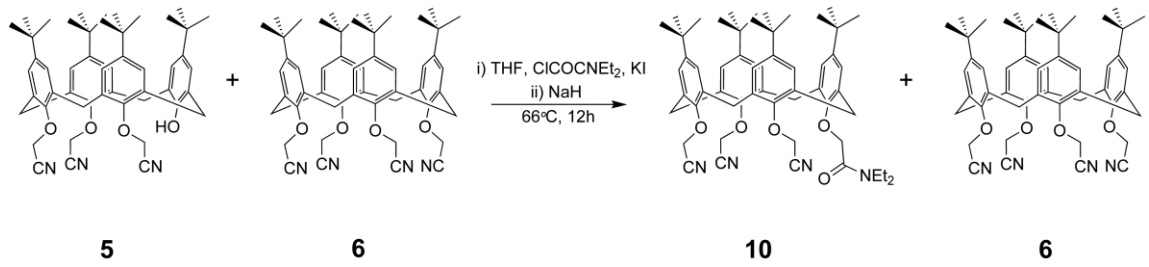

Figure 2.7: Mixed tri/tetra-nitrile route to produce calixarene 10.

The synthesis of **10** from the tri/tetra-nitrile mixture was attempted *via* conventional conditions for tetra-alkylation of the calixarene. Chloro-diethylacetamide was reacted with the mixture of nitrile calixarenes **5** and **6** and NaH as the base. This resulted in similar degradation problems as seen, in Section 2.1.2, when producing the tetra-nitrile calixarene **6**. Despite this, fine tuning of the reaction conditions was successful in the formation of the mono-amide tri-nitrile calixarene **10**. It is interesting to note that unlike both the di-amide di-nitrile and tetra-nitrile calixarenes, different conformations of calixarene **10** were not evident within the crude product mixture.

A rational synthesis of the mono-amide tri-nitrile calixarene **10** was also explored, as it could simplify access to pure tri-nitrile **5**. The initial scheme involved protection of one phenolic group, subsequent addition of the nitrile moieties to the other three positions before deprotection and optional addition of the final amide group to the remaining phenol. Unfortunately this method for obtaining **10** and **5** through the same reaction scheme was unsuccessful, with the actual scheme having to follow the one shown in Figure 2.8.

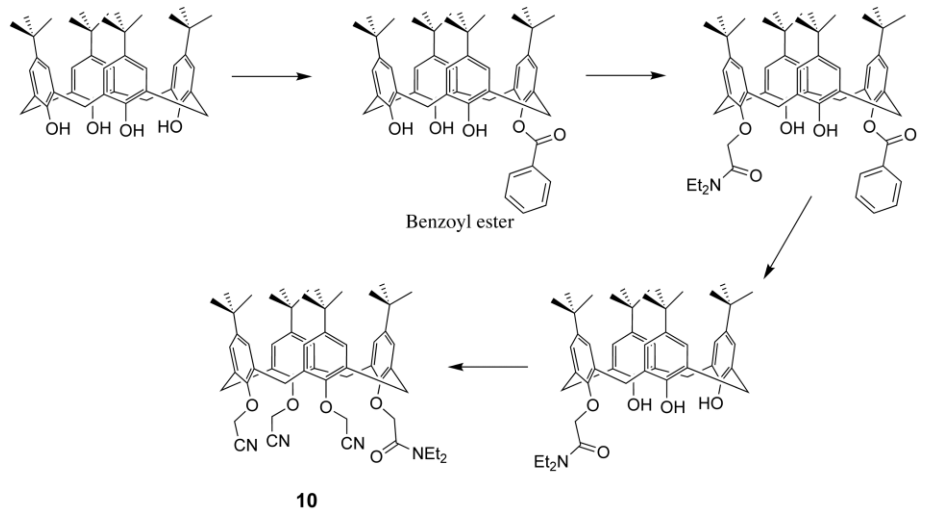

Figure 2.8: Benzoyl protected route to produce calixarene 10.

The benzoyl ester was synthesised according to literature, and was a protecting group readily hydrolysed from the calixarene lower rim under mild conditions.[146] All attempts to substitute the remaining three positions on the lower rim of the calixarene with nitrile moieties, allowing access to pure tri-nitrile calixarene **5**, resulted in failure. The isolated material from this synthesis was not the desired tri-nitrile substituted product, instead the nitrile group exclusively substituted in the distal "3" position to the benzoyl group. Hence a variation of the reaction conditions using the chloro-diethylacetamide alkylating agent was devised, giving the same persistent product as the nitrile reaction. This slightly altered scheme shown in Figure 2.8 could still be used to isolate **10**, but not the pure tri-substituted **5**.

2.2.2 Di-amide di-nitrile calixarene

As mentioned previously, one of the reasons that the diethylamide substituents were added to the lower rim of the calixarene was to complete the tetra-substitution of the calixarene. The conversion of the nitrile functional groups on the di-amide di-nitrile calixarenes to the corresponding tetrazole derivatives was to be used as a comparison with the di-tetrazole calixarene **1**. Calixarene **8** could be synthesised from either the di-amide or di-nitrile calixarenes, as both allowed for successful tetra-substitution. As

the di-nitrile calixarene **4** was already readily available, it was decided to utilise this as the starting material for this reaction scheme (see Figure 2.9).

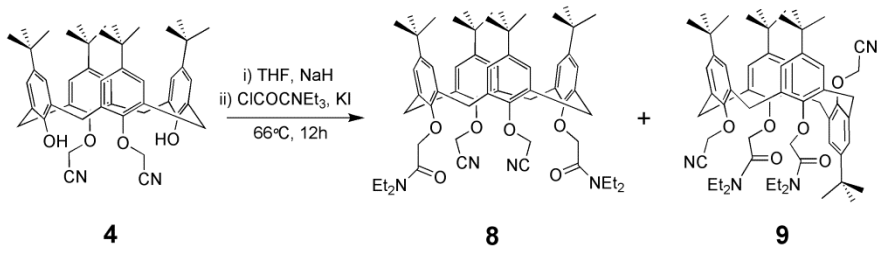

Figure 2.9: Synthesis of the cone and partial cone conformers of the di-amide di-nitrile calixarenes.

Addition of chloro-diethylacetamide as the alkylating agent, along with NaH as the base did cause some degradation similar to that seen in Section 2.1.2. Despite this, the reaction still proceeded in 88% yield with the other 12% attributed to the degradation product, *tert*-butyl calixarene. After column chromatography of the product it became evident that the di-amide di-nitrile calixarene produced was actually a mixture of two different conformers (**8** and **9**). They were easily separated and subsequent ^{1}H NMR studies showed that they were the cone and partial cone conformers, in an average synthetic distribution of 25:75 respectively. This ratio is unsurprising as the increased steric bulk of one diethylamide group added on the lower rim would cause intra-annular rotation of an adjacent nitrile substituted phenyl ring, which is then locked into position.

2.3 Nitrile to tetrazole conversion

As discussed in Section 1.2, there are many literature methods for the formation of tetrazoles.[40,41,43,47] The employment of organic nitrile groups as the substrate is the more traditional approach to forming tetrazoles, and is the one applied in this thesis. The method first implemented by Sharpless using water as the solvent cannot be employed here, as the calixarene nitriles are lipophilic and thus insoluble in water or a water/isopropanol mixture.[41] The Finnegan method, utilising sodium azide with ammonium chloride in DMF had more potential as the calixarene is soluble in DMF, however the workup of this procedure proved to be difficult.[40] As a result the Koguro method was found to be the method of choice, as it involves the use of hot toluene as the

solvent, in which the nitrile calixarenes are soluble.[43] The workup of this reaction was extremely simple with only an acid wash being required in each case.

2.3.1 Synthesis of the tetrazole calixarenes

Upon addition of sodium azide, along with ammonium chloride as a proton source, the nitrile group undergoes a 1,3 dipolar cycloaddition forming the deprotonated tetrazole, which is subsequently protonated upon acidic workup of the reaction. The reaction to form the tetrazoles on the calixarene requires longer reaction times than that described by Koguro.[43] This slower reactivity can be attributed to likely steric crowding on the lower rim of the calixarene preventing rapid conversion of the nitrile substrate.

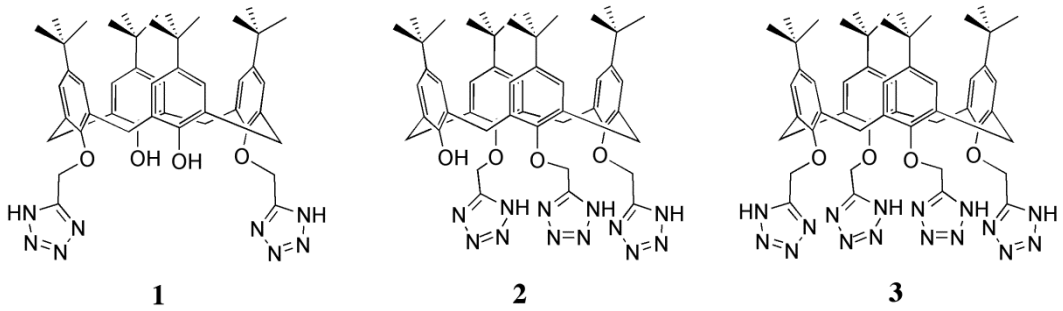

1 **2** **3**

Figure 2.10: Tetrazolyl-functionalised calixarene ligands synthesised; di-tetrazole calixarene 1, tri-tetrazole calixarene 2 and tetra-tetrazole calixarene 3.

Typically reactions to form calixarenes **1**, **2** and **3** were left heating for up to three days, maximising conversion. The tetrazolation reactions proceeded with a high yield, however, because of the slow kinetics of the reaction partially reacted products could occasionally be isolated and characterised. One of these products was the di-tetrazole mono-nitrile calixarene which was isolated as a reaction by-product in up to 5% yield. This product was characterised by ^{1}H NMR and MS after separation by HPLC (Figure 2.12). A further complication of the tetrazolation reaction was the occurrence of intra-annular rotation of the nitrile substituted phenyl rings under the Koguro conditions. Evidence of this rotation during the tetrazolation reaction of the di-nitrile calixarene **4** was obtained with the isolation and crystallisation of the di-tetrazole calixarene in the 1,2-alternate conformation (Figure 2.11). This

demonstrated that at high temperatures the cone conformation of the nitrile starting material is not always conformationally rigid. This phenomenon will be discussed in more depth in Chapter 3.

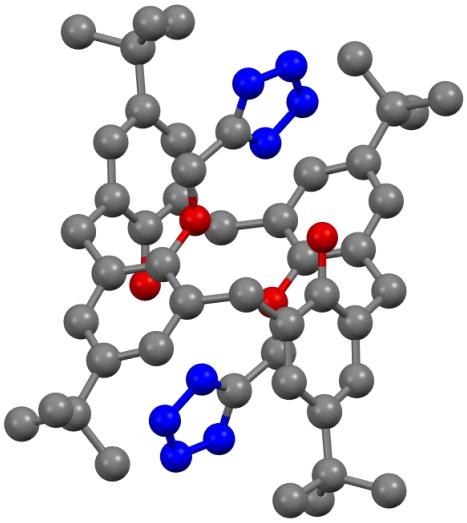

Figure 2.11: X-ray crystal structure of the di-tetrazole calixarene in the 1,2-alternate conformation.

Conversion of the amide/nitrile functionalised calixarenes **8**, **9** and **10** was attempted using the same Koguro conditions. The successful conversion of the solely nitrile substituted calixarene derivatives **4**, **5** and **6** indicated that conversion of nitrile moieties to tetrazoles when attached to calixarenes was possible. However, despite this, employment of similar Koguro conditions on all the mixed amide/nitrile functionalised calixarenes failed to react, with starting material being isolated in high yields. After unsuccessfully attempting the Koguro method, the Finnegan method and the Sharpless method with water/isopropanol as the solvent, it was decided that the lack of reactivity was unknown.

2.3.2 Isolation and purification

Isolation of the calixarene tetrazoles from the reaction mixture needed to be altered from Koguro's paper due to the hydrophobic nature of the calixarene product. According to the literature, the sodium salt of the tetrazole products readily transfer into the water layer during an extraction of the toluene. Upon subsequent acidification of the aqueous

layer, the protonated tetrazole would then precipitate out of solution. In contrast, the calixarene derivatives in this thesis are insoluble in the aqueous layer, even as the sodium salt. Thus the workup was adapted to exploit the insoluble nature of the calixarene to isolate it from the by-products and other reagents. Firstly the toluene was washed with acidic water and then evaporated under reduced pressure until completely dry. This powder is only partially protonated and contains unreacted nitrile calixarene. The powder was then dissolved in ethyl acetate and washed with acidic water several times to ensure complete protonation had occurred. Subsequent drying and removal of the ethyl acetate leaves the tetrazole calixarene as an impure product. The purification procedure required for each tetrazole calixarene differed depending on the number of moieties attached.

Purification of the di-tetrazole calixarene **1** was relatively straightforward, as the starting di-nitrile reagent **4** generally contained no by-products. The di-tetrazole calixarene **1** is initially isolated as an off yellow/cream solid. Dissolving the yellow solid in minimal hot chloroform or dichloromethane and then placing into the freezer to cystallise results in the formation of crystals typically 24 hours after cooling. The white needle-like crystals evolved over this time are then immediately vacuum filtered and washed with a minimum amount of cold chloroform. The recrystallisation could be repeated several times until the isolated crystals turned yellow suggesting incorporation of the impurity. This workup procedure allowed for consistent isolation of the calixarene tetrazole **1** in moderate to high yields (65% - 85%).

Contrary to the straightforward purification of the di-tetrazole calixarene **1** *via* recrystallisation, isolation of pure tri- and tetra-tetrazole **2** and **3** proved to be substantially more difficult. As discussed in Section 2.1.3, due to the nature of the reaction to produce the tri-nitrile calixarene **5**, some of the tetra-substituted product **6** was also synthesised. Separation of these different nitrile derivatives proved to be extremely difficult with conventional chromatography methods. The tetrazole

derivatives were not much more conducive, fortunately the polarity difference afforded by an additional tetrazole group proved significant when analysing by HPLC. Hence, the tri- and tetra-tetrazole calixarenes **2** and **3** were separated through the use of a Waters HPLC system with a preparative reverse phase C18 column. Trifluoroacetic acid was added to the acetonitrile/water solvent system to ensure that the tetrazoles remained protonated, thereby avoiding any potential difficulties that arise from variably deprotonated systems. As illustrated in Figure 2.12, the retention times for this solvent system allowed not only separation of the different substitutions but also different conformers. The partial cone tetra-tetrazole calixarene eluted at 11.5 minutes with the cone tetra-tetrazole **3** eluting at 15.4 minutes. The tri-tetrazole calixarene **2** took substantially longer to elute at 28.4 minutes and the partially converted di-tetrazole mono-nitrile, previously mentioned, eluted last at 33.9 minutes.

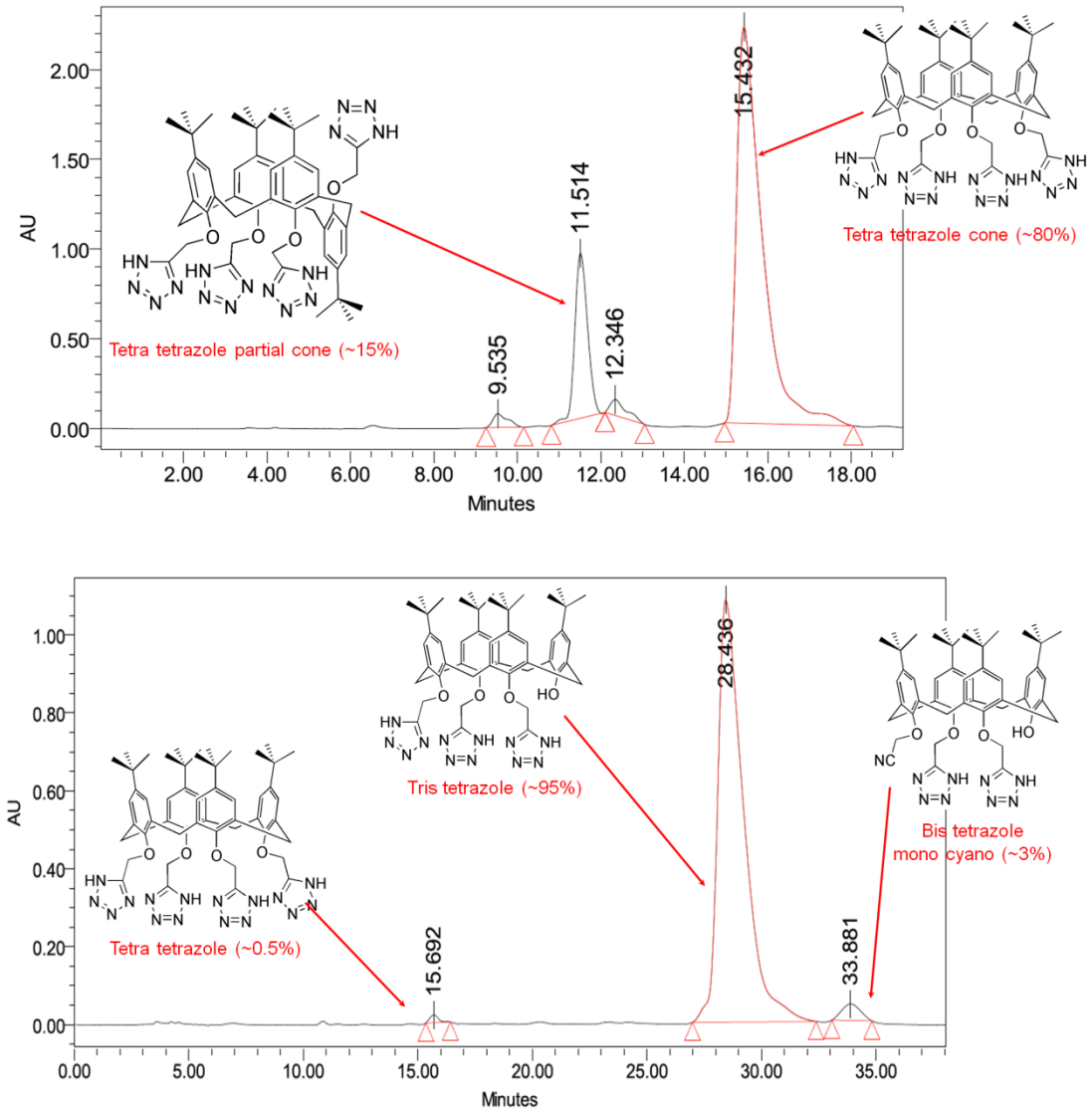

Figure 2.12: HPLC traces showing the elution times of the various tetrazole calixarenes.

2.4 Conclusions

Synthesis of three new calixarene tetrazolato ligands was successful upon conversion of the lower rim nitrile substituents to tetrazole moieties. Optimisation of the reaction conditions to form the nitrile starting materials was required as significant degradation was evident. Unsuccessful formation of the tetra-nitrile calixarene **6** from *tert*-butyl calixarene required the employment of the isolated di-nitrile calixarene **4** to be used as an intermediate. It was observed that at high temperatures the nitrile substituted

calixarenes may not be conformationally stable, leading to the formation of calixarene tetrazoles not in the desired cone conformation. Conversion of the nitrile groups to tetrazole moieties was achieved *via* a 1,3 dipolar cycloaddition with sodium azide, as demonstrated in the literature. A slight deviation in the workup of the Koguro tetrazolation reaction resulted in the isolation of the hydrophobic calixarene tetrazole ligands **1**, **2** and **3** in moderate to high yield.

3 Conformational rotation of cyanomethoxy-substituted calixarenes

Calix[4]arenes are able to assume four well-defined conformations; cone, partial cone, 1,2-alternate, and 1,3-alternate (see Figure 1.5).[1,25] Literature studies have demonstrated that attachment of nitrile substituents on the lower rim of the calixarene does not stop the rotation of the calixarenes phenyl groups.[15,21,147] A systematic study to investigate the conformational equilibrium for two initially pure conformers has not been previously performed. Nitrile groups on the calixarene framework are important precursors to many different functional groups.[17,108,144,145,148] One such example seen in the previous chapter is the conversion of the nitrile moiety to a tetrazole. As such, it is important to have a complete understanding of the possible conformations naturally adopted by the calix[4]arene when nitrile substituents are attached to the lower rim. This understanding also needs to extend to the ability of the nitrile-substituted phenyl groups to rotate and hence interconvert between conformers (noting that this interconversion can only occur with the smallest such group, the cyanomethoxy substituent).

At room temperature, rapid interconversion among the unsubstituted conformers occurs by the "oxygen through the annulus" pathway.[15,141,147,149] If the calixarene undergoes nucleophilic substitution on the lower rim, replacing the free OH groups with sterically hindered substituents, the conformational interconversion is curtailed, and conformationally stable compounds can be isolated and characterised, most often by NMR spectroscopy and/or single crystal X-ray diffraction.

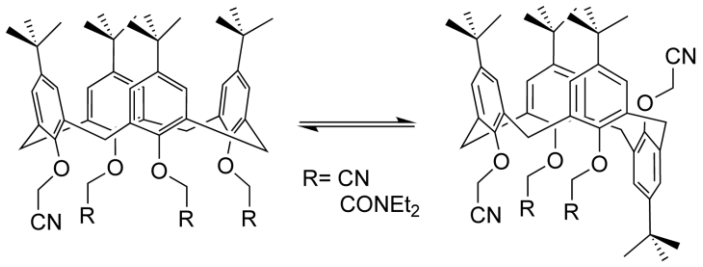

Figure 3.1: Rotation through the annulus by the lower rim nitrile functional groups.

There are many known examples of lower rim calixarene substituents undergoing rotation through the annulus, in particular methyl and ethyl groups.[13,20,25,147,150] It has been shown that the smallest functional group necessary to prevent rotation appears to begin with the propyl group.[15,141,147] Given the sequence of OMe, OEt and OPr, it is of interest to determine where the cyanomethoxy substituent falls into this progression of effective group size, Figure 3.1. Previous investigations of rotation associated with nitrile substituted phenyl rings of the calixarene have shown that there is rotation of the moieties at differing rates depending on the upper rim substituents.[21,147]

3.1 Crystal structures

Of the nitrile substituted calixarenes studied in this thesis, there were several that had not been previously structurally characterised (**5**, **7**, **8**, **9** and **10**). Single crystals of these derivatives, appropriate for structural determination, were obtained. These structures are reported below.

3.1.1 Nitrile substituted calixarenes

The two nitrile substituted calixarenes present within this thesis, yet to be structurally determined, are the tri-nitrile calixarene **5** and the partial cone conformer of the tetra-nitrile substituted calixarene **7**.

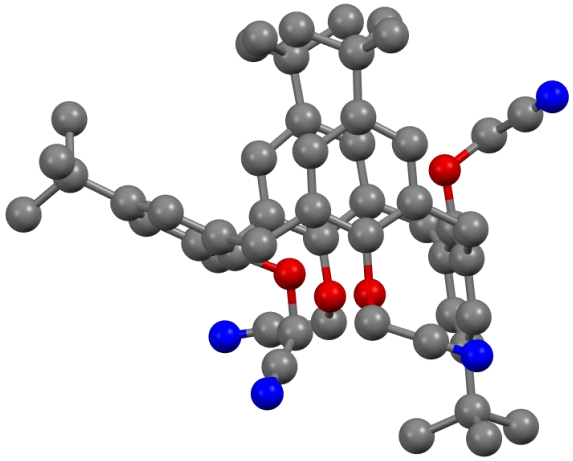

Figure 3.2: X-ray crystal structure of the tetra-nitrile substituted calixarene 7.

The tetra-nitrile calixarene **7** assumed the partial cone conformation. Three of the phenyl rings are virtually perpendicular to the plane defined by the methylene C atoms, with interplanar angles of 91°, 86°, and 90°. The remaining phenyl ring (distal to the rotated ring) is lying at a much more acute angle of 30° with respect to the methylene plane. As is typically the case with a "pinched" conformation, the calixarene cavity is unoccupied.

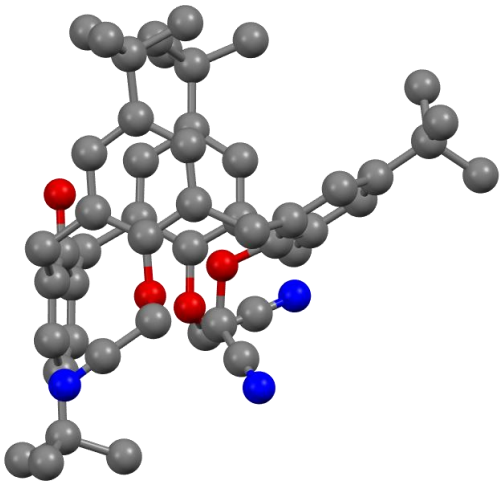

Figure 3.3: X-ray crystal structure of the tri-nitrile substituted calixarene 5.

The structure of the tri-substituted calixarene **5** is remarkably similar to that of the partial cone tetra-substituted **7**. Like calixarene **7**, **5** exists in the 'three down, one up' or partial cone configuration (see Figure 3.3). The phenyl group rotated with respect to the methylene plane is the only unsubstituted phenyl ring in the molecule. This phenol and the vicinal nitrile substituted phenyl rings are virtually perpendicular to the methylene C_4 plane, with dihedral angles of 94°, 88°, and 87°. The phenyl ring distal to the rotated phenol lies at a much more acute angle with a dihedral angle of 29°.

3.1.2 Amide/nitrile substituted calixarenes

The di-amide di-nitrile calixarenes in both the cone and partial cone conformation (**8** and **9**), along with the cone conformer of the tri-nitrile mono-amide calixarene **10** all reported in this thesis, have not been previously structurally characterised *via* X-ray crystallography.

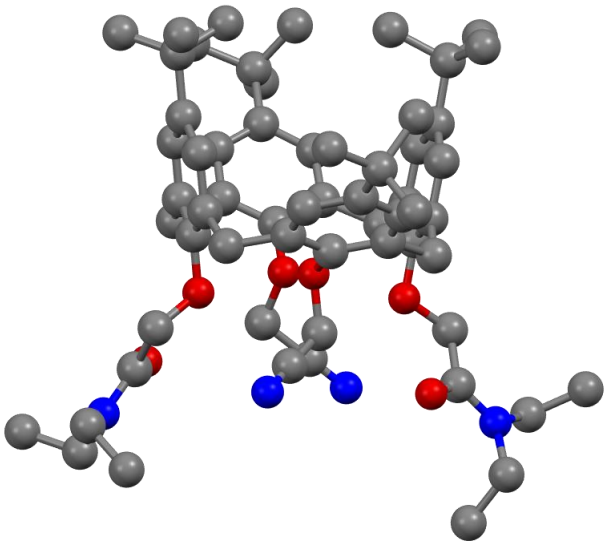

Figure 3.4: X-ray crystal structure of the cone di-amide di-nitrile substituted calixarene 8.

There are two crystallographically independent molecules in the asymmetric unit of calixarene **8**, which are related by a pseudo *a*/2 translation, one of which is shown in Figure 3.4. The calixarene is in the cone conformation, with the two opposing phenyl rings containing the amide groups almost co-planar, the dihedral angle between the two planes being 15° for both molecules. This co-planar nature is also reflected in the

dihedral angles between the phenyl rings and the C_4 methylene plane of the calixarene, with the rings being almost perpendicular to the plane (98° and 82° for molecule 1 and 90° and 75° for molecule 2). The dihedral angles between the methylene plane and the nitrile substituted phenyl rings are more acute with angles of 34° and 47° for molecule 1 and 34° and 48° for molecule 2.

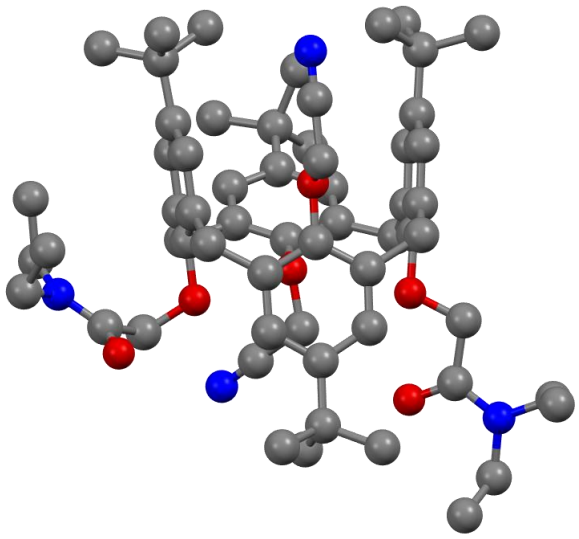

Figure 3.5: X-ray crystal structure of the partial cone di-amide di-nitrile substituted calixarene 9.

The phenyl rings of calixarene **9** are arranged in the 'three down, one up' partial cone configuration, with one of the nitrile substituted phenyl rings being in the rotated position as demonstrated in Figure 3.5. The two opposing phenyl rings with the amide groups attached are almost co-planar, with only an 8° dihedral angle between the two planes. This is also reflected in the dihedral angles between these phenyl rings and the methylene plane being almost perpendicular (93° and 84°). The angle between the methylene plane and the rotated phenyl ring is 87°, which shows that this is also close to perpendicular. The dihedral angle for the remaining phenyl ring is 36°.

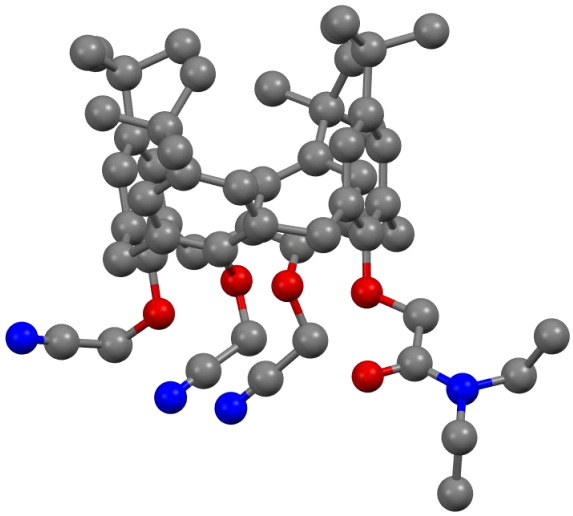

Figure 3.6: X-ray crystal structure of the mono-amide tri-nitrile substituted calixarene 10.

The mono-amide tri-nitrile derivative **10** crystallised in the cone conformation. The cone conformer is "pinched", with the two distal phenyl rings, including the amide-substituted phenyl group, being almost co-planar (dihedral angle of 8°). These two co-planar phenyl rings are also almost perpendicular to the methylene plane, having dihedral angles of 84° and 87°. The dihedral angles between the methylene plane and the two remaining phenyl rings are 46° and 41°. The calixarene cavity is unoccupied as demonstrated in Figure 3.6, however, there is a hydrogen bond between a residual ethanol and the amide oxygen atom, see Appendix C.

3.2 Identification of different conformers

The di-, tri- and tetra-nitrile calixarenes (**4**, **5**, **6** and **7**) and the sterically bulky amide/nitrile calixarenes (**8**, **9** and **10**) were utilised for the rotation experiments. This is predominantly due to their isolation in pure form for the two conformers, cone and partial cone. The easiest way to differentiate between the conformers was through the use of NMR spectroscopy. Detailed observation of both the aromatic region (6.7-7.4 ppm) and the methylene ether linkage region (4.8-5.2 ppm) of the ^{1}H NMR spectra allowed for rapid identification of each conformer, even within a complex mixture. The assignment of individual peaks was also determined through NMR spectra, but in this case 2D COSY and HSQC experiments were performed.

3.2.1 Nitrile substituted calixarenes

The ^{1}H NMR spectra associated with the four nitrile substituted calixarenes were studied in terms of symmetry, confirming the assumed conformations.

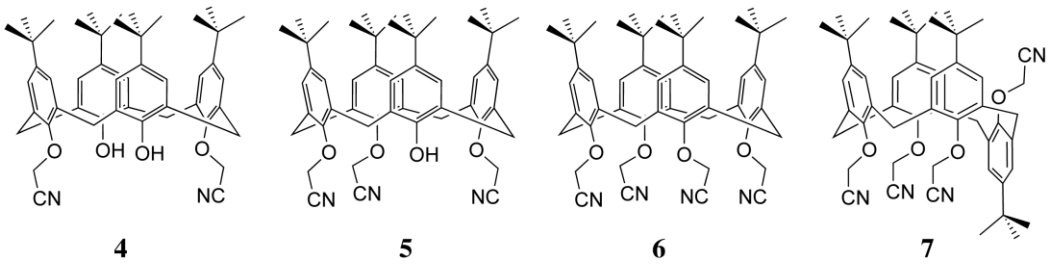

Figure 3.7: The nitrile substituted calixarenes utilised for the rotation experiments.

The symmetry and selected ^{1}H NMR peak assignments of the 1,3-substituted calixarene **4** in the cone conformation are shown in Figure 3.8 below.

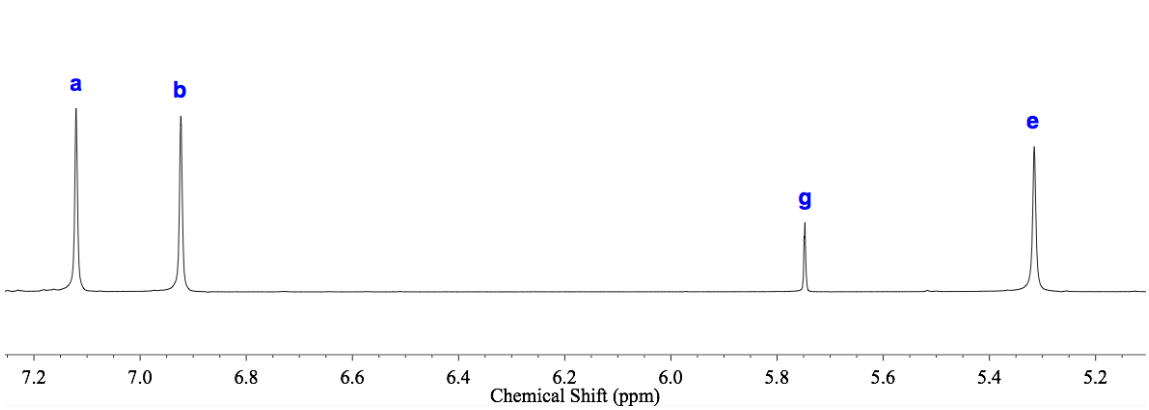

Chemical shift	Multiplicity	Corresponding hydrogen	Relative integration
7.12	Singlet	a	4
6.92	Singlet	b	4
5.31	Singlet	e	4
5.75	Singlet	g	2

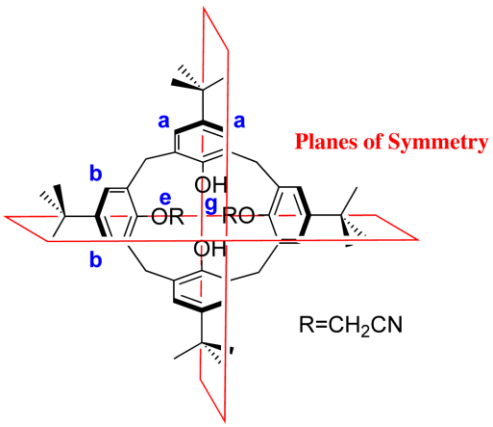

Figure 3.8: ^{1}H NMR spectrum and symmetry diagram for the di-nitrile calixarene 4 in the cone conformation.

The two bisecting planes of symmetry present within **4** simplify the ^{1}H NMR spectrum to the point where there are only four peaks present within the diagnostic region.

Confirmation of di-substitution is two-fold, firstly the relative integration of the peak at 5.75 ppm is two, which corresponds to two free phenols. Secondly the relative integration (four) of the methyl ether linkers also matches with di-substitution of the calixarene.

The tri-substituted calixarene **5** was unable to be isolated in a pure state due to a lack of difference in polarity between the product and the starting material. As a consequence there are peaks within the ^{1}H NMR spectrum, Figure 3.9, which have been assigned previously to the di-substituted **4**, and have been denoted with an asterix.

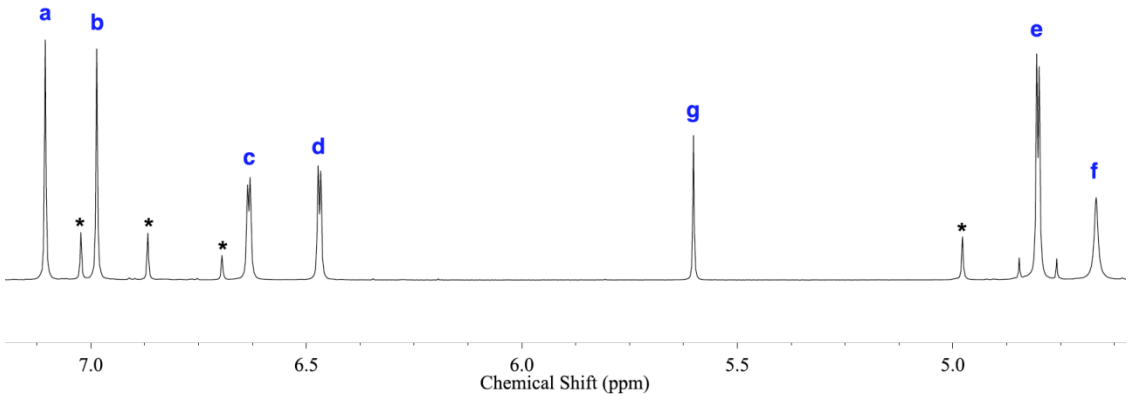

Chemical shift	Multiplicity	Corresponding hydrogen	Relative integration
7.27	Singlet	a	2
7.15	Singlet	b	2
6.80	Doublet	c	2
6.63	Doublet	d	2
4.97	Doublet	e	4
4.83	Singlet	f	2
5.76	Singlet	g	1

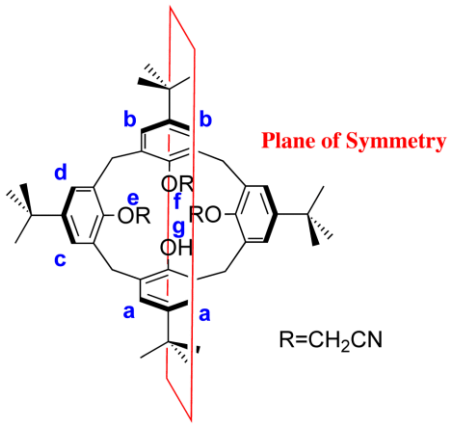

Figure 3.9: ^{1}H NMR spectrum and symmetry diagram for the tri-nitrile calixarene 5 in the cone conformation. * denotes di-nitrile impurity.

As a result of tri-substitution on the lower rim, there is only one plane of symmetry within the molecule. This single mirror plane bisects the unsubstituted aromatic ring

resulting in an increased number of peaks in the ^{1}H NMR spectrum. There are four peaks assigned to the hydrogens of the phenyl rings. There are two singlets (a,b) and two doublets (c,d), which arise from *meta* coupling of the non-equivalent *meta* hydrogens. Similar to the splitting of the non-equivalent aromatic hydrogens (c,d), there is also splitting of the methyl ether linkers of the nitrile groups on the lower rim. These hydrogens (e) both split into doublets with an integration ratio of four. This splitting is a consequence of the two vicinal phenyl groups being non-equivalent. The other methyl linker CH_2 has a relative integration of two and is only a singlet. The integration of the three peaks (e,f) have an overall integration of six which is consistent with what is expected for the tri-substituted calixarene **5**. The peak at 5.76 ppm corresponds to the hydrogen of the free phenol and integrates to one as there is now only the single free unsubstituted phenol on the lower rim of the calixarene.

The fully substituted nitrile calixarenes **6** and **7** were independently isolated from the initial reaction mixture and analysed *via* X-ray crystallography to support the hypothesis that they were indeed different conformational isomers. The cone conformation **6** was easily identified by ^{1}H NMR spectroscopy, as it has a four-fold rotational axis of symmetry, which makes each of the hydrogen atoms on the phenyl rings of the calixarene equivalent. This ensures that the spectrum has only one singlet in the ^{1}H NMR spectrum of Figure 3.10 for each hydrogen environment (discounting the methylene bridges of the macrocycle which are doublets). As expected for complete substitution of the lower rim of the calixarene, there is no peak for the hydrogen of the free phenols as observed for the previous two calixarenes.

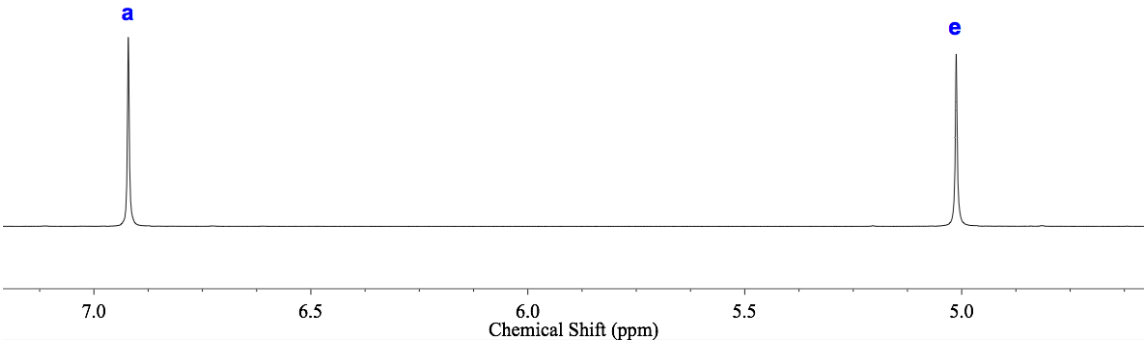

Chemical shift	Multiplicity	Corresponding hydrogen	Relative integration
6.91	Singlet	a	8
5.00	Singlet	e	8

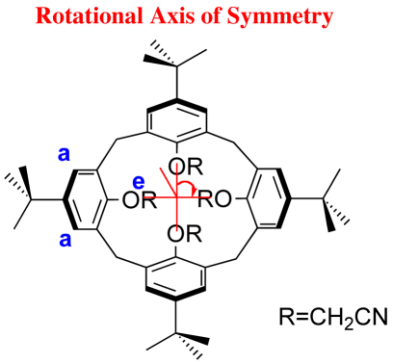

Figure 3.10: ^{1}H NMR spectrum and symmetry diagram for the tetra-nitrile calixarene 5 in the cone conformation.

In contrast to the relatively simple ^{1}H NMR spectra of the cone conformation, the partial cone calixarene **7** has a ^{1}H NMR spectrum which is similar to the tri-substituted calixarene **5**.

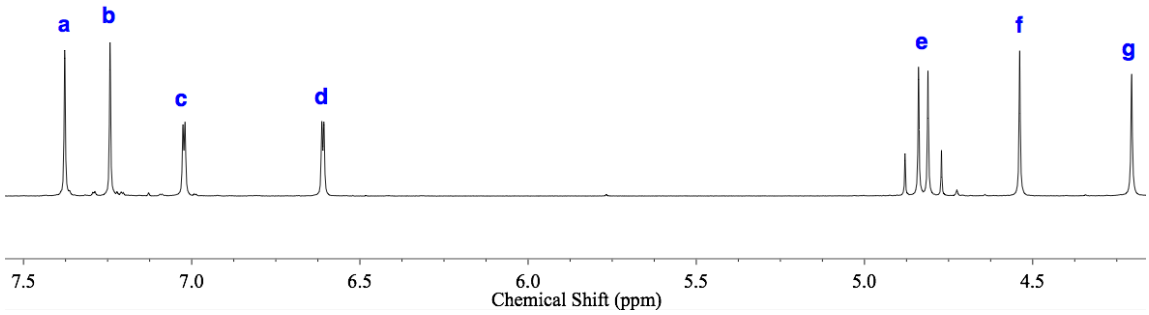

Chemical shift	Multiplicity	Corresponding hydrogen	Relative integration
7.37	Singlet	a	2
7.23	Singlet	b	2
7.02	Doublet	c	2
6.60	Doublet	d	2
4.81	Quartet	e	4
4.53	Singlet	f	2
4.20	Singlet	g	2

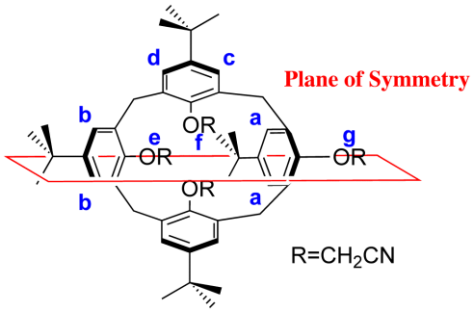

Figure 3.11: Splitting of the tetra-nitrile calixarene 7 ^{1}H NMR spectrum when in the partial cone conformation.

Only one plane of symmetry exists in calixarene **7**, with this mirror plane bisecting the rotated phenyl group (see Figure 3.11). This results in there being two singlets (a,b) and two doublets (c,d) in the aromatic region of the spectrum. For calixarene **7**, the methyl ether hydrogens have split into two overlapping peaks, making an apparent quartet (e), with two additional singlets further upfield (f,g). These peaks have an integration ratio of four:two:two. In addition to the correct integration for tetra-substitution of the methyl ether linkers, the absence of any hydroxyl signal attributed to a free phenol further supports the assumption that tetra-substitution has occurred.

3.2.2 Amide/nitrile substituted calixarenes

In addition to the purely nitrile substituted calixarenes, amide moieties were also substituted on the lower rim of the calixarene (see Section 2.2). The increased steric bulk of the diethylamide substituent was expected to affect not only the rate at which rotation

of the nitrile substituted phenyl groups occurred, but also affect the equilibrium distribution of the different conformers. Three amide-nitrile substituted calixarenes were investigated; the cone conformation of the mono-amide tri-nitrile calixarene **10**, the di-amide di-nitrile calixarene in cone conformation **8** and partial cone conformation **9** (see Figure 3.12).

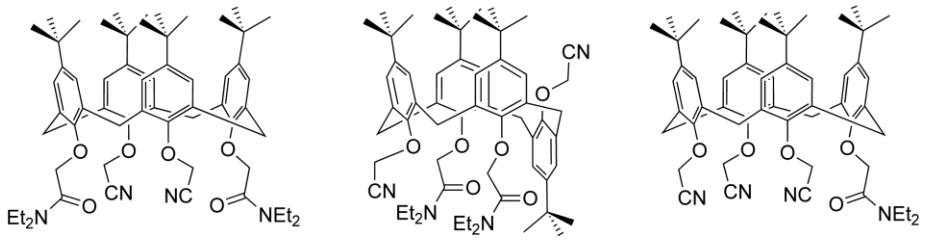

8 **9** **10**

Figure 3.12: The amide-nitrile substituted calixarenes utilised for the rotation experiments.

The simplification of the ^{1}H NMR spectrum in Figure 3.13 is a result of the higher levels of symmetry present within calixarene **8** in comparison to the partial cone conformer **9**.

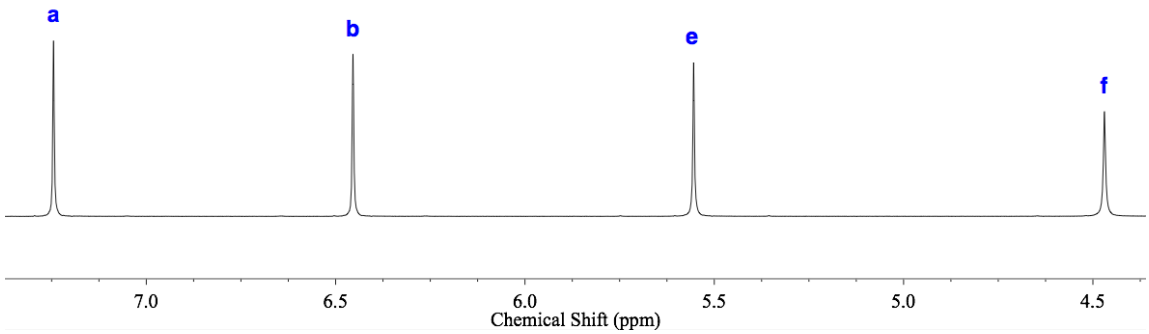

Chemical shift	Multiplicity	Corresponding hydrogen	Relative integration
7.25	Singlet	a	4
6.45	Singlet	b	4
5.55	Singlet	e	4
4.47	Singlet	f	4

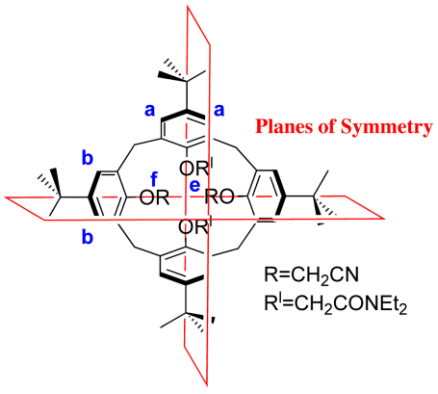

Figure 3.13: ^{1}H NMR spectrum and symmetry diagram for the di-amide di-nitrile calixarene 8.

The spectrum in Figure 3.13 contains only two singlets (a,b) in the aromatic region, as a result of there being two planes of symmetry in the molecule. The methyl ether linkers have significantly different chemical shifts as a result of the different substitution on the lower rim. The more deshielded singlet (e) at 5.55 ppm has been assigned to the CH_2 linking the phenyl ring with the amide moiety, as a result of the stronger electron withdrawing nature of the amide when compared with a nitrile group. The nitrile methylene peak at 4.47 ppm is consistent with that observed for the nitrile substituted calixarenes discussed in Section 3.3.1.

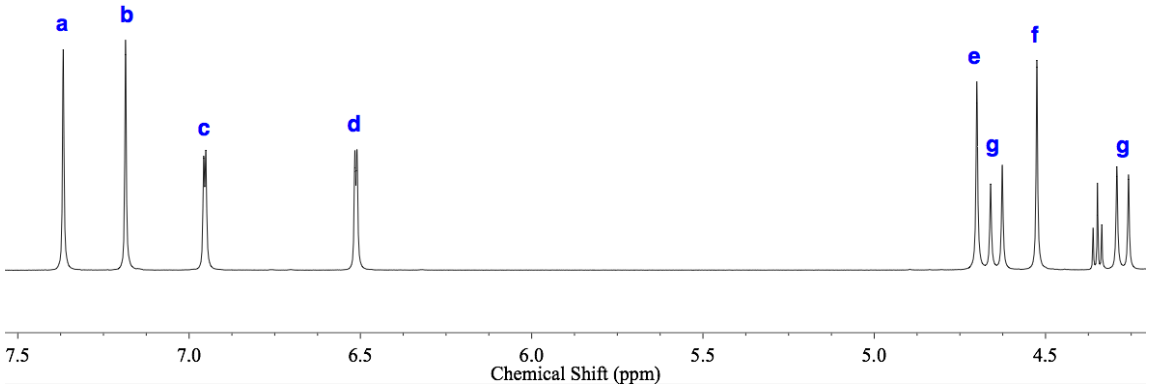

Chemical shift	Multiplicity	Corresponding hydrogen	Relative integration
7.36	Singlet	a	2
7.18	Singlet	b	2
6.95	Doublet	c	2
6.50	Doublet	d	2
4.69	Singlet	e	2
4.63	Doublet	g	2
4.52	Singlet	f	2
4.26	Doublet	g	2

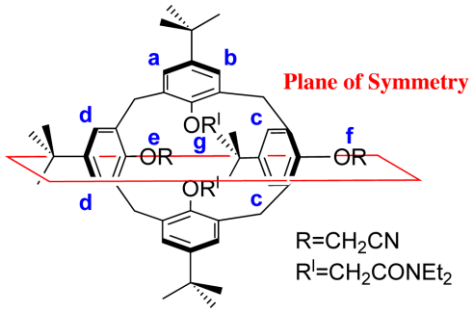

Figure 3.14: Splitting of the ^{1}H NMR spectrum upon inversion to the partial cone calixarene 9.

The partial cone conformation of the di-amide di-nitrile calixarene **9** has a significantly different ^{1}H NMR spectrum as a result of the difference in symmetry present in the molecule. There is now only a single plane of symmetry upon rotation of one nitrile substituted phenyl group (see Figure 3.14). The mirror plane which has been lost is the

one bisecting the phenyl groups substituted with the diethylamide moieties. This loss also affects the hydrogens of the methyl ethyl linker to the amide groups, which shift upfield and split into two doublets (g). The signals representing the CH_2 linkers to the nitrile moieties also split into two singlets representing the rotation of one of the phenyl groups (e,f).

Calixarene **10** has only one plane of symmetry when in the cone conformation as graphically represented in Figure 3.15. The tetra-substitution of the lower rim of **10** once again ensures that there are no peaks associated with the hydrogen of a free phenol.

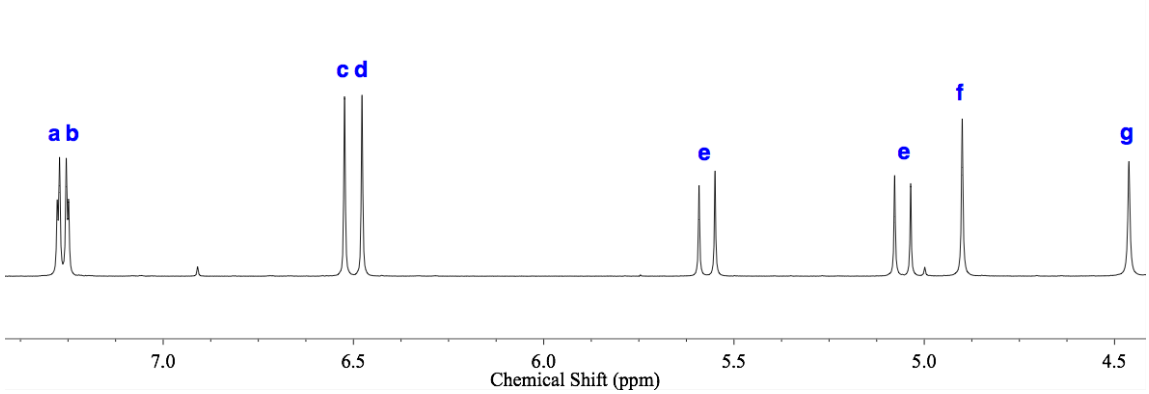

Chemical shift	Multiplicity	Corresponding hydrogen	Relative integration
7.28	Doublet	a	2
7.25	Doublet	b	2
6.52	Singlet	c	2
6.48	Singlet	d	2
5.57	Doublet	e	2
5.06	Doublet	e	2
4.90	Singlet	f	2
4.46	Singlet	g	2

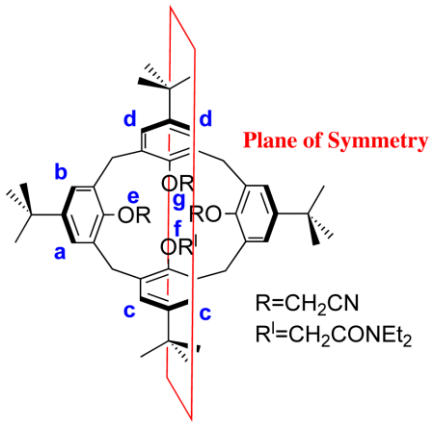

Figure 3.15: ^{1}H NMR spectrum of the mono-amide tri-nitrile calixarene 10 in the cone conformation.

As with the previous calixarenes that possess only one plane of symmetry, the peaks in the aromatic region have split into two doublets (a,b) and two singlets (c,d). The methyl ether linkers associated with the phenyl units perpendicular to the plane of symmetry (e)

are non-equivalent, resulting in the hydrogens coupling to each other and hence the doublets. The signals associated with the amides (f) are further downfield due to the electron withdrawing nature of the moiety, with the nitrile singlet (g) being the remaining peak recorded. Integration of the peaks identified as representing the hydrogens of the methyl ether linkers on the lower rim sum to eight, which is consistent with tetra-substitution of the calixarene.

3.3 Conditions required for rotation

The conditions required for rotation of the nitrile moieties were considerably different from that reported in the limited literature.[21,147] Nam reports that equilibrium was achieved at room temperature over the course of ten days, while higher temperatures could reduce this to one hour. This equilibrium was for calixarene species with either no or less sterically bulky substituents on the upper rim. Of the calixarenes studied here, no rotation was observed below 100°C for any species. As such, systematic studies were performed using deuterated dimethyl sulfoxide (d_6-DMSO) as the solvent, with the solutions heated at a constant 150°C. It was found that this temperature was appropriate in achieving equilibrium while limiting degradation. ^{1}H NMR spectra were recorded at daily intervals to track the progression of both the evolution of the new species, as well as the degradation of the calixarene. In most cases this equilibrium was established within ten days or complete degradation of the substrate had already occurred. ^{1}H NMR measurements were performed at room temperature, which effectively stopped the rotation while the spectra were obtained.

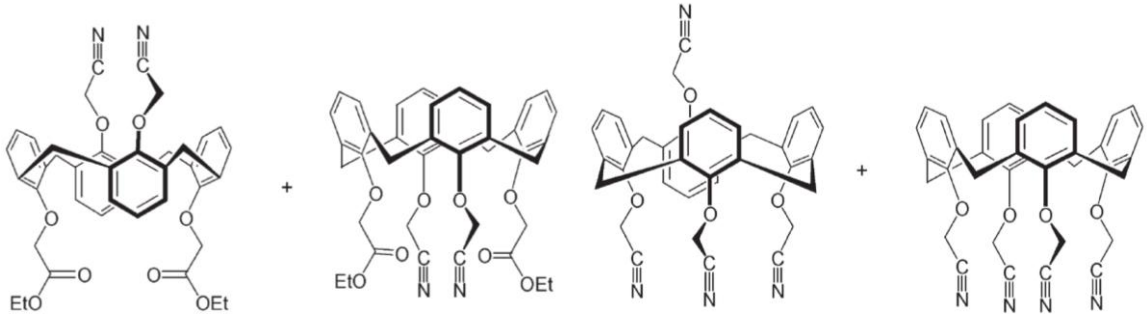

Figure 3.16: Examples of the nitrile calixarenes studied within the literature. [21]

3.4 Equilibrium of conformational distribution

Individual isolation of each pure conformer of the substituted calixarenes allowed for determination of the equilibrium percentage for the conformational isomer present in solution. Where possible, equilibrium was approached from each direction, commencing with the pure conformational isomer. Approaching equilibrium using both pure conformational isomers provides confirmation that an equilibrium point had been achieved. Isolation of each pure conformer was possible with the cone/partial cone pairs for the tetra-nitrile system **6** and **7**, and the di-amide di-nitrile **8** and **9**. Only one isomer was available for the other nitrile substituted calixarenes, **4**, **5** and **10**. Here, equilibrium was assumed to have been reached if there was no significant change over two consecutive days.

The ratio of each conformer was determined by integration of two individual, non-overlapping peaks within the aromatic region of the spectra. Degradation of the calixarene was accounted for by means of a relative ratio. Assigning the integration of the peak in the initial spectra with the value of one, any reduction in this value in subsequent spectra should be directly proportional to the increase in the new peak (conformer). Any discrepancy in the sum of these two integrations not being equal to one is considered degradation of the system as only two conformers were observed in every case.

3.4.1 Tetra-nitrile substituted calixarenes

The isolation of the two different isomers (**6** and **7**) of the tetra-nitrile substituted calixarene allowed for easy identification of the equilibrium point at which both conformers no longer interconverted. It can be seen in Figure 3.17 that upon prolonged heating of the cone tetra-nitrile calixarene **6**, there is a rapid decrease in the amount of cone conformer present in solution, with an associated increase in the concentration of the partial cone conformation.

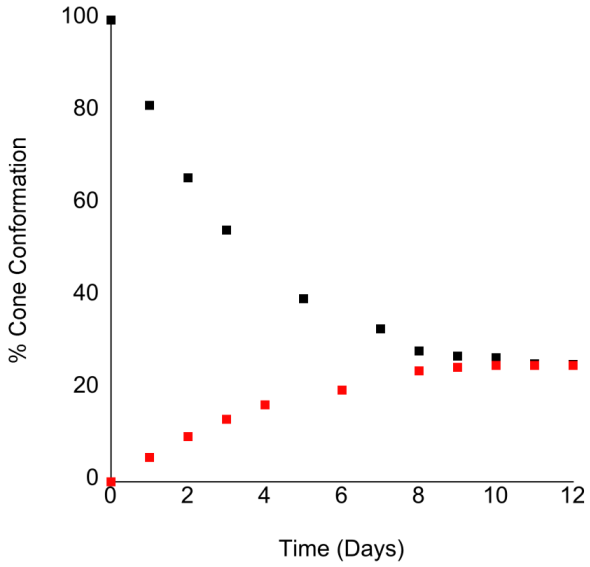

Figure 3.17: Percentage cone conformation distribution of the two pure isolated conformers over time, cone (black) and partial cone (red).

Integration of the ^{1}H NMR spectra for both species suggests that the conformational distribution reaches an equilibrium percentage of 76% partial cone and 24% cone conformation. This ratio is in direct contrast with the proportion of partial cone conformer present within the reaction mixture upon initially synthesising the tetra-nitrile substituted calixarenes.

Table 3.18: Comparison of conformational distribution between synthesis and rotation experiments.

	Cone	**Partial cone**
Rotation equilibrium	24%	76%
Synthetic isolation	94%	6%

It can be suggested that the discrepancy in conformational distribution between the rotation experiments and the synthetic isolation, shown in Table 3.18, may be a result of preorganisation of the calixarene. It is well known that sodium can interact with the lower rim of a calixarene, and might in this case cause the equilibrium to favour the cone conformation *via* a metal templating effect.[13,22,138]

3.4.2 Amide/nitrile substituted calixarenes

In a similar fashion to the tetra-nitrile calixarenes, the di-amide di-nitrile calixarenes (**8** and **9**) also underwent rotation of one nitrile-phenyl group. The conformational inversion for the di-amide di-nitrile calixarene system occurred at a faster rate when compared with the tetra-nitrile calixarene (see Figure 3.19).

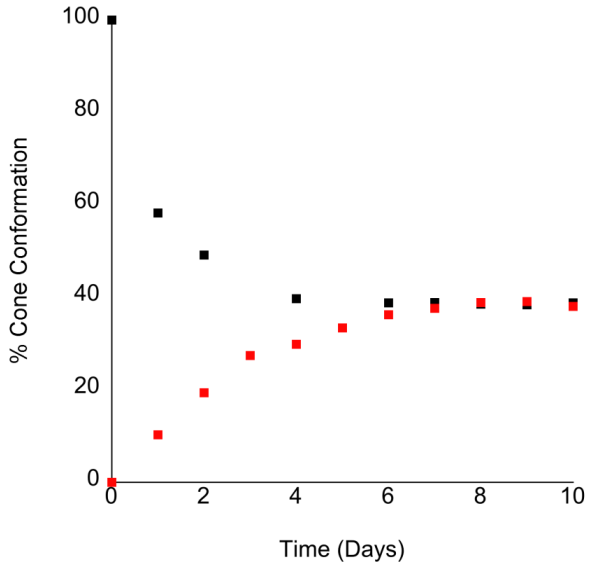

Figure 3.19: Percentage cone conformation distribution of the two pure isolated conformers 8 and 9 over time, cone (black) and partial cone (red).

As in the previous case of the nitrile substituted calixarenes, the partial cone conformation is once again favoured due to it being the more stable, less sterically crowded conformer.[13,15] In contrast to the tetra-nitrile substituted calixarenes, the equilibrium distribution of the conformations is not much different from that isolated in the synthesis reaction, Table 3.20. The only small difference is the slightly higher proportion of cone conformation present in the rotation experiments. This may seem counter intuitive considering the hypothesis that the metal mediated templating effect should produce a higher concentration of the cone conformer in the synthetic reaction. However, the steric crowding on the lower rim of the calixarene in this instance could overcome the templating effect of the sodium ion, thereby producing a higher proportion of the partial cone conformation.

Table 3.20: Comparison of conformational distribution between synthesis and rotation experiments.

	Cone	Partial cone
Rotation equilibrium	38%	62%
Synthetic isolation	25%	75%

Upon heating calixarene **10** at 150°C, the ^{1}H NMR spectrum contained a significantly higher number of peaks. This change is consistent with a complete loss of symmetry within the molecule suggesting that one of the nitrile groups adjacent to the diethylamide moiety and on the remaining plane of symmetry had rotated.

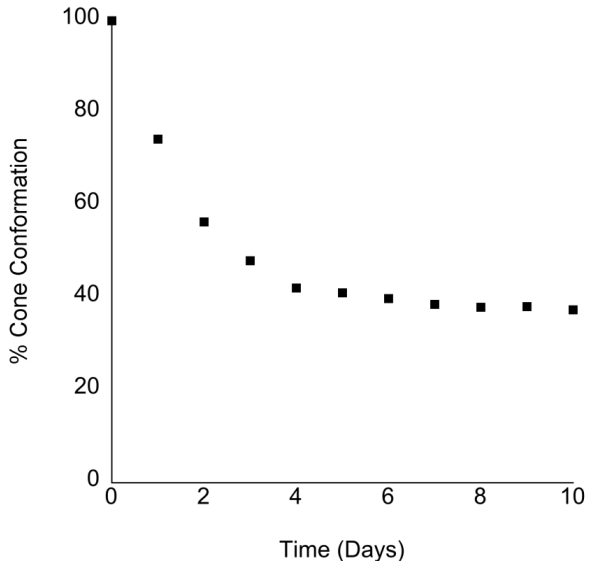

Figure 3.21: Mono-amide tri-nitrile calixarene 10 conformational distribution over time.

Over the course of eight days it can be seen in Figure 3.21 that there was a 62% conversion of the cone conformer. The extent of interconversion is identical to the di-amide di-nitrile experiment, most likely due to the presence of similar groups on the lower rim of both calixarenes. The rotation of one nitrile substituted phenyl group is once again likely to be driven by the reduced steric crowding in the partial cone conformation.[13,15]

As with the other nitrile calixarenes, constant heating at 150°C caused the di-nitrile calixarene **4** to degrade. Unfortunately this degradation proceeded at a much faster rate

than the tetra-substituted derivatives (**6** and **7**). In fact after nine days of constant heating, no starting material or substituted calixarene remained. Despite the degradation, the ^{1}H NMR spectrum of the calixarene **4** d_6-DMSO solution suggested that after three days there was up to 83% conversion of the cone di-nitrile calixarene to the partial cone conformation (see Figure 3.22). The partial cone conformer was able to be identified, as the rotation of one nitrile substituted phenyl ring will result in the loss of a plane of symmetry. This will cause splitting of the *meta* hydrogens on the unsubstituted phenols, becoming two doublets, along with a separation of the *meta* hydrogens on the substituted phenols into two new singlets. The methyl ether hydrogens also split into two singlets reflecting the different environments of the two nitrile groups in the partial cone conformer. The percentage conversion remained relatively constant until after day five where the proportion of dealkylated calixarene began to significantly increase. After nine days the degradation was complete with only *tert*-butyl calixarene remaining as a recognisable calixarene signature in the ^{1}H NMR spectrum.

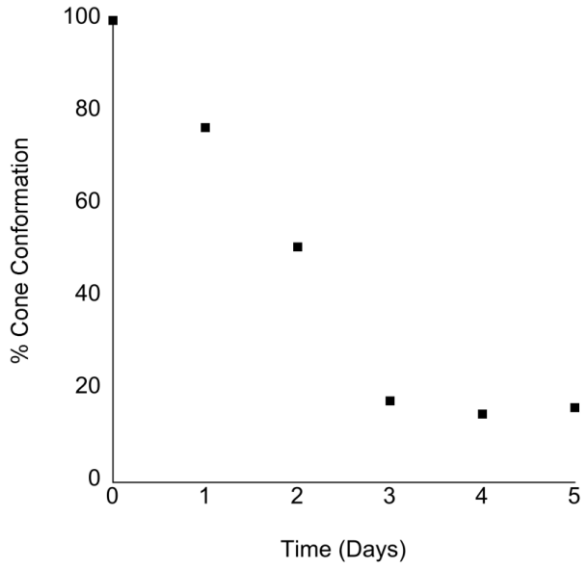

Figure 3.22: Di-nitrile calixarene 4 interconversion percentages suggesting equilibrium present at 83% conversion before complete decomposition of the calixarene.

Tri-nitrile calixarene **5** also underwent degradation upon heating at 150°C. This degradation also occurred at a rapid rate until no calixarene remained after three days. As a result no useful data was obtained for the tri-nitrile calixarene conformational inversion.

3.5 Conclusions

The newly characterised nitrile containing calixarenes; tri-nitrile **5** and tetra-nitrile calixarene **7** were both crystallised in the partial cone conformation. The mono-amide tri-nitrile calixarene **10** synthesis was confirmed by the X-ray crystal structure obtained, also confirming the cone conformation. Conformational mobility of the cyanomethoxy substituted calixarenes was found to exist at elevated temperatures (**>** 100°C). This rotation through the annulus was tracked *via* ^{1}H NMR spectroscopy, with a conversion ratio able to be calculated upon accounting for the degradation of the calixarene. Confirmation of the equilibrium conversion percentage was attained by performing the experiment on the two pure conformations. The percentage distribution of the conformations between the synthesis solutions and those from the rotation experiments was found to be dissimilar for both the tetra-nitrile and di-amide di-nitrile calixarenes. The tetra-nitrile experiment had a percentage cone conformation of 24% within the rotation experiments in comparison to synthetically isolating it in 94%. In contrast the di-amide di-nitrile calixarene solution equilibrated at a cone conformation percentage of 38% which is higher than the synthetically isolated percentage of 25%. The discrepancy between percentages was hypothesised to be a consequence of the metal templating effect where an alkali metal, sodium in this case, preferentially preorganises the calixarene in a particular conformation before addition of the nitrile functional groups.

4 Lanthanoid complexes of the tetrazole calixarenes

The lanthanoids are classified as hard acids, and are known to prefer interactions with hard donor moieties such as neutral (eg. amide carbonyl) or negatively charged (eg. carboxylate) oxygen atoms. The high affinity for oxygen atoms results in the lanthanoid ions having a strong tendency to bind water. In order to displace the water from the coordination sphere of the lanthanoid and replace it with a non-oxygen donor, a negatively charged or bidentate ligand is generally employed. As a result, there is limited literature investigating the interaction between tetrazoles and lanthanoids. Appropriate functionalisation of a calixarene allows for multidentate coordination of the lanthanoid by tetrazole moieties, and the lanthanoid coordination chemistry of such ligands is the focus of this chapter.

4.1 Tetrazole calixarene ligands

Successful isolation of the suite of tetrazole calixarenes (see Chapter 2) allowed for the characterisation of the ligands *via* numerous methods including X-ray crystallography. Each of the ligands was confirmed to be in the cone conformation with the anticipated number of tetrazole groups on the lower rim. As can be expected for a ligand with numerous hydrogen bond donors and acceptors, there is an extensive hydrogen bond network that is observed with each of the ligands and their metal complexes in the solid state.[45,138,151]

The solid state structure of di-tetrazole ligand **1** is shown in Figure 4.1. The calixarene assumes the cone conformation, with 1,3-substitution at the lower rim. Intra-molecular $O_{ooo}O$ hydrogen bonds between the neighbouring substituted and unsubstituted phenol O atoms is observed, typical of the cone conformation.[1,13,22] The tetrazole ring containing N312 (Tz3) has a hydrogen bond to the oxygen of the closest phenol with a bond distance of 3.022 Å. The N–H hydrogen of the other tetrazole (Tz1) forms a hydrogen bond to the nitrogen of an acetonitrile molecule. A dimeric structure is formed, with interleaving of the tetrazole substituents from a neighbouring molecule, disposed about an inversion centre. There is a close approach (3.002 Å) of N312 and N313 on neighbouring molecules, possibly indicating that the $N312_{ooo}O21$ hydrogen bond is bifurcated with N313, supporting the dimer.

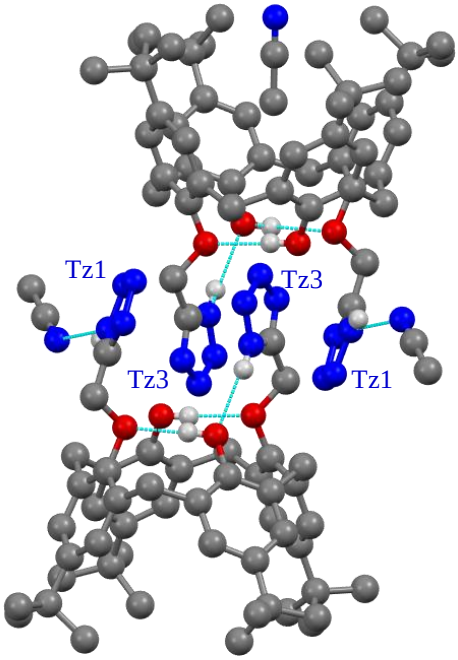

Figure 4.1: The di-tetrazole calixarene ligand 1 in the cone conformation, showing the dimeric structure observed in the crystal structure. Tetrazole moieties are numbered to clarify in-text discussion.

Considering the calixarene conformation in more detail, the two opposing unsubstituted phenolic rings have a dihedral angle between the phenyl rings and the C_4 methylene plane of 56° and 58°. The two tetrazole-substituted phenyl rings are slightly more pinched with dihedral angles to the methylene plane being 64° and 71°. This is a relatively symmetrical cone conformation, leaving room for the inclusion of solvent in the cavity,[100,138] and as can be observed in Figure 4.1, there is in fact one molecule of acetonitrile within the cavity of the calixarene.

The structure of tri-tetrazole calixarene **2** is shown in Figure 4.2. Here the calixarene assumes a much more pinched cone conformation, with the two opposing tetrazole-substituted phenyl rings having a dihedral angle between the two planes of 6°. This is also reflected in the dihedral angles between these phenyl rings and the C_4 methylene plane, with angles of 88° and 85°. The angle between the unsubstituted phenol ring and the methylene C_4 plane is 26°, possibly as a result of the strong intra-molecular hydrogen bond formed between the N-H (N312) of the central tetrazole (Tz3) and the phenolic oxygen (O11). This hydrogen bond is bifurcated with there being

a possibility of a hydrogen bond between the N-H and the oxygen of the vicinal substituted phenyl ring (2.925 and 2.835 Å respectively).

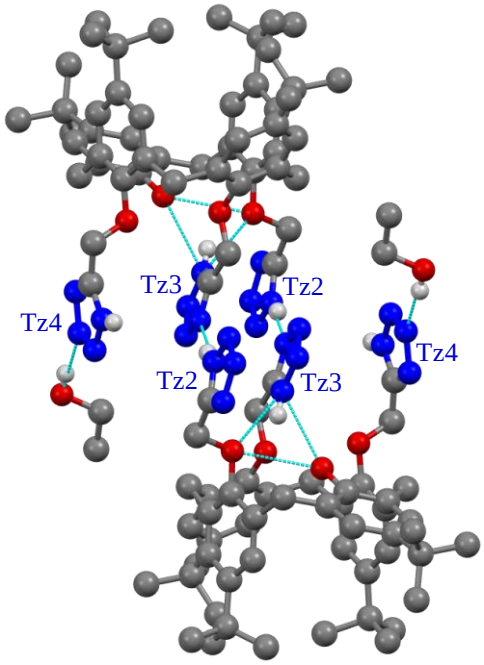

Figure 4.2: The tri-tetrazole calixarene ligand 2 in the pinched cone conformation, again showing the dimeric structure observed in the crystal structure. Tetrazole moieties are numbered to clarify in-text discussion.

Again, a dimeric structure is found in the solid state, with tetrazole substituents Tz2 and Tz3 forming a complementary pair of hydrogen bonds. The remaining tetrazole Tz4 is involved in a hydrogen bond from the N-H hydrogen to another calixarene, generating a 1D hydrogen bonded polymer. The intra-molecular hydrogen bond from Tz3 to the phenoxy oxygens (O11 and O21) helps to create a linear arrangement of the three tetrazole substituents. It must be noted that this linear arrangement could support π-stacking interactions, however recent literature discussing π-π interactions has questioned if they are appropriate to describe situations in which two or more aromatic rings are associated in some fashion, considering the strength of other interactions.[152,153] Despite this, the two planes of tetrazoles Tz2 and Tz3 are almost co-planar with an angle of 8° and a distance of 3.22 Å between them. The two Tz3 tetrazoles, from each calixarene of the dimer, are co-planar (0°) at a distance of 3.29 Å.

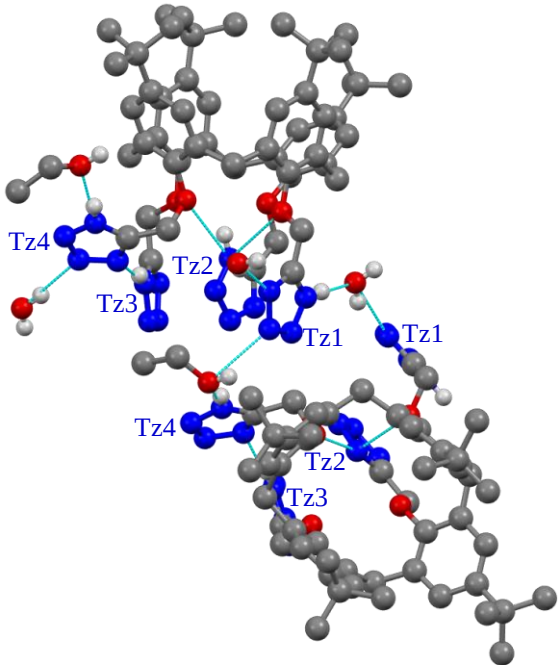

Figure 4.3: The tetra-tetrazole calixarene ligand 3 in the pinched cone conformation, showing the hydrogen bonded dimeric structure observed in the crystal structure. Tetrazole moieties are numbered to clarify in-text discussion.

The tetra-tetrazole calixarene **3** is different to the other ligand solid state structures, in that there are no direct inter-molecular hydrogen bonds between neighbouring calixarenes. However, the structure still has the bifurcated intra-molecular hydrogen bond between the N–H of Tz2 and the phenoxy oxygens O11 and O41, similar to the tri-tetrazole calixarene **2**. This hydrogen bond has a distance of 2.972 Å to O41 and 3.017 Å to O11 suggesting that, like the tri-tetrazole calixarene **2**, the intra-molecular hydrogen bond to the phenoxy oxygens is driving three of the tetrazole units to be somewhat stacked, with the fourth tetrazole not interacting in the same manner. These three stacked tetrazole rings (Tz1, Tz2, Tz3) have interplanar ring angles of 10° (Tz1-Tz2) and 27° (Tz2-Tz3) with distances of 3.397 and 3.24 Å respectively. Tetrazole rings Tz1 and Tz4 have hydrogen bonds with solvent, three water and two ethanol molecules. Calixarene **3** is also in the pinched cone conformation, with two opposing phenyl rings having a dihedral angle of only 9°, and angles with the C_4 methylene plane of 82° and 88°. The dihedral angles between the methylene plane and the two less pinched substituted phenyl rings are more acute, with angles of 56° and 50°.

4.2 Tetrazole calixarene complexes

Crystallisation of lanthanoid complexes with calixarene tetrazole ligands **2** and **3** was consistently unsuccessful. The only structural evidence of successful solid state coordination with these ligands was the isolation and characterisation of the sodium salts by X-ray crystallography. These dimeric and tetrameric sodium complexes are shown below in Figures 4.4 and 4.5.

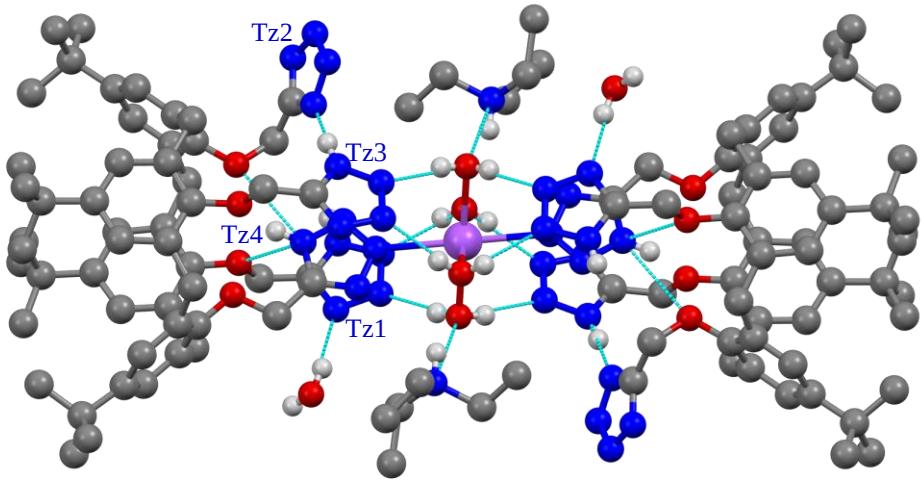

Figure 4.4: Sodium bridged tetra-tetrazole calixarene 3 dimer in the crystal structure of $[Na(1\text{-}1.5H)_2(H_2O)_6(HNEt_3)_2]$. Tetrazole moieties are numbered to clarify in-text discussion.

The tetra-tetrazole ligand **3** forms a sodium bridged dimer which is heavily hydrogen bond stabilised. The formula for the complex is $[Na(\mathbf{1}\text{-}1.5H)_2(H_2O)_6(HNEt_3)_2]$. The charge of both the triethylammonium and tetra-aqua sodium ion is balanced by the deprotonation of one tetrazole per calixarene (Tz2), plus an additional deprotonation disordered over the two coordinating tetrazole moieties (Tz4). The intra-molecular hydrogen bonds stabilising the complex are hydrogen bonds from the four water molecules to the Tz1 and Tz3 tetrazoles. The other tetrazoles are involved in inter-molecular hydrogen bonds with either water or neighbouring calixarene molecules. The triethylammonium cations sit in the second coordination sphere of the sodium cation, forming $N\text{-}H_{ooo}O$ hydrogen bonds to aqua ligands. In this structure, the tetra-tetrazole calixarene ligand **3** assumes a similar conformation to the free ligand. The tetrazole substituents Tz1, Tz3 and Tz4 are all relatively linear and co-planar with interplanar distances of 3.16 Å (Tz1-Tz4) and 3.14 Å (Tz4-Tz3) and angles of 7° and

15° respectively. As previously mentioned, a possible reason for the calixarene tetrazole groups forming the linear ring assembly could be the N-H_{ooo}O intra-molecular bifurcated hydrogen bond between nitrogen N412 and the phenoxy oxygens O21 (3.026 Å) and O11 (2.996 Å).

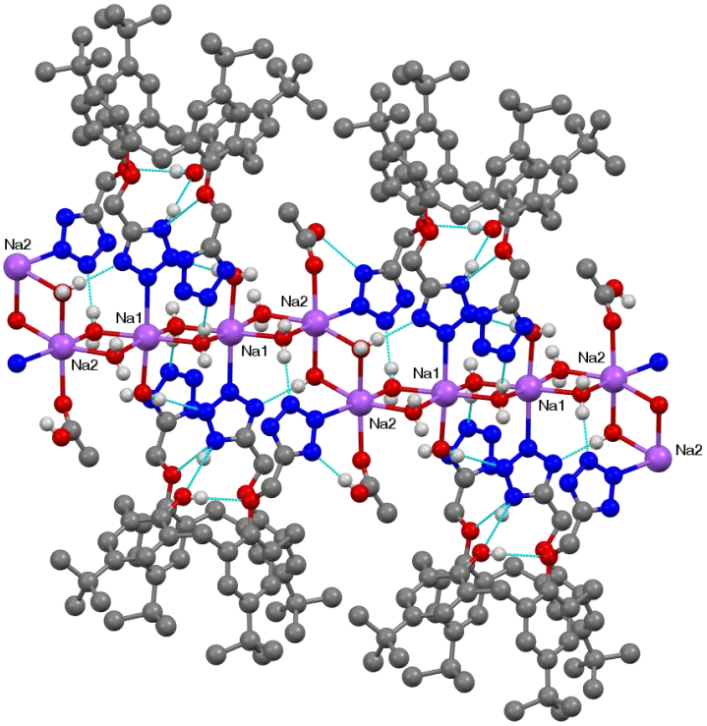

Figure 4.5: Linear tetrameric sodium polymer with calixarene ligand 2, observed in the crystal structure of [(2-2H)$Na_2(H_2O)_5(CH_3COOH)$].$(CH_3CH_2OH)(H_2O)_3$.

The sodium complex with the tri-tetrazole ligand **2** crystallised as a linear polymer, where the asymmetric unit is [(**2**-2H)$Na_2(H_2O)_5(CH_3COOH)$].$(CH_3CH_2OH)(H_2O)_3$. Two of the tetrazole units of the calixarene have been deprotonated, with the third tetrazole protonated at N(315) and N(313) bonded to one of the sodium ions (Na1). The coordination sphere of this sodium is completed by five water molecules, of which four bridge to adjacent Na^+ ions. A dimer is formed through a crystallographic inversion centre bridging the Na1 ions through a pair of O(1) water molecules. The second Na^+ ion, Na2 is also six coordinate, with the coordination sphere consisting of four water molecules, the acetic acid molecule and a N atom of one of the deprotonated tetrazole units of the substituted calixarene group related by the inversion centre. This forms a one dimensional polymer along the *b*-axis. A portion of this polymer is illustrated in

Figure 4.5. Similar water bridged sodium polymeric structures have been isolated previously, however unlike this example, there are only three sodium atoms in each linear section instead of four.[154,155] As is the case for the previous tetra-tetrazole structure in Figure 4.4, the tri-tetrazole calixarene ligand **2** in this sodium polymer is in a similar conformation to the ligand only structure. The three tetrazole rings have interplanar angles of 20° and 11° at distances of 3.1 Å and 3.31 Å respectively. The central tetrazole is fixed into a somewhat linear arrangement with the other tetrazoles by the same bifurcated intra-molecular hydrogen bond present in the ligand solid-state structure. This hydrogen bond is similar to the tri-tetrazole ligand structure with $N_{ooo}O$ bond distances of 2.982 Å and 2.826 Å for O11 and O41 respectively. As is often the case with tetrazole ligands, there are a significant number of hydrogen bonds along the length of the polymer, which presumably help to stabilise the structure. This tetrazole binding with the acetate species acting as a co-ligand is very similar to the structures seen in Section 4.4.1.

Failure to form 1:1 complexes between the tri/tetra-tetrazole calixarene ligands and lanthanoid ions has been hypothesised to be a result of the intra-molecular interactions that are present within the molecule, especially the hydrogen bond between the N-H of the tetrazole and the oxygens of the phenoxy rings. This hypothesis is supported by the characterisation of the only lanthanoid complex that could be isolated and structurally characterised with the tri- or tetra-tetrazole calixarene ligands.

In this structure, involving the tri-tetrazole ligand **2**, there is an associated praseodymium atom interacting with the central tetrazole moiety. Contrary to other similar structures, the coordinated tetrazole is still protonated, allowing for it to be involved in the intra-molecular hydrogen bond which gives the ligand its familiar linear tetrazole formation.[57,85,88,89] The persistence of a similar conformation to the ligand within the solid state suggests that the tetrazoles may require additional energy input to disrupt the inter- and intra-molecular contacts present within these ligands.

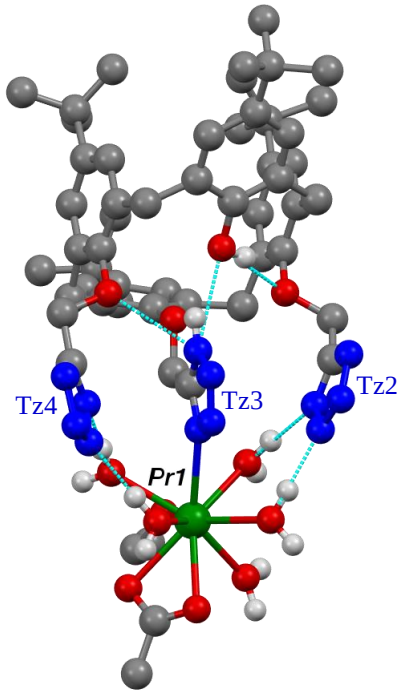

Figure 4.6: The tri-tetrazole calixarene 2 forming a complex with Pr^{3+}, with the observed formulation; $[Pr(2\text{-}2H)(CH_3CO_2)(EtOH)(H_2O)_5]$. Tetrazole moieties are numbered to clarify in-text discussion.

The formula of the complex was found to be $[Pr(\mathbf{2}\text{-}2H)(CH_3CO_2)(EtOH)(H_2O)_5]$. The Pr^{3+} atom is nine-coordinate, with a coordination sphere consisting of five water molecules, a bidentate acetate anion, an ethanol molecule and most importantly a single bond to the calixarene at the central tetrazole (Tz3) *via* the N1 position (N312). The calixarene **2** is once again in the pinched cone conformation, with the dihedral angle between the two tetrazolyl-functionalised phenyl groups being 9°. This is also reflected in the perpendicular nature of the dihedral angles between the planes of the phenyl rings and the methylene C_4 plane, being 81° and 87°. The dihedral angles between the C_4 plane and the phenyl rings of the free phenol and the central tetrazole substituted phenyl ring are 26° and 45° respectively. The smaller angle for the tetrazole substituted phenyl group allows that tetrazole to assume a position between the two external tetrazoles possibly allowing for the π stacking interactions which have been discussed previously. The molecule is stabilised through several intra- and inter-molecular hydrogen bonds. There are intra-molecular hydrogen bonds from coordinated water molecules to nitrogen atoms of the two deprotonated external tetrazole units (Tz2 and Tz4). There is also a

hydrogen bond between the phenolic hydrogen to the phenoxy oxygen atom of the adjacent phenyl group, and the typical tetrazole N-H bifurcated hydrogen bond to the phenol and phenoxy oxygen atoms (O11 and O41). The inter-molecular hydrogen bonds originate from hydrogen atoms of water molecules bound to the praseodymium to both tetrazole units and water molecules of neighbouring molecules.

4.3 Di-tetrazole calixarene 1:1 complexes

Addition of triethylamine to the crystallisation solutions of ligand **1** deprotonates the tetrazoles and increases the likelihood of couloumbic interactions with the lanthanoid.[89] Under these conditions, the formation of 1:1 lanthanoid complexes is observed.

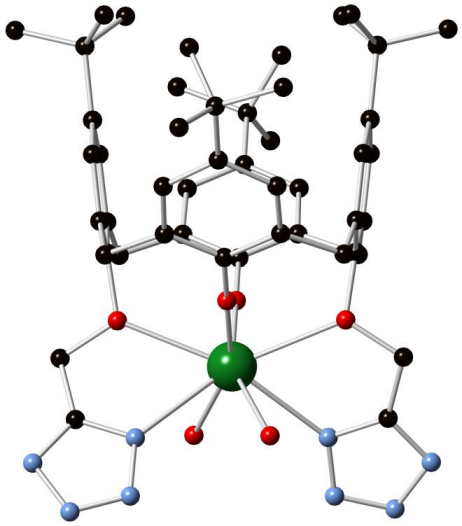

Figure 4.7: The di-tetrazole calixarene 1 forming an octacoordinated 1:1 complex with Eu^{3+} $[(1\text{-}3H)Eu(H_2O)_2]$.

Overall, the observed coordination chemistry of **1** is typical of a calixarene ionophore substituted at the lower rim. The results are consistent with the formation of a 1:1 complex, with the eight-coordinate Eu^{3+} atom bound to the four phenol O atoms, two tetrazole N1 atoms, and two water O atoms (see Figure 4.7). It is clear from the coordination geometry of the Eu^{3+} ion, and the bond Eu-O distances, that the hydroxyl groups of the phenols have been deprotonated.[99] The deprotonated phenols have Eu-O distances of 2.20 Å and 2.15 Å, while both the alkylated phenoxy oxygens have bond lengths of 2.57 Å. The neutral overall charge of the molecule also suggests that one

tetrazole moiety has been deprotonated upon addition of triethylamine. The calixarene is in the pinched cone conformation, with the two tetrazolyl-substituted phenyl rings being almost co-planar, a dihedral angle of 12°, to accommodate the lanthanoid within the lower rim of the calixarene. The two tetrazole rings are offset from each other so that they are not lying in the same plane, with both tetrazoles having hydrogen bonds to water molecules attached to the neighbouring lanthanoid.

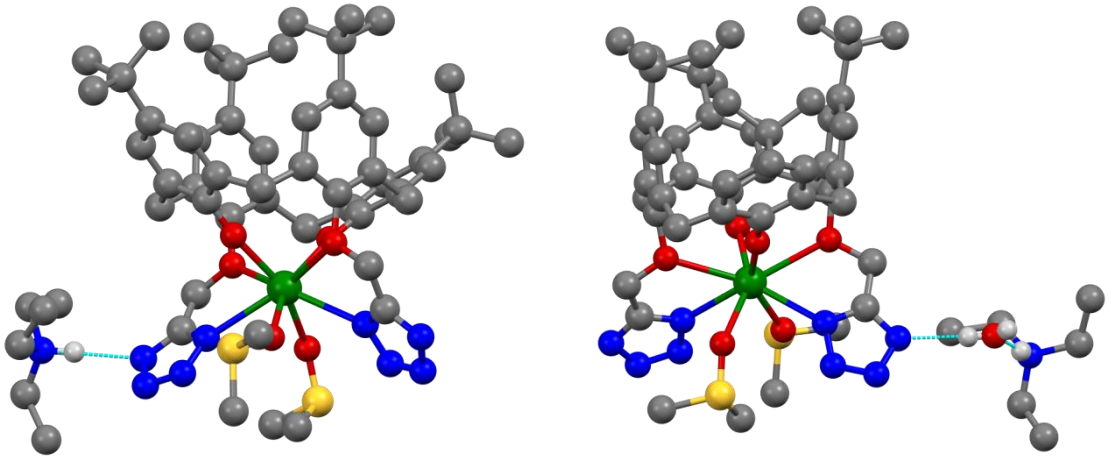

Figure 4.8: The di-tetrazole calixarene 1 forming an octacoordinated 1:1 complex with Nd^{3+}, showing both crystallographically independent molecules $[(HNEt_3)(1\text{-}4H)Nd(DMSO)_2]$ and $[(H_2O)(HNEt_3)(1\text{-}4H)Nd(DMSO)_2]$.

In a similar fashion to the previous 1:1 complex in Figure 4.7, the Nd^{3+} complex with calixarene **1** is also in the pinched cone conformation, with 10° between the two planes of the substituted tetrazole rings. Within the crystal, there are two independent molecules per asymmetric unit. The difference between the molecules are their second sphere interactions. One of the calixarenes has an inter-molecular hydrogen bond between the N1 position of the tetrazole and the N-H of a triethylammonium species. The other calixarene has the same hydrogen bond to the N1 position, however it is to the O-H of a water molecule which then bridges *via* a hydrogen bond to a triethylammonium cation. In both cases, the triethylammonium cation balances the charge of the fully deprotonated calixarene. Both Nd^{3+} atoms are eight coordinate, with the coordination sphere being best described as square antiprismatic. Unlike the previous example, the coordination sphere of the lanthanoid is not completed by water molecules as is often the case. This is most likely a result of growing the crystals in a DMSO

solution which would have shifted the equilibrium to exclude water. Once again as can be seen in Figure 4.8, there is torsion between the two tetrazole rings, as they are no longer lying in the same plane. This may be necessary to accommodate the slightly larger lanthanoid by increasing the bond length between the N1 position of the tetrazole and the Nd^{3+} atom. With bond lengths of 2.67 Å and 2.64 Å these are slightly longer than the europium structure which had bond lengths of 2.60 Å. The phenols are once again deprotonated with Nd-O bond distances of 2.22 Å and 2.19 Å, in comparison to the substituted phenyl rings which have distances of 2.66 Å in both instances.

In contrast to the two previous examples of 1:1 lanthanoid complexes formed with the di-tetrazole calixarene ligand **1** and triethylamine, when base is omitted from the crystallisation solutions, a structure with the lanthanoid outside the cavity was characterised. This structure is very similar to the praseodymium complex with the tri-tetrazole ligand **2** (see Figure 4.6).

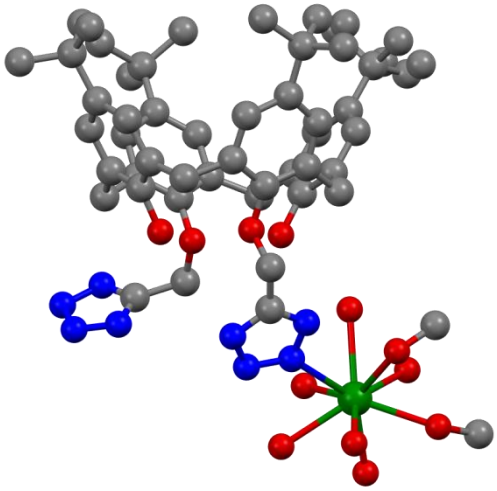

Figure 4.9: The di-tetrazole calixarene 1 forming a nonacoordinated 1:1 complex with La^{3+}, showing only the species [1($La(H_2O)_6(HOCH_3)_2$)] from the unit cell.

The structure was modelled as consisting of four unique species within the unit cell. These species are; [$La(H_2O)_9$], [**1**($La(H_2O)_6(HOCH_3)_2$)], [**1**($La(H_2O)_7$)] and [$\mathbf{1}_2$]. The species in Figure 4.9, [**1**($La(H_2O)_6(HOCH_3)_2$)], is the most relevant here, as it shows coordination through one of the deprotonated tetrazoles to the La^{3+} ion. It is unknown

exactly why the metal is not forming a 1:1 complex within the cavity of the calixarene, however, two possibilities could be suggested. Firstly, the lack of base deprotonating the calixarene reduces the electrostatic interactions the lanthanoid would have with the ligand. Secondly, the larger ionic radius of lanthanum means it is possible that the tetrazolyl calixarene cannot distort to an extent where the metal is able to be incorporated within the cavity. The lanthanum atom is nine-coordinate with six water molecules, two methanol molecules, while the tetrazole completes the coordination sphere with binding from the N2 position. The other components of the structure are linked by an extensive array of hydrogen bonds.

4.4 Bottlebrush clusters

Addition of triethylamine to the crystallisation solutions containing a lanthanoid cation and ligand **1** was shown to crystallise the 1:1 complexes as demonstrated previously in Section 4.3. However, upon addition of an aqueous neutral buffer, ammonium acetate, the formation of new lanthanoid complexes was induced. These did not resemble the previously isolated 1:1 complexes, in fact the structures were rod-like lanthanoid hydroxo clusters. These clusters comprise of a nineteen lanthanoid atom core surrounded by the calixarene ligand **1**. The formula for these large structures is; $[Ln_{19}(\mathbf{1}\text{-}3H)(\mathbf{1}\text{-}2H)_{11}(CH_3CO_2)_6(OH)_{26}(H_2O)_{30}]$. This lanthanoid clusters resemble the bottlebrush or ‘Callistemon citrinus’ flower native to Australia and as such has been named the ‘bottlebrush’ cluster. Henceforth, any mention of the bottlebrush is in reference to this elongated linear lanthanoid hydroxo cluster motif.

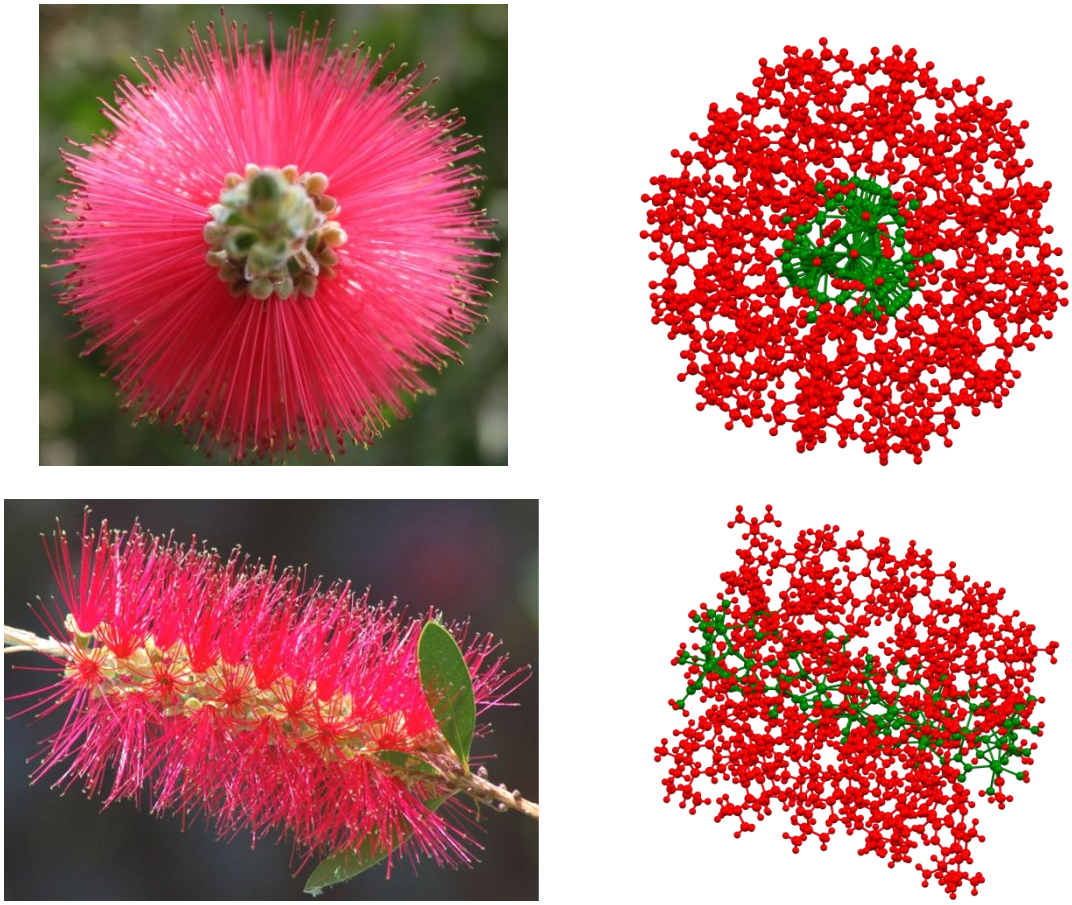

Figure 4.10: Elongated lanthanoid hydroxo cluster resembling the Bottlebrush flower native to Australia.

There are three major components required for the formation of the bottlebrush cluster; ligands, metal salt and solvent. There are two ligands, the di-tetrazole calixarene **1** along with an aqueous solution of a co-ligand, in this case one from the carboxylate family. The metal source can be any of a variety of lanthanoid salts, although usually the nitrate DMSO salt. The last key parameter is the choice of solvent, either ethanol or a 1:1 mixture of ethanol and ethyl acetate. Each parameter of the crystallisation solutions was tested and substituted as part of an in-depth investigation into the range of conditions which resulted in the formation and crystallisation of the bottlebrush cluster (see Section 4.4.2).

In an attempt to determine the reproducibility of the cluster species, multiple crystallisations were performed under identical conditions utilising different batches of reagents, including; di-tetrazole ligand **1**, metal salt, co-ligand and also solvent. Based

on unit cell determinations, isomorphous nineteen lanthanoid clusters (Ln_{19}) are formed upon addition of the heavier lanthanoids, from Sm to Lu (Figure 4.11, see Appendix A for full list of data). The trend in the formation of the bottlebrush cluster across the series is consistent with the reduction in ionic radii of the lanthanoids. It could be suggested that the 'lanthanide contraction' of the 4*f* orbitals, reducing the size of the ions is affecting the speciation and hence the crystallisation of the cluster.[95,98]

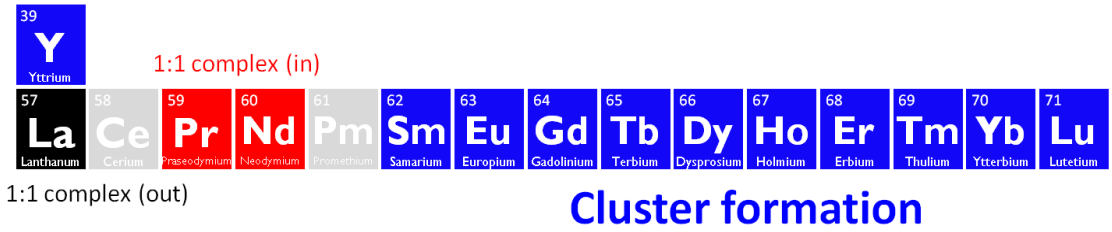

Figure 4.11: Isolated crystalline species for ligand 1 upon addition of ammonium acetate to solution.

The crystal morphology was found to be a good indicator of the product formed, which was confirmed upon unit cell determinations. While yields varied, presumably as a result of subtle changes in the ambient laboratory conditions, the cluster synthesis was found to be consistently reproducible.

4.4.1 Structural description

Slight changes in the crystallisation conditions resulted in the isolation of three different crystal morphologies (see Figure 4.12). These different morphologies corresponded to different unit cells as determined by X-ray diffraction. There were two structures possessing a monoclinic (Ln_{19}-A, Ln_{19}-B) space group with the other (Ln_{19}-C) in a trigonal space group. Each species had one parameter slightly altered causing the different crystal morphology and different unit cells. The Ln_{19}-A species grew from an ethanol only solution, in contrast to the 1:1 mixture of ethanol/ethyl acetate used for both Ln_{19}-B/C. The difference between Ln_{19}-B/C is the equivalents of aqueous ammonium acetate added to the crystallisation solutions. Ln_{19}-B has 5 equivalents of ammonium acetate, while Ln_{19}-C has 10 equivalents. While there were some subtle variations in the co-ligand distribution in these clusters, leading to variations in the crystal packing, the key features were common to all structures.

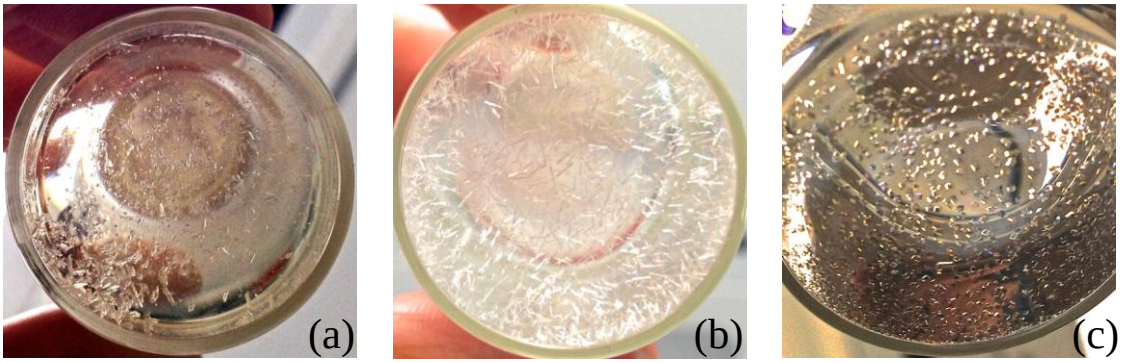

Figure 4.12: The crystal morphologies of the clusters *in situ*: (a) Ln_{19}-A, (b) Ln_{19}-B and (c) Ln_{19}-C.

The cluster cores of Ln_{19}-A/B/C contain nineteen lanthanoids and are identical in all cases. The lanthanoid atoms form a sequence of apex-sharing trigonal bipyramids with 2-fold rotational symmetry perpendicular to the long axis of the core, and *quasi* 3-fold symmetry along the long axis.

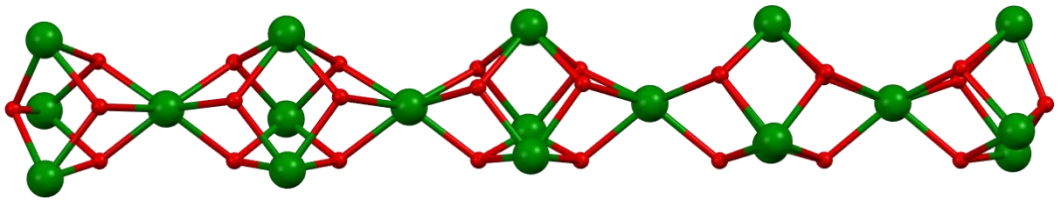

Figure 4.13: The lanthanoid hydroxo core of the Ln_{19} species showing the apex sharing trigonal bipyramids.

The cluster is terminated at each end with a μ_3-O atom replacing the apical metal atom, and *syn-syn* acetate anions bridging the terminal metal atom triangles. The metal equatorial triangles are close to parallel (deviation of less than one degree) but are rotated; relative to the central metal triangle, the penultimate triangles deviate by ~12°, and the terminal triangles by ~20°. Each triangular face of the trigonal bipyramids is capped with a μ_3-O atom. This cluster is only the second example of trigonal bipyramidal geometry in a lanthanoid cluster, the first being a single bipyramid supported by carboxylate ligands.[156] The remainder of the lanthanoid coordination spheres comprise of terminal hydroxo O atoms. The equatorial Ln atoms are eight-coordinate (N_2O_6, or for the terminal Ln atoms, NO_7) with a geometry best described as a distorted square antiprism, and the apical Ln atoms are nine coordinate (N_3O_6, distorted tricapped trigonal prism).

The individual clusters characterised for both Ln_{19}-B and Ln_{19}-C are identical. The clusters are formulated as $[Ln_{19}(\mathbf{1}\text{-}3H)(\mathbf{1}\text{-}2H)_{11}(CH_3CO_2)_6(OH)_{26}(H_2O)_{30}]$. It seems likely that the calixarene ligand **1** is key to the stabilisation of these cluster species. The cluster contains twelve calixarene molecules along the long sides of the cluster, giving the "bottlebrush" appearance.

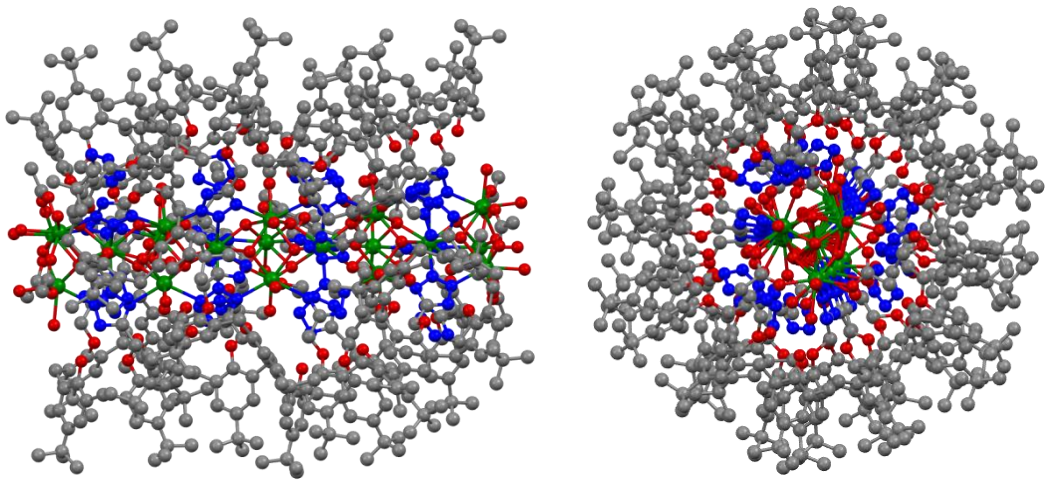

Figure 4.14: The crystal structure of Ln_{19}-B/C, side and end view. Hydrogens and second sphere solvent molecules have been omitted for clarity.

In terms of the ligand-metal interactions, the calixarene ligand can be placed into two groups: "central" molecules and those associated with the terminus. In both cases, the calixarene is coordinated to the primary coordination sphere through only one of the two tetrazolyl moieties. The tetrazole in the primary coordination sphere acts as a $\mu_{1,2,3}$-tetrazolate bridging ligand, connecting three different lanthanoids. While tetrazole ligands are well known as bridging ligands in coordination polymers,[58,79,80] their presence as bridging ligands in discrete clusters is rare and virtually unknown in a lanthanoid-based system.[81,157] The calixarenes also interact with the second coordination sphere of the metal centres, through hydrogen bonds between the tetrazole N atoms and phenol O atoms of the ligand, and hydroxo O atoms of the core. While the details vary between "central" and "terminal" calixarenes, the interactions are extensive in both cases and presumably must strengthen the stabilising effect of the ligand on the metal-hydroxo core (See Figure 4.15).

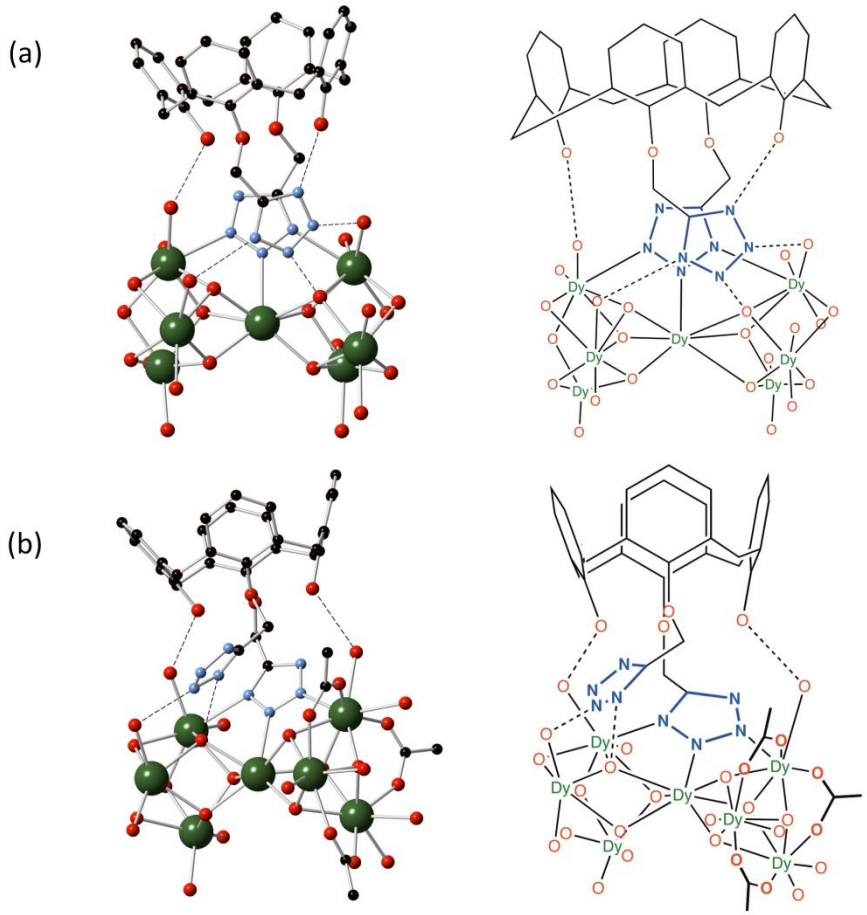

Figure 4.15: The interactions observed for the two classes of calixarene ligand (a) central and (b) terminal.

Although the molecular makeup of the two isolated clusters Ln_{19}-B and Ln_{19}-C are identical, the packing of the crystals and hence unit cell are considerably different. The Ln_{19}-C cluster crystallised in a rhombohedral form, with the cluster lying along a 3-fold rotation axis with quasi 2-fold symmetry perpendicular to the cluster axis. As such, it has a much more densely packed unit cell with closely packed end-to-end bottlebrush molecules in comparison to the Ln_{19}-B crystals (Figure 4.16).

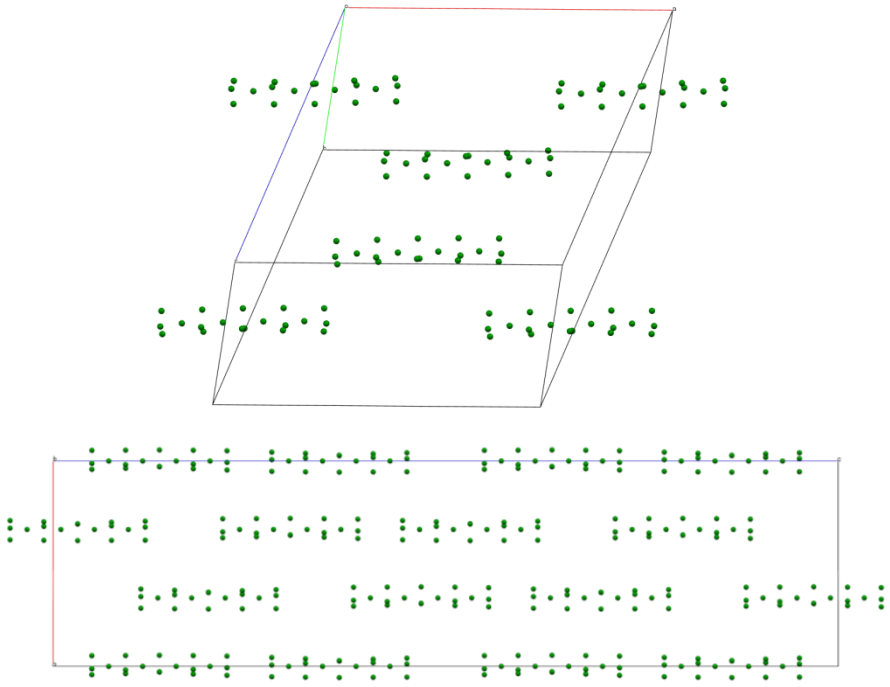

Figure 4.16: The unit cell packing of the cluster cores for Ln_{19}-B (top) and Ln_{19}-C (bottom).

The difference in the minimum distances, end-to-end, between the cores is significant, 18 Å and 9 Å for Ln_{19}-B and Ln_{19}-C respectively, while side-to-side the distances are more comparable at 26 Å and 24 Å. A possible explanation for the comparable side to side values is that this distance is actually a minimum measurement before the *tert*-butyl groups from adjacent molecules begin to overlap and interact. This is confirmed upon inspection of the packing in the example of the high ammonium acetate crystal structure (Figure 4.17). It is unknown why the addition of further equivalents of ammonium acetate leads to the increase in packing density.

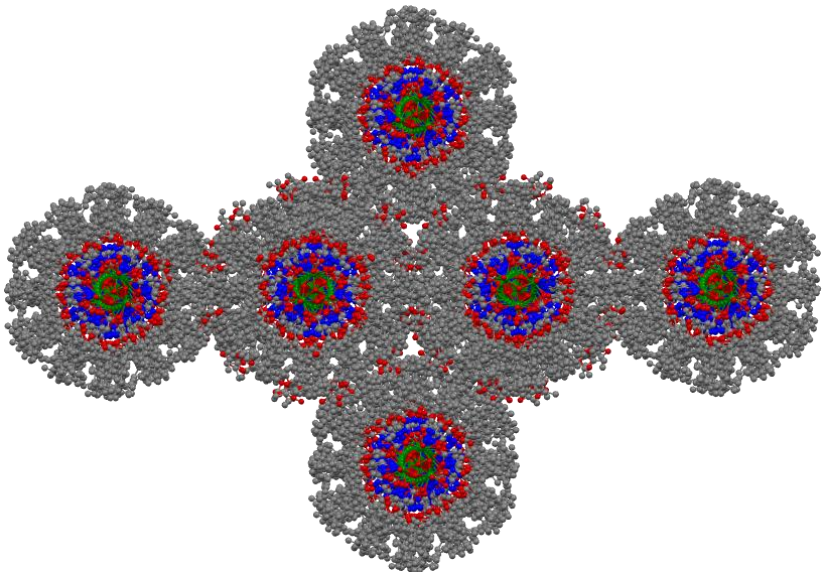

Figure 4.17: Dense packing of the Ln_{19}-C, high ammonium acetate crystal.

The crystallisation conditions were slightly different for Ln_{19}-A in comparison to Ln_{19}-B/C, as the solvent was straight ethanol instead of a 1:1 mixture of ethanol/ethyl acetate. Despite this change, a neutral cluster similar to the previous examples was still characterised. It has a different formula from that of Ln_{19}-B/C in that there is one less acetate and an additional calixarene ligand **1** associated with the cluster. As such, the formula for Ln_{19}-A was found to be $[Ln_{19}(\mathbf{1}\text{-}2H)_{12}(CH_3CO_2)_5(OH)_{26}(H_2O)_{30}]$:(**1**-2H). In a similar fashion to the other Ln_{19} clusters, Ln_{19}-A has a 3-fold symmetry along the axis, with a 2-fold rotational symmetry perpendicular to the core. The loss of a terminal acetate group, being replaced by two water molecules, resulted in a charge imbalance present in the system. However, the missing negative charge is tentatively placed on an additional calixarene **1** molecule residing in the second coordination sphere of the cluster. This calixarene molecule links two cluster molecules end-to-end through two hydrogen bonds between hydrogens of terminal O-H unidentate water molecules to the nitrogens of one tetrazole (N1 and N3), see Figure 4.18. The other tetrazole of this second sphere ligand is not participating in the bridging of the clusters, it is simply hydrogen bonding to only one of the clusters, once again between the O-H of water molecules and the N1 and N2 nitrogens of the tetrazole.

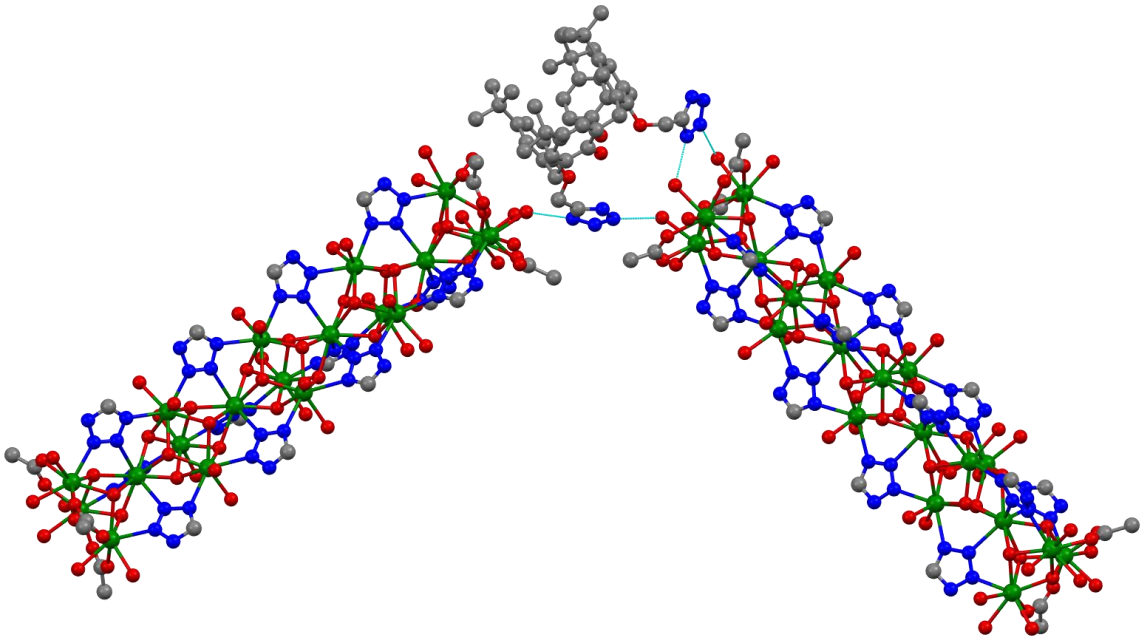

Figure 4.18: Ligand 1 creating a hydrogen bonded dimer of the Ln_{19} cluster.

A simple alteration of the system was made by substituting ammonium acetate with ammonium benzoate under the same reaction conditions. Regular crystals formed upon slow evaporation of the 1:1 ethanol/ethyl acetate solution (see Appendix B). The structure determination of this Ln_{12} species gave results consistent with a cluster formulated as $[Ln_{12}(\mathbf{1}\text{-}3H)_3(\mathbf{1}\text{-}2H)_3(PhCO_2)_6(OH)_{16}(H_2O)_{21}]$. Remarkably, the core of the cluster is constructed from the same trigonal bipyramidal motif as the Ln_{19}-A/B/C, but is shorter in length.

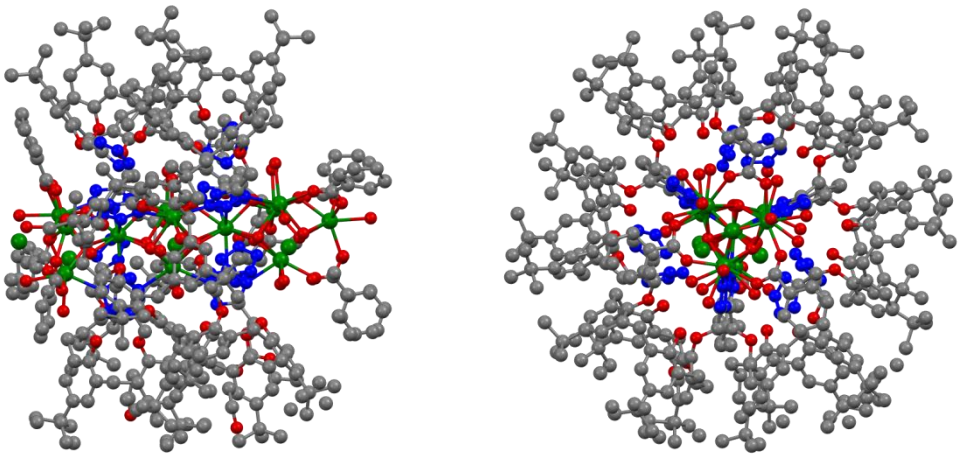

Figure 4.19: The shorter Ln_{12} cluster possessing the same trigonal bipyramidal cluster motif, side/end view.

In comparison to the Ln_{19} clusters, Figure 4.19 shows that there are only six calixarene molecules along the length of the cluster, with six associated benzoates capping the end of the lanthanoid hydroxo core. The core consists of twelve lanthanoids arranged in the same trigonal bipyramidal motif. One end of the metal core is terminated with an apical Ln atom, with the associated trigonal bipyramidal edges bound to disordered benzoate anions and water molecules, rather than tetrazole moieties. The other end of the cluster is essentially the same as found in the acetate systems. The Ln_{12} species crystallised in the rhombohedral form with a trigonal space group similar to Ln_{19}-C. The packing of the crystal involves six individual clusters spaced side-to-side, with the distance between cores at approximately 21 Å (see Figure 4.20). This is comparable with the side-to-side measurement for each of the Ln_{19} clusters giving additional evidence to the hypothesis that this is the minimum distance allowed between this cluster framework.

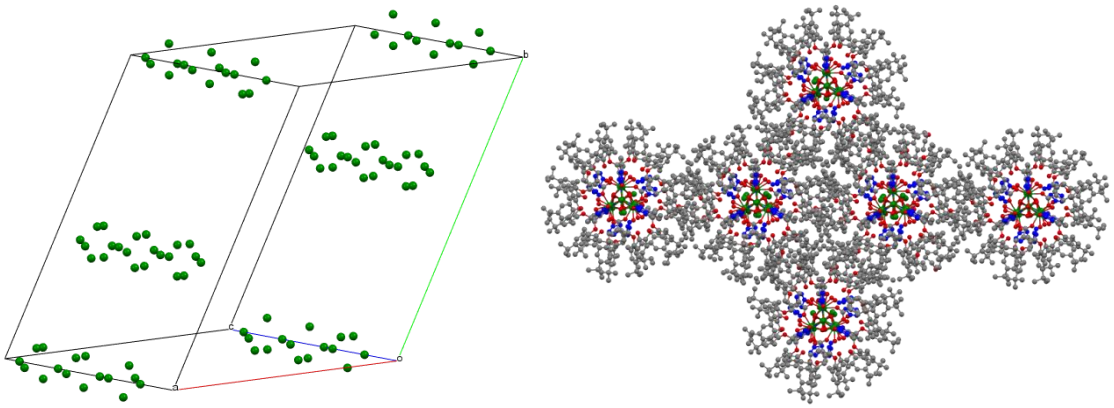

Figure 4.20: Cluster unit cell packing of the Ln_{12} species.

4.4.2 Alteration of parameters

An attractive feature of the Ln_{19} clusters, is the distinction between the calixarenes bound to the side faces of the rod-like cluster, and the acetate capping ligands. This distinction suggested a potential to change the length of the cluster by altering the ratio of the two ligands. As such, an explorative investigation of the crystallisation conditions was undertaken to not only try and change the length of the cluster, but also determine the key parameters which influenced the formation of the species.

In an attempt to alter the length of the cluster, variation in the number of equivalents of ammonium acetate was undertaken. Unfortunately reducing the number of equivalents only changed the crystal growth by causing a significant reduction in the yield of the bottlebrush crystals. This is a logical outcome as the formation of the cluster requires the presence of ammonium acetate in solution, and once that reagent is consumed no more cluster will crystallise. In contrast to the reduction in equivalents, an increase in ammonium acetate did have an effect on the crystals morphology forming in solution. A doubling of the concentration of the co-ligand produced cubic crystals, which was initially hoped to represent a change in length of the cluster (see Figure 4.12 (c)). Upon performing diffraction experiments, it was discovered that the clusters were still the same Ln_{19} motif (Ln_{19}-C), however the crystal packing of the molecule had been altered (see Figure 4.16). Increasing the concentration of the ammonium acetate co-ligand even further to 10 M saw a further change in the crystal morphology grown from solution. Subsequent analysis of this crystal showed that there was no bottlebrush cluster present, instead a $[Ln_2(OAc)_8]$ species had crystallised from solution as seen in Figure 4.21.

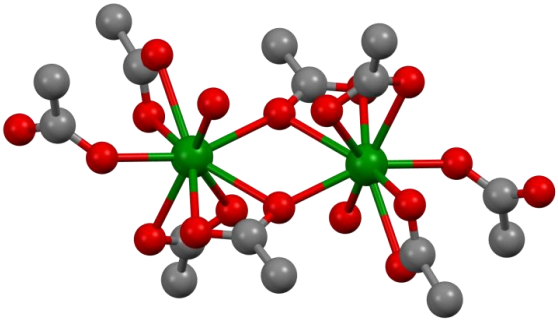

Figure 4.21: $Ln_2(OAc)_8$ species crystallised upon addition of 10 M ammonium acetate.

A possible explanation for the inability to change the length of the cluster by altering the concentration of the co-ligand was revealed upon addition of the ammonium benzoate buffer. The benzoate anions were situated at each end of the cluster, in a similar fashion to the acetate molecules. However, on the end terminated by an apical Ln atom, the associated benzoates could also be described as taking a position on the long side of the rod-like cluster (see Figure 4.22). Hence, the selectivity of the ligands between the capping positions (end) and sides of the cluster may not be as high as the initial acetate

structures suggested. This may explain why altering the carboxylate:calixarene ratio does not affect the cluster length isolated.

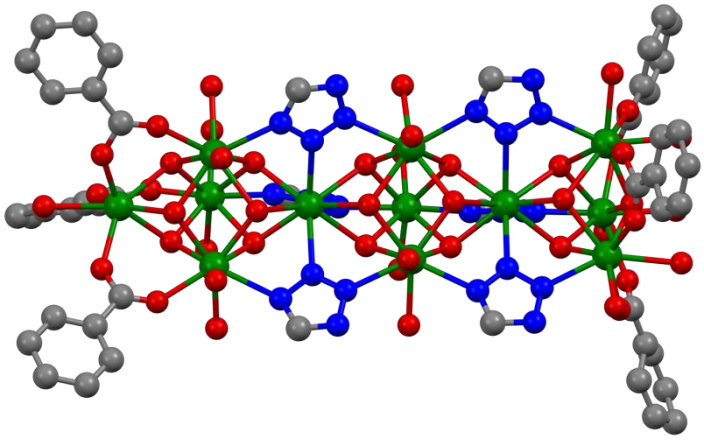

Figure 4.22: Ambiguity of the benzoate 'capping' ligands interacting with the sides of the cluster.

Figure 4.22 clearly shows that the benzoate anions are not acting as purely capping ligands which terminate the growth of the cluster, but also have some interaction with the side of the cluster. The benzoates coordinated to the apical lanthanoid are also coordinated to the next row of lanthanoids, bridging along an edge of the trigonal bipyramid rather than bridging along the base as is the case for the other end.

In another attempt to alter the cluster species crystallising from solution, different solvents and metal salts were substituted into the crystallisation conditions. The metal salts used were the lanthanoid chloride, picrate and nitrate DMSO. In each case the bottlebrush cluster persisted with no change from those described previously. Methanol, ethyl acetate and acetonitrile were all used as solvents for the crystallisation experiments. In the case of methanol and acetonitrile the ligand, di-tetrazole calixarene **1** crystallised from solution, with the ethyl acetate solution failing to form any crystals.

The co-addition of triethylamine or sodium hydroxide along with ammonium acetate to the crystallisation solution interestingly resulted in no alteration of length or crystal packing of the bottlebrush cluster. The only indication that the bases were having any

influence on the speciation of the cluster was an approximate halving of the average yield. This reduction in the yield of the cluster may be due to a shift in the equilibrium towards the 1:1 complex upon addition of base. Unfortunately, the solid state results do not provide any direct indication of the species present in solution, and thus an investigation of the solution phase was initiated, see Section 4.5.

From the range of different parameters tested, it was determined that there are two key parameters which result in the successful formation of the cluster. The first factor is the use of the correct ligands, calixarene ligand **1** and a carboxylate co-ligand, in this case acetate or benzoate. Secondly the solvent used for the crystallisation, as any variation from the ethanol or ethanol/ethyl acetate mixture prevented the formation of crystals characterised as the bottlebrush cluster. The lack of crystallisation of the bottlebrush does not necessarily indicate that there is no formation within solution, however the solid state evidence is that in all instances, the di-tetrazole calixarene **1** crystallised without any interactions with a lanthanoid. The failure to form bottlebrush crystals, if it is forming in solution, may be due to the change in polarity of the solvents. This difference may result in the crystallisation of the ligand prior to the cluster causing the equilibrium to shift to favour the crystallising species.

4.5 Solution state studies

The potential for solutions containing both ligands and lanthanoids to result in a complex mixture of species is well established.[76,85,95] The results described above suggested that the bottlebrush clusters could form under a range of conditions, provided it was in the appropriate solvent. This could be either due to the low solubility of the bottlebrush clusters relative to the other components of the equilibrium, or might indicate that the bottlebrush cluster was the dominant species in solution. The reaction mixtures were studied in an effort to determine which of these scenarios was occurring.

4.5.1 Dynamic Light Scattering (DLS)

Dynamic Light Scattering (DLS), also known as Photon Correlation Spectroscopy is not a direct measurement of particle size, rather the monitoring of Brownian motion. The technique correlates the movement of particles over time to the size of the particles. The relationship between the size of a particle and its movement due to Brownian motion is defined in the Stokes-Einstein equation.

$$D = \frac{kT}{6\pi\eta R}$$

Figure 4.23: Stokes-Einstein equation.

Essentially, the smaller the particle is, the further the particle will move over a given time. The Zetasizer machine applies this principle to mathematically solve the size of the particles in solution.

Although it is probable that various cluster morphologies and sizes are produced within solution, the least soluble component of these will crystallise. A reversible equilibrium present within the crystallisation solutions will increase the yield of that component until all reagents are consumed. The DLS measurements were performed to try and quantify the particle size of the species in solution, as well as testing their reversibility in response to a change of conditions. According to the manufacturer, the Zetasizer Nano ZS can perform accurate measurements as low as 0.3 nm at a minimum concentration of 0.1 g/L. An approximation the software has to make in order to calculate the volume of the particles, is the assumption that the particles are all spherical in nature.[158] Figure 4.24 shows that the bottlebrush particles are not entirely spherical, instead they are elongated in one dimension making them oblong in shape. This approximation, along with the knowledge that the machine is nearing the limits of its capabilities results in the values calculated being approximate. Despite this, a trend of size increase should still be observable, with any values obtained from the output treated qualitatively rather than quantitatively.

Based on the crystal structures in Figure 4.24, an estimation of the clusters' dimensions can be determined. This estimation includes the lanthanoid hydroxo core and also the surrounding calixarene ligands, but does not take into account any solvation spheres. Consequently, the data obtained can only be used to observe trends in size difference rather than an exact size.

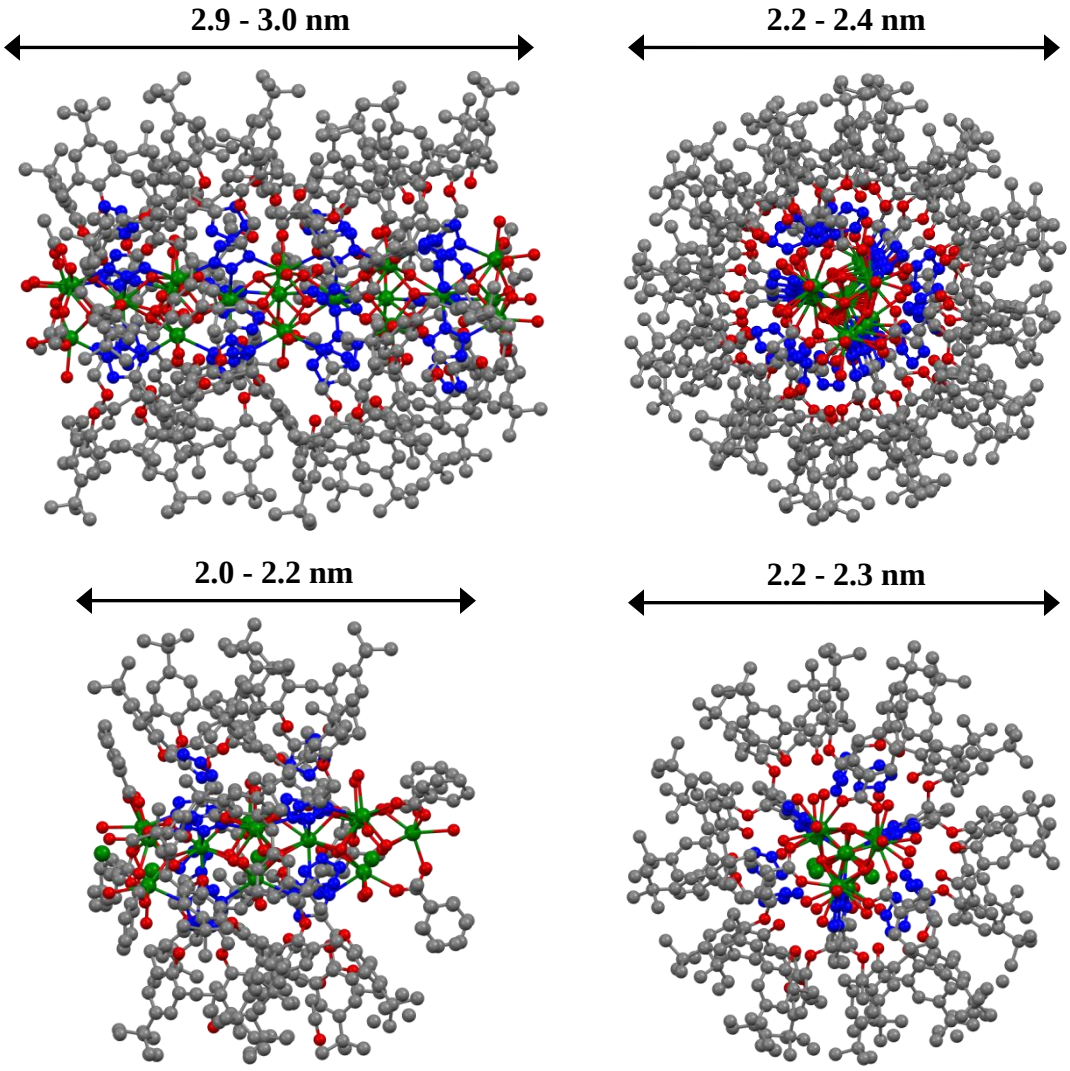

Figure 4.24: Dimensions of the Ln_{19} (top) and Ln_{12} (bottom) clusters.

For the DLS measurements, aqueous ammonium acetate was titrated into metal-ligand solutions at two different concentrations. The first concentration tested was the same as employed for the crystallisation experiments, 0.0018 M, the results of which can be seen below in Figure 4.25(a). The second concentration was considerably more concentrated,

0.1 M, designed to try and increase the signal to noise ratio, and hence the accuracy of the measurements performed.

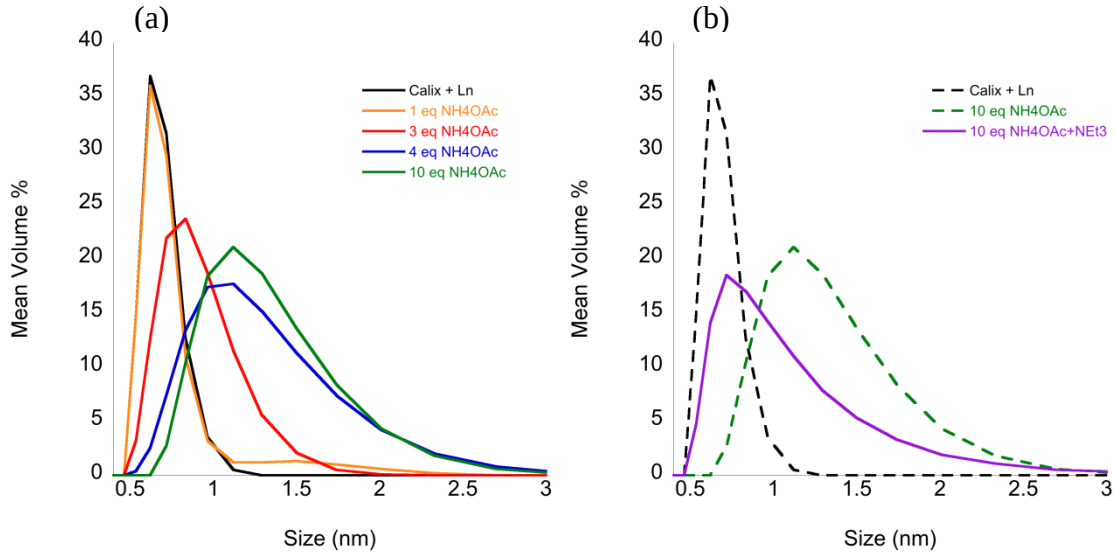

Figure 4.25: (a) Overlayed spectra at a concentration of 0.0018 M, and addition of triethylamine (b).

There are two main trends which can be observed from the overlayed spectra in Figure 4.25(a), a steady increase in the average particle size and an associated increase in the peak width. The increase in peak width represents a wider size range of species in solution, consistent with the formation of lanthanoid clusters. The particle size of the calixarene-lanthanoid solution with no ammonium acetate is virtually identical to that of a calixarene only solution. This suggests that there may only be minimal interactions between the lanthanoid and the calixarene consistent with no addition of base or co-ligand. As the titration progresses, there is a steady increase in the average particle size in solution. The lack of response upon initial addition of ammonium acetate is most likely a result of the low concentration of the larger particles in solution. Upon further addition, there is a significant increase in the average particle size in solution along with the increase in peak width which increases from 0.5 nm to 2.5 nm.

It could be suggested that the observed increase in particle size upon addition of aqueous ammonium acetate to the solution is a consequence of uncontrolled hydrolysis of the lanthanoid salt resulting in precipitation of lanthanoid hydroxide particles. If uncontrolled hydrolysis was occurring, the increased basicity induced by triethylamine

would likely cause further increase in particle size. The data shown in Figure 4.25(b) clearly demonstrates that upon addition of triethylamine to the solution, the average size significantly decreases similar to the original size of the calixarene only result. This reduction of the average particle size, is consistent with the size range of the 1:1 complex, known to form when triethylamine is added in the presence of ligand **1** and lanthanoids.[53] Despite the shift in the peak maxima to a lower average size, there is still retention of a significant peak width (2.5 nm), suggesting the presence of an equilibrium with some of the larger cluster size particles remaining within solution. This hypothesis is supported by the isolation of crystals under these conditions which were confirmed by X-ray crystallography to consist of the bottlebrush cluster (see Section 4.4.3).

There is significant evidence that there is an increase in particle size upon addition of ammonium acetate at the concentration of 0.0018 M. Unfortunately, the low counts obtained as a result of the dilute solution gave an inaccurate average particle size being calculated. To try and rectify this, the concentration of the solution was increased to the point of saturation of the solution. The highest concentration at which all the reagents would dissolve in the ethanol/ethyl acetate solvent was 0.1 M. The DLS results obtained at this concentration are shown in Figure 4.26(a).

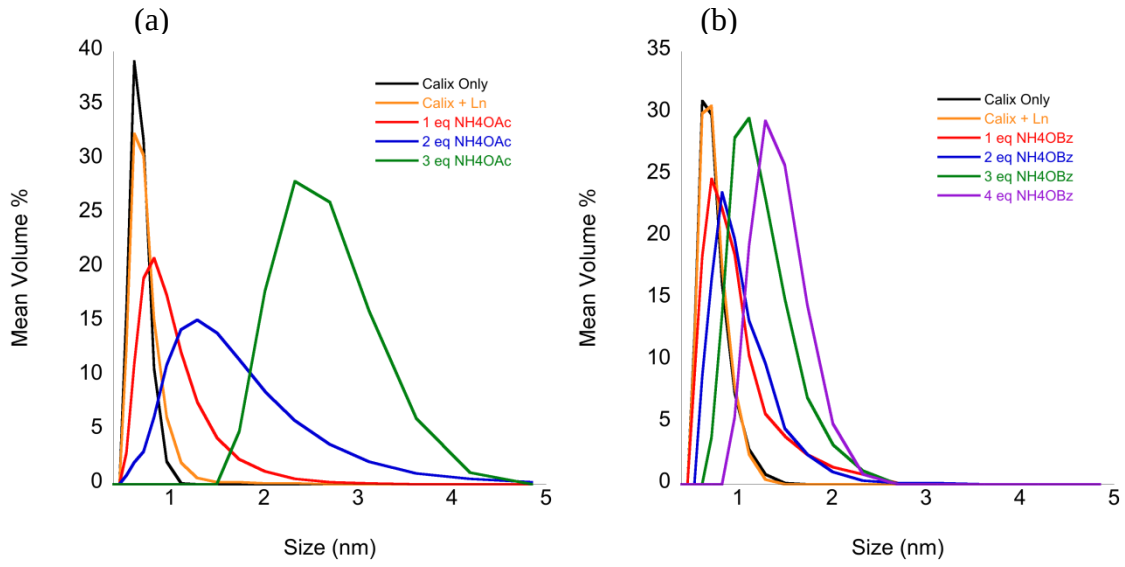

Figure 4.26: DLS overlayed spectra at 0.1 M concentration, acetate (a) and benzoate (b).

In a similar fashion to the lower concentration titration, the overlayed acetate plot exhibits an increase in the average particle size upon addition of aqueous ammonium acetate. The comparison between the two solutions of different concentrations fails after the third addition of ammonium acetate, as there was formation of a significant quantity of precipitate in solution. After filtering the precipitate, light scattering measurements were performed again, however this measurement failed to detect the presence of any particles in solution, suggesting that all the calixarene had precipitated. Despite this, Figure 4.26(a) shows that before the calixarene and lanthanoid precipitated, the increase in particle size is approaching the size value estimated for the Ln_{19} bottlebrush cluster.

Figure 4.26(b) is the titration of ammonium benzoate into the calixarene ethanol and ethyl acetate solution, also performed at the higher concentration of 0.1 M. In a similar fashion to the ammonium acetate titrations, the plot indicates that there is an increase in the average particle size within solution, until precipitation of the calixarene complexes occurred. There was also an increase in the peak width, albeit to a lesser extent than the ammonium acetate system. Remarkably, the maximum size and peak width observed are both less than that found in the acetate system, which is consistent with the solid state results where benzoate was found to support a smaller cluster, see Figure 4.24.

The trends observed in both the ammonium acetate and benzoate solutions are consistent with the formation of the bottlebrush cluster, possibly as a dominant species, although it is highly likely that there are numerous species present.[76,85,95] However, given the limitations of the DLS technique used here, particularly the application of a spherical shape factor, these results must be considered to be qualitative rather than quantitative.

4.5.2 NMR experiments

To further investigate the solution phase behaviour of the bottlebrush clusters, ^{1}H NMR spectroscopy experiments were performed. The isolated crystals of the bottlebrush

cluster were unfortunately insoluble in all available deuterated solvents. As a result, the NMR experiments were performed replicating the experimental conditions used to crystallise the clusters. Due to the expense of deuterated ethanol and ethyl acetate, only three independent solutions were analysed. All of the solutions contained yttrium and calixarene **1** in the solvent mixture, with one solution having aqueous ammonium acetate in deuterated water added, another having only deuterated water added, and the last one having only triethylamine (Et_3N) added. The first solution was used to try and detect the formation of the cluster, with the second solution discounting any changes upon addition of deuterated water from solution one. The third solution as previously discussed should indicate formation of the 1:1 complex upon addition of triethylamine.

Performing ^1H NMR spectra on clusters is usually avoided as the spectra of clusters can often be of limited use, as they tend towards being broad and featureless due to the complex equilibria, and large molecule sizes. For the sake of discussion in this chapter, the stacked plot in Figure 4.27 only shows the peaks in the aromatic region of the spectra. These peaks will be used as an analytical tool to observe any changes in solution, as there are no residual solvent peaks in that region and the starting material di-tetrazole calixarene **1** has only two singlets.

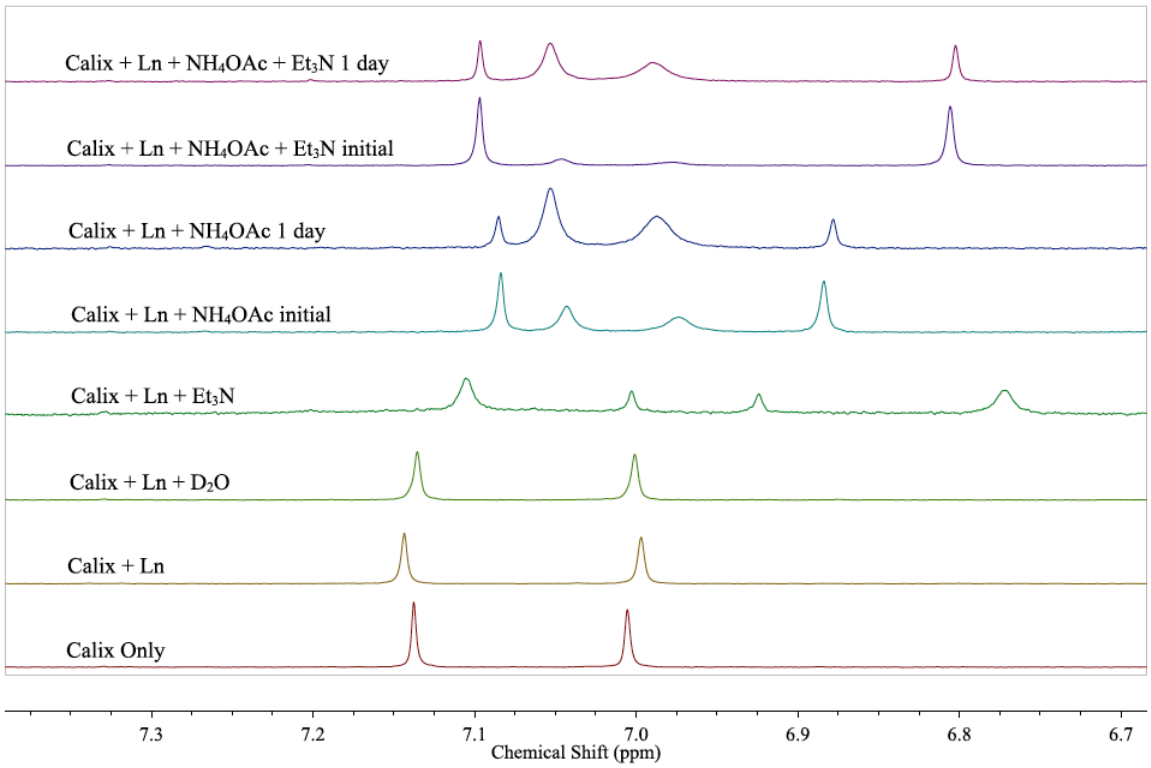

Figure 4.27: Aromatic region of the ^{1}H NMR spectra showing evolution of new peaks.

From the stacked plot, it can be observed that the addition of either ammonium acetate or triethylamine results in the evolution of additional peaks in the aromatic region of the spectra. In conjunction with these additional peaks, the peaks assigned to the di-tetrazole calixarene **1** have shifted from their original position. The shifting of the original peaks is expected as upon addition of acetate and triethylamine, the calixarene is known to interact with the metal in solution, changing the electronic environments of the hydrogens within the system.[89,99] It can be observed that the ^{1}H NMR spectra recorded after leaving the solutions for 1 day show an increase in the proportion of the additional peaks between 6.9-7.1 ppm. This suggests that the system may be slow to achieve equilibrium.

Both DLS and ^{1}H NMR measurements suggest a complex equilibrium is present within solution, where the lanthanoid may not be interacting with the di-tetrazole ligand **1** in a conventional manner. This equilibrium allows for formation of the cluster due to the metal being outside the cavity of the calixarene while still remaining in close association

with the lower rim tetrazoles. The NMR series seems to support the observation as there is evidence of new species that form upon titration of ammonium acetate into the solution. These peaks may not necessarily represent the cluster, however they are different to the peaks evolved upon addition of triethylamine to the solution.

4.5.3 Photophysical measurements

Similar to the DLS and ^{1}H NMR experiments, solution state photophysics of the crystallisation mixture was performed to analyse the species formed in solution. The titration of ammonium acetate was complemented by a comparative parallel experiment involving titration with triethylamine, as previous measurements have suggested that triethylamine addition favours the formation of the 1:1 complex.[53] Monitoring the changes in the absorbtion, excitation, emission spectra and fitting of the lifetime decay upon sequential addition, allows for comparison between titrations. Terbium is the lanthanoid used in these experiments as europium undergoes charge transfer processes, quenching the emission.[53,159,160]

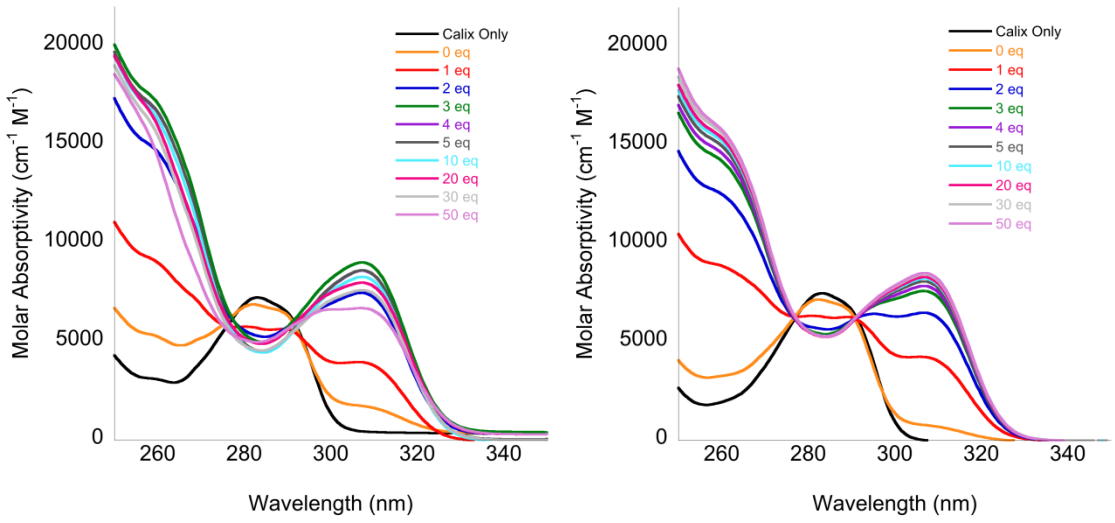

Figure 4.28: Absorption spectra of the di-tetrazole/terbium titrations with aqueous ammonium acetate (left) and triethylamine (right), in an ethanol/ethyl acetate solution.

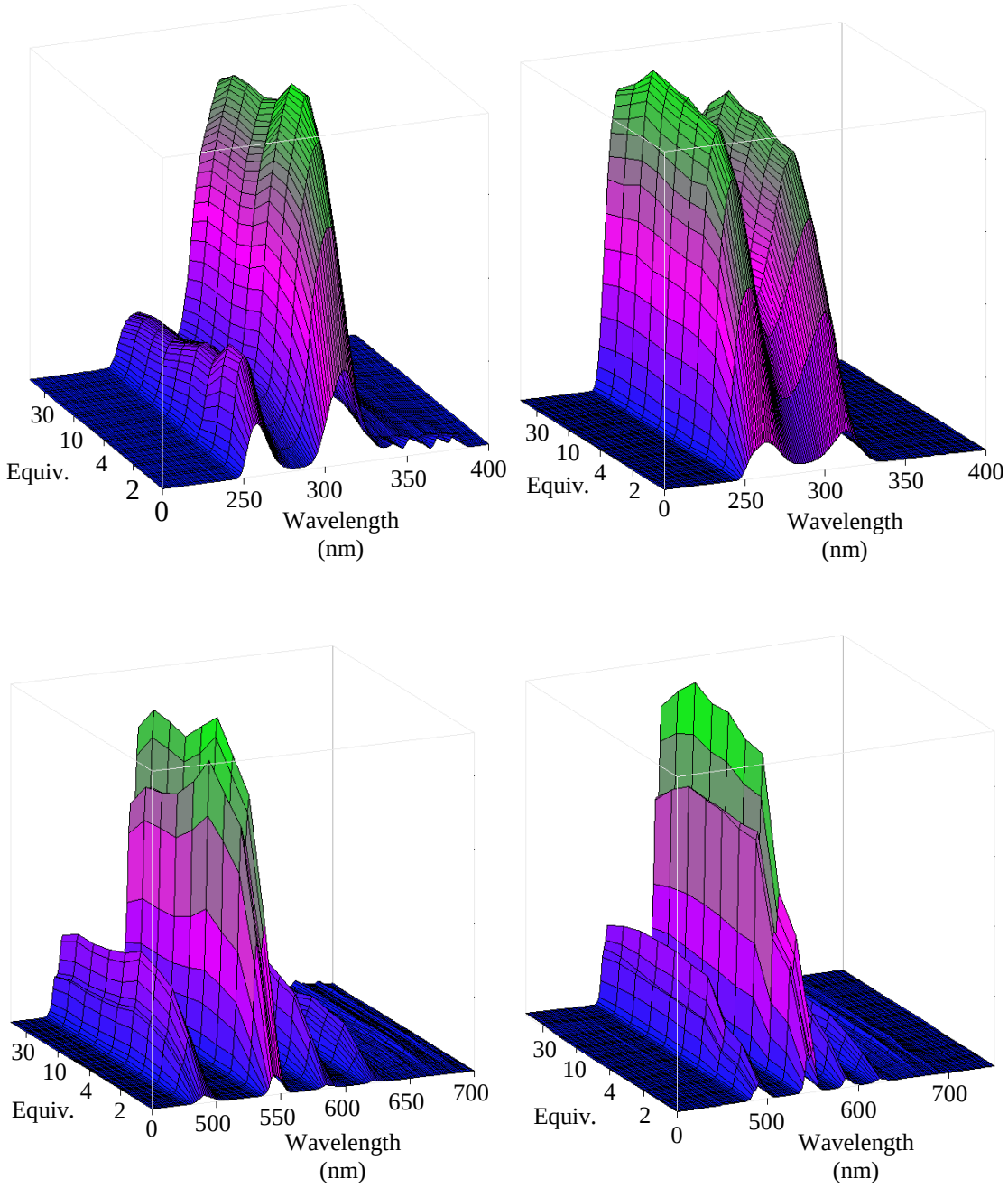

Figure 4.29: Excitation (top) and emission (bottom) spectra of the di-tetrazole/terbium titrations with aqueous ammonium acetate (left) and triethylamine (right), both in an ethanol/ethyl acetate solution.

The initial absorbtion spectrum of a 1×10^{-4} M solution containing the protonated calixarene shows a broad and slightly structured band between 260-300 nm. This is attributed to the $^{1}\pi\pi^{*}$ transition which is most likely centered on the phenyl rings of the calixarene, along with the tetrazoles attached to the lower rim. Figure 4.28 shows that upon addition of a lanthanoid to the solution, a small red-shifted shoulder at

approximately 310 nm is observed, which is attributed to the $^{1}\pi\pi^{*}$ of the partially deprotonated phenolates or tetrazolato portions of the ligand-lanthanoid complex. The intensity of the shoulder increases upon addition of both acetate and base, suggesting that the solutions are behaving in a similar manner. As it is expected that the base is deprotonating the calixarene, it can be hypothesised that the acetate is causing further interaction between the calixarene and the lanthanoid, favouring deprotonation.

Excitation of the solution at the wavelength of the red shifted shoulder (310 nm) results in the usual terbium emission, $^{5}D_{4} \rightarrow {}^{7}F_{J}$ (J = 6, 5, 4, 3) transitions. Similar spectra for the absorption and excitation measurements, monitoring the terbium emission, confirm that the lanthanoid is undergoing sensitization *via* the antenna effect from the calixarene phenyl rings. The excitation spectrum of the ammonium acetate solution in Figure 4.29 shows a small amount of direct excitation of terbium. This emission from terbium is from metal centres that have not been excited *via* the antenna effect, and becomes negligible upon subsequent additions of the aqueous acetate solution. This observation indicates that at initial stages of the titration there could be a small proportion of uncoordinated terbium not undergoing the antenna energy transfer process, while in contrast, at higher equivalents of added acetate the majority of the free terbium is coordinated. The loss of terbium direct excitation is consistent with the increase in emission intensity, supporting the hypothesis that addition of acetate is inducing interaction between the calixarene and lanthanoid. Between three and four equivalents of added base/acetate, a plateau of emission intensity is established, suggesting that there is either complete coordination of the metal, or the system is at an equilibrium at which additional coordination of the terbium to the calixarene is no longer favoured.

Table 4.30: Lifetime data, monitoring 545 nm, for the di-tetrazole calixarene titrations.

	Ammonium acetate			Triethylamine	
No. of eq.	τ_1	τ_2	τ_3	τ_1	τ_2
Metal			796 µs		796 µs
0	55 µs (56%)		677 µs (44%)	49 µs (42%)	740 µs (58%)
1	54 µs (64%)		756 µs (36%)	46 µs (58%)	792 µs (42%)
2	54 µs (65%)		718 µs (35%)	45 µs (63%)	730 µs (37%)
3	55 µs (69%)		782 µs (31%)	48 µs (59%)	691 µs (41%)
4	54 µs (81%)		697 µs (19%)	48 µs (61%)	670 µs (39%)
5	53 µs (92%)		714 µs (8%)	48 µs (64%)	680 µs (36%)
10	55 µs			47 µs (71%)	729 µs (29%)
20	59 µs			48 µs (74%)	701 µs (26%)
30	50 µs (61%)	151 µs (39%)		49 µs	
50	51 µs (25%)	158 µs (75%)		47 µs	

Both of the terbium titration solutions initially exhibited bi-exponential behaviour, comprising of one short and one long lifetime. The similarity between the longer mono-exponential lifetime (796 µs) and the longer lifetime component upon addition of base supports the hypothesis that there is usually a component of 'free' terbium not coordinated to the calixarene in the early stages of the titrations. The shorter lifetime component of both solutions was suggested to be the 1:1 complex as demonstrated in previous work.[53]

The ammonium acetate titration reached a mono-exponential lifetime upon addition of ten equivalents (see Table 4.30). The short component of the lifetime is again consistent with the presence of the 1:1 complex with ligand **1**. The bi-exponential nature of the lifetime at lower equivalents of ammonium acetate helps to support the previous findings from this chapter, where it is suspected that there is an equilibrium within solution. At higher number of equivalents there is evolution of an additional lifetime, which, not only increases in proportion with increasing acetate but is also shorter than the 'free' terbium lifetime. As this lifetime is not evident in the triethylamine titration,

this may indicate the presence of the bottlebrush species or a terbium acetate complex as previously discussed (Figure 4.21). The evolution of a new lifetime component also confirms that there is a difference in solution upon addition of ammonium acetate when compared with triethylamine.

4.6 Solid state studies

Single crystal X-ray diffraction is a solid state method utilised to confirm the presence of the bottlebrush cluster within the isolated crystals, however this method does not confirm the bulk purity of the sample, and is biased to the well crystallised component. Confirmation of bulk purity for the isolated crystals is therefore required before analysing the crystals for their chemical and photophysical properties. There are several methods that were readily accessible to help determine the bulk purity of the sample, including; elemental analysis, total metal content and thermogravimetric analysis. Analysis using these techniques not only provides information on the purity of the isolated sample, but also an indication on whether the bottlebrush cluster persists upon isolation from the crystallisation solution. Figure 4.31 shows an example of the crystals in solution and upon isolation under ambient conditions.

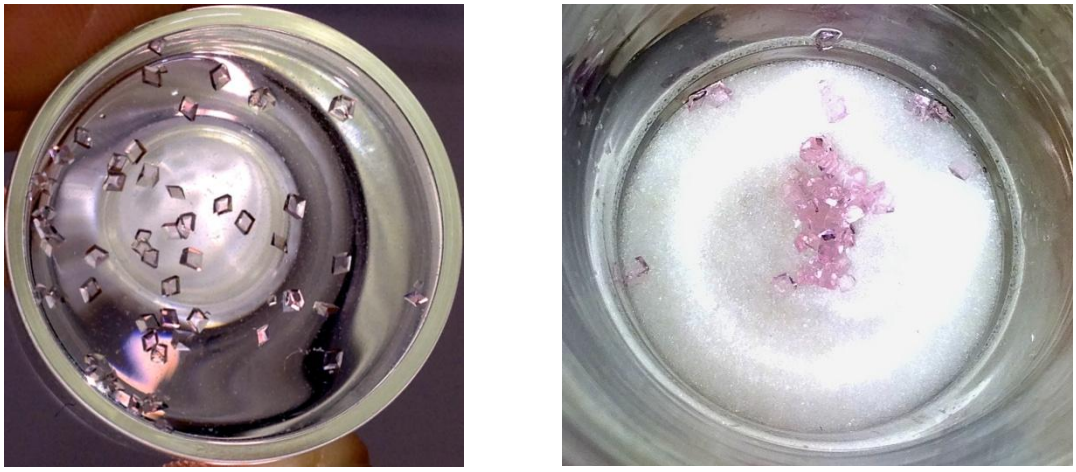

Figure 4.31: Crystal morphology of Ln_{12} crystals *in situ* and upon isolation in atmospheric conditions.

From the images above, it can be observed that there appears to be very little difference in the crystal morphology between the crystals grown in solution and those isolated.

This suggests a high possibility of the bottlebrush cluster being retained along with the majority of the solvent upon isolation of the crystals. This is critical information when analysing the bulk sample, as the data obtained can then be related back to the crystal structure of the cluster.

4.6.1 Bulk purity analysis

Both elemental analysis and digestion for total metal content are techniques which analyse the bulk purity of the crystalline sample isolated as the bottlebrush cluster. However, when dealing with such large structures, the voids between molecules can be significant and variable solvation upon isolation can skew the results, complicating the analysis of the bulk sample.

Table 4.32: Elemental results obtained for both acetate and benzoate systems.

Sample ID	Metal Source	% C expt (calc)*	% H expt (calc)*	% N expt (calc)*
Dy_{19}-B	Picrate	50.37 (49.11)	5.72 (6.21)	18.40 (8.36)
Dy_{19}-B	Nitrate DMSO	46.51 (49.11)	5.24 (6.21)	8.66 (8.36)
Yb_{19}-B	Nitrate DMSO	44.25 (48.50)	5.18 (6.14)	8.21 (8.26)
Er_{19}-B	Nitrate DMSO	48.15 (48.83)	5.75 (6.18)	9.74 (8.32)
Dy_{12}	Nitrate DMSO	46.86 (48.42)	5.45 (5.68)	7.16 (7.81)
Er_{12}	Nitrate DMSO	46.82 (48.10)	5.63 (5.64)	7.08 (7.76)

***Formula used for calculations; $[Ln_{19}(1\text{-}3H)(1\text{-}2H)_{11}(CH_3CO_2)_6(OH)_{26}(H_2O)_{30}.(EtOAc)_{12}(EtOH)_8(H_2O)_{24}]$ and $[Ln_{12}(1\text{-}3H)_3(1\text{-}2H)_3(PhCO_2)_6(OH)_{16}(H_2O)_{21}.(EtOAc)_3(EtOH)_6]$**

From the results of the elemental analysis shown in Table 4.32, the samples of the acetate containing cluster gave inconsistent results. It can be suggested that the high value of both nitrogen and carbon in the first Dy_{19}-B sample is attributed to the presence of picrate, which has high carbon and nitrogen content, within the crystal matrix. The additional picrate from the metal salt is not present within the other Dy_{19}-B sample as they were crystallised with the nitrate DMSO salt. It also suggests that there is significant inclusion of solvent and ions such as picrate within the voids of the crystal, making analysis of the bulk sample difficult.

Combustion of the benzoate samples resulted in more consistent results when compared to the acetate samples. Although the results were outside the acceptable error of the expected values, there was less than 0.4% difference between the samples analysed. This suggests that there may be a higher proportion of retained impurities/solvent for the Ln_{19} samples when compared to the Ln_{12} species.

Analysis of the isolated crystalline cluster for total metal content involved the digestion in acidic media after extensive drying was carried out on the sample. Quantitative analysis of dysprosium metal content was then performed.

Table 4.33: Total metal content results obtained for both acetate and benzoate systems.

Sample ID	% Ln Calculated	% Ln Found
Dy Acetate	21.81	21.85
Dy Benzoate	24.17	22.88

As a result of extensive drying of the samples prior to analysis, the calculated values in the table above used the non-solvated formula of both the acetate and benzoate clusters; $[Dy_{19}(\mathbf{1}\text{-}3H)(\mathbf{1}\text{-}2H)_{11}(CH_3CO_2)_6(OH)_{26}(H_2O)_{30}]$ for the acetate sample and $[Dy_{12}(\mathbf{1}\text{-}3H)_3(\mathbf{1}\text{-}2H)_3(PhCO_2)_5(OH)_{16}(H_2O)_{21}]$ for the benzoate bottlebrush. The results from the analysed samples, Table 4.33, were found to be closer to the calculated values than the values obtained from elemental analysis. Unfortunately once again, it seems reasonable to suggest that the difference between the calculated and observed values is directly linked to the variation in the impurities remaining within the crystal upon isolation.

4.6.2 Thermogravimetric Analysis (TGA)

Thermogravimetric Analysis (TGA) is a bulk analysis method which provides additional insight on the stability and constitution of any molecule.[58,161] The stability is directly related to the temperature at which degradation begins, and also % weight lost over a temperature range. Typically, the results obtained when performing TGA of clusters can be broken down into three main sections. Firstly, solvent molecules, whether free or

involved in second sphere interactions are removed. After the solvent has been removed, other loosely coordinated molecules also evaporate. Occasionally these two portions are overlapping depending on the strength of the interactions within the cluster. Secondly, the tightly coordinated first coordination sphere molecules undergo combustion. This leaves the metal core, which in the case of lanthanoid clusters is predominantly lanthanoid hydroxo species which can eventually at high temperatures dehydrate to the lanthanoid oxide.[58,60]

The output of the TGA analysis is percentage mass lost as a function of temperature over a given time. This allows for the calculation of the individual sections as a percentage, which will give an indication as to the proportional constituents of the cluster molecule. In the case of the bottlebrush cluster this is only an estimate as it is impossible to gauge the number and hence mass of solvent molecules which remain within the crystal matrix upon isolation. Despite this Figure 4.34 displays the three distinct regions usually present for a TGA trace.

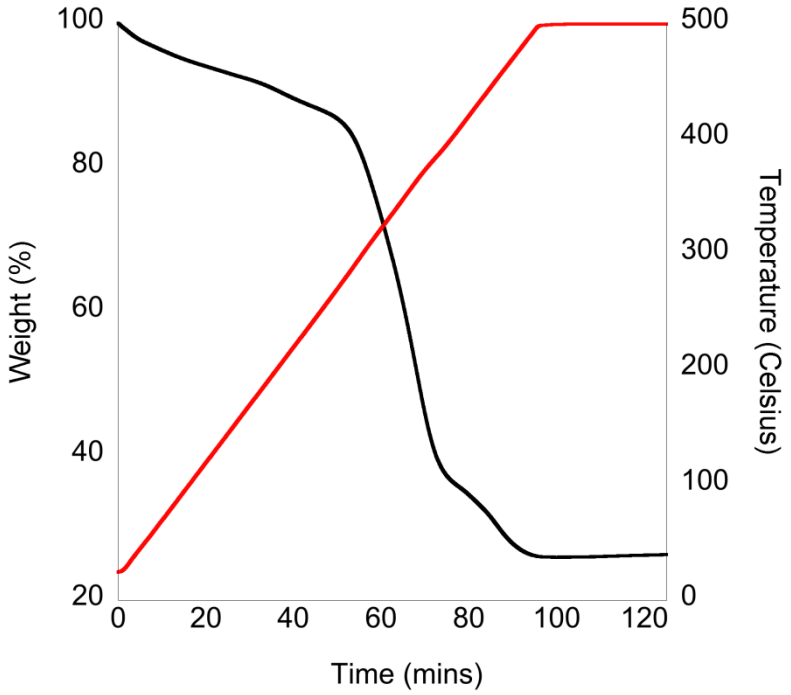

Figure 4.34: TGA output of Ln_{19} acetate bottlebrush cluster in air. Black line corresponds to weight loss, red line corresponds to temperature.

The three sections can be approximated to percentages of 14%, 64% and 22%. Calculations estimating the mass of solvent in the second coordination sphere can be seen in Appendix F. The resulting numbers closely follow what would be expected for the formulation of the cluster as determined by X-ray crystallography. The calculations show that if the acetate caps (2.2%) are considered to be loosely coordinated, and hence are included in the solvent combustion portion of the TGA plot there will be a percentage mass of 14%. The remaining calixarene molecules and water molecules external to the core would be removed next in the temperature range of 280-500°C. The twelve di-tetrazole calixarene molecules surrounding the cluster core correspond to a percentage mass of 62%. This leaves the remaining 24% as being the lanthanoid hydroxide cluster core, which is consistent with calculations. A Raman spectrum of the residue remaining after heating the sample to 1100°C, is consistent with the lanthanoid sesquioxide, providing evidence that there is a lack of organic material remaining after combustion.

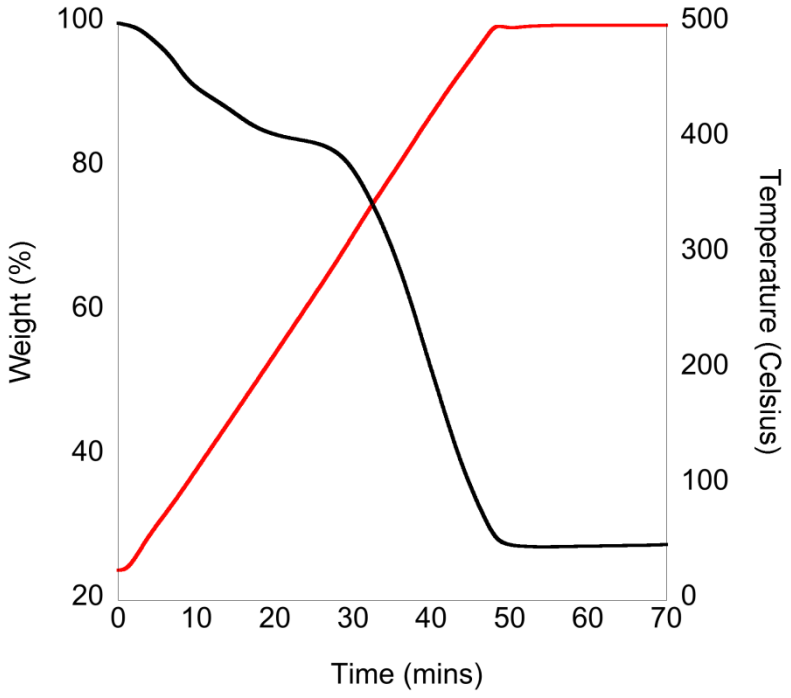

Figure 4.35: TGA output of Ln_{12} benzoate bottlebrush cluster in air. Black line corresponds to weight loss, red line corresponds to temperature.

Combustion of the benzoate Ln_{12} cluster gave the results seen in Figure 4.35, which are similar to those obtained for the acetate structure. There are three, possibly even four

sections which can be approximated to percentages of 7%, 8%, 59% and 26%. Once again the first portion of weight loss (7%) would correspond to solvent in the crystal, the next section could be suggested to be the benzoate caps on the ends of the cluster (8%). The last weight loss would correspond to the combustion of the organics and water molecules attached to the core (59%), leaving behind the lanthanoid hydroxo core (26%). Calculations (Appendix F) have estimated the percentages of each of these portions, finding that all values are remarkably similar. The calculations show that solvent in the second coordination sphere corresponds to approximately 6% of the overall mass of the structure. The benzoate caps correspond to 8% of the structure, while the remaining organic and water molecules correspond to 60% of the overall weight. This leaves 26% as the internal lanthanoid hydroxo core, which is consistent with observations. Once again, a Raman spectrum of the residue remaining after heating the sample to 1100°C, is consistent with the lanthanoid sesquioxide, providing evidence supporting the lack of organic material remaining after combustion.

4.7 Conclusions

The newly synthesised calixarene tetrazolato ligands **1**, **2** and **3** have been tested for their coordination ability to the lanthanoids. Failure to characterise 1:1 ligand-lanthanoid complexes for both the tri- and tetra-tetrazole calixarene ligands **2**/**3** was suggested to be a result of inter- and intra-molecular interactions persistent in both the ligand and metal complex X-ray crystal structures. The di-tetrazole ligand **1** did not have the same interactions, and as such 1:1 lanthanoid complexes were characterised. Addition of an aqueous carboxylate co-ligand, ammonium acetate, allowed the formation of a new rod-like lanthanoid hydroxo cluster. Alteration of the length of the cluster was attempted by changing the equivalents of the acetate co-ligand with no success. However, upon changing the co-ligand to ammonium benzoate, a shorter cluster was isolated. This structure had an identical cluster motif with one less repeating unit. Attempts were made to study the speciation of the cluster in solution, using DLS, photophysics and ^{1}H NMR spectroscopy. The solution state studies gave consistent results all indicating the presence of a complex equilibrium within solution. Despite this

a consistent size of each cluster is continually obtained (Ln_{19} and Ln_{12}). This suggests that, relative to the other components, the bottlebrush clusters are the least soluble component within solution, driving the equilibrium to formation of that particular size. Bulk purity of the isolated crystals gave inconsistent results for both elemental analysis and total metal content, however this is most likely due to the variable quantity of solvent remaining within the crystals upon isolation. In comparison, TGA measurements were more consistent, with reasonable accuracy being obtained for the percentages of each component.

5 Photophysics of the lanthanoid-calixarene tetrazolato complexes

5.1 Introduction to photophysics

The lanthanoids and their complexes are known to exhibit photoluminescence in both solution and solid state. Their emission is characterised by line-like bands, typically 100-300 cm^{-1} in width, and often relatively long luminescent lifetimes.[89,162,102,163] Apart from lanthanum and lutetium, which do not have any *f-f* transitions, all the lanthanoid elements are luminescent. The transitions of the lanthanoids can be separated into three separate groups; UV emitters, visible emitters and near-infrared (NIR) emitters. These transitions can either be fluorescent or phosphorescent in nature. The line-like emission of the lanthanoids is relatively unaffected by the nature of the ligand, due to the inner core nature of the 4*f* orbitals (see Section 1.3.2).[74]

5.1.1 Electronic transitions

For a given electronic configuration, there may be multiple ways to allocate the electrons to the set of seven 4*f* orbitals. Hence, specific spectroscopic terms must be introduced to take into consideration the interelectronic repulsion. The spectroscopic term of a lanthanoid ion can be read as $^{2S+1}L_J$. The spin multiplicity (2S+1) is obtained through the summation of the individual spin angular momenta. The orbital angular momenta of the individual electrons add to form a total orbital angular momentum L, while the coupling of L and S calculates the total angular momentum, J. Coupling associated with the lanthanoid individual momenta cause the energy of the 4*f* orbitals to be non-degenerate and split, represented pictorially below in Figure 5.1.[164]

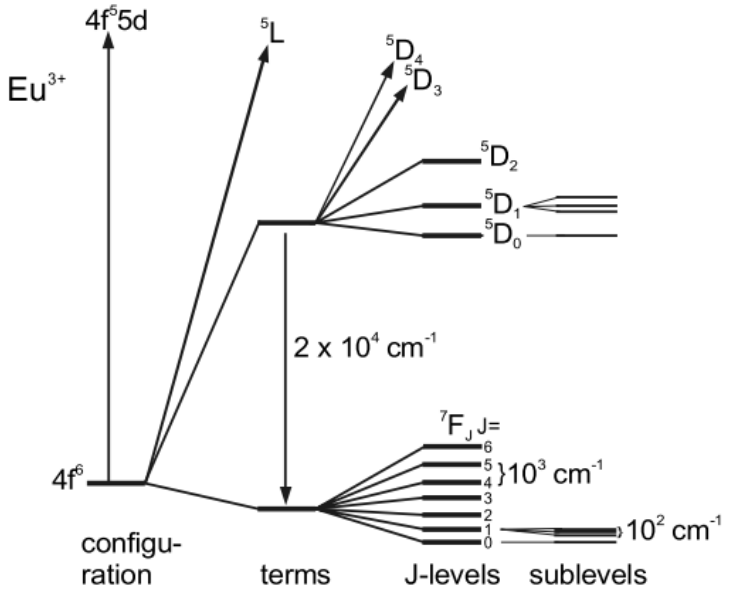

Figure 5.1: Derivation of the ground term for europium, describing all the quantum terms.[164]

Each $^{2S+1}L_J$ term has a multiplicity of 2J+1 degenerate levels, with this splitting known as the Stark effect. The energy difference between states is typically only a few hundred cm^{-1}, which progressively increases as the crystal field symmetry is lowered.

5.1.2 Selection rules

For all electronic transitions there exists a set of rules which govern whether a transition is allowed or forbidden.[96,160] There are two main rules which need to be considered when studying the lanthanoids. These rules are the spin selection rule, and the orbital angular momentum selection rule. The spin selection rule states that there must be no change in the spin of an electron within a given transition. For lanthanoid complexes, the spin selection rule can be relaxed through spin-orbit coupling, for the coupling results in the total spin of the 4*f* electrons no longer being accurately defined. The orbital angular momentum rule dictates that there must be a change in the angular momentum during a transition. This is as a result of a photon having a spin angular momentum of one which must be conserved in the transition. Due to spin-orbit coupling, L couples with S resulting in J, and since the spin selection rule states that S cannot change, L is the only value that can change when a photon is absorbed, ie. $\Delta L = 0$ or ± 1. Together, these rules establish the probability of any lanthanoid electronic transition occurring.

5.1.3 Antenna Effect

Emission from any lanthanoid ion requires an electron to be excited to a position of higher energy within the 4*f* shell, usually with an energy difference comparable to visible light. Excitation can occur directly, ie. excitation of the metal, however, this is usually an inefficient process as a result of both the spin and parity forbidden nature of the transitions (see Section 5.1.2), as such the absorption coefficients of lanthanoid ions are very low (typically less than 10 $M^{-1}cm^{-1}$). As a result, an important feature of luminescent lanthanoid ions is that their luminescence can be photosensitised by an appropriate antenna chromophore through a process known as the "antenna effect".[165] The coordinating chromophore absorbs the incoming energy, usually in the UV, or visible spectral region, which is then transferred to a lanthanoid excited state *via* energy transfer, resulting in subsequent emission. Figure 5.2 shows this process pictorially.

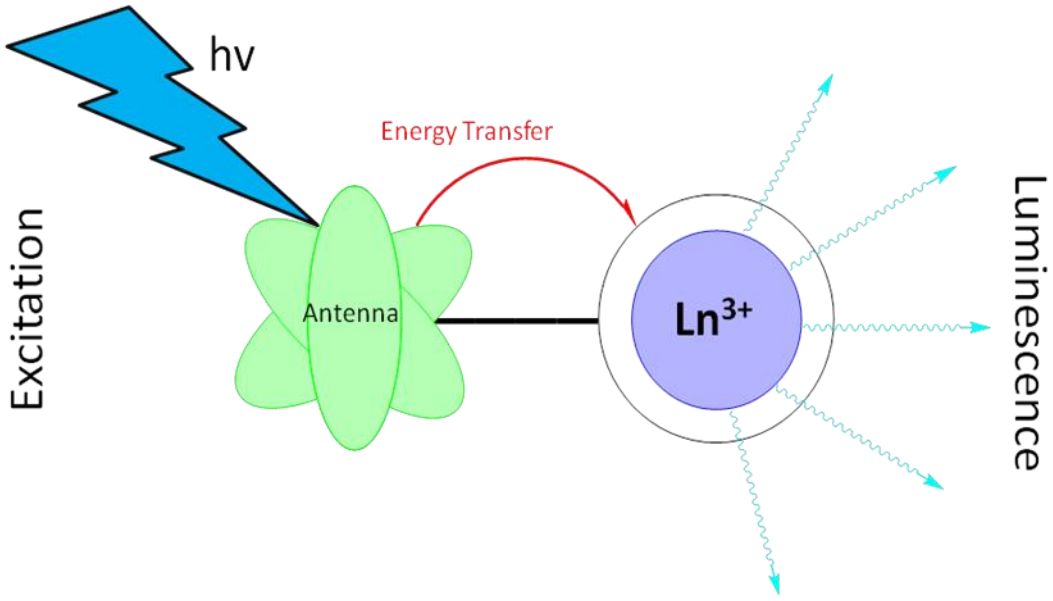

Figure 5.2: Schematic representation of lanthanoid luminescence *via* the antenna effect.

Excitation of the organic chromophore involves promotion of an electron to an orbital of higher energy which is known as the singlet excited state when referring to a Jablonski diagram (see Figure 5.3). Before transferring the energy to the lanthanoid, a proportion of the excited electrons within the ligand orbitals undergo a spin forbidden transition, known as intersystem crossing, to the triplet excited state. Intersystem crossing is a non-radiative process involving transition between two electronic states with different spin multiplicity, and is enhanced by the strong spin-orbit coupling caused by the presence of the heavy lanthanoid ion. Energy transfer from the ligands triplet excited state has been proposed to occur *via* Dexter and/or Förster mechanisms.[166,167] The excited lanthanoid then relaxes to its ground state, accompanied by either the typical line like emission characteristic of the lanthanoids, or other non-radiative processes. Although energy transfer is generally considered to originate from the triplet state, it cannot be excluded that energy from the singlet does not contribute towards excitation of the lanthanoid.

5.1.4 Triplet state

To optimise the antenna effect, two parameters are important: the difference in energy between the singlet and triplet state within the ligand, as well as the difference in energy between the triplet state and the lanthanoid accepting state, Figure 5.3.

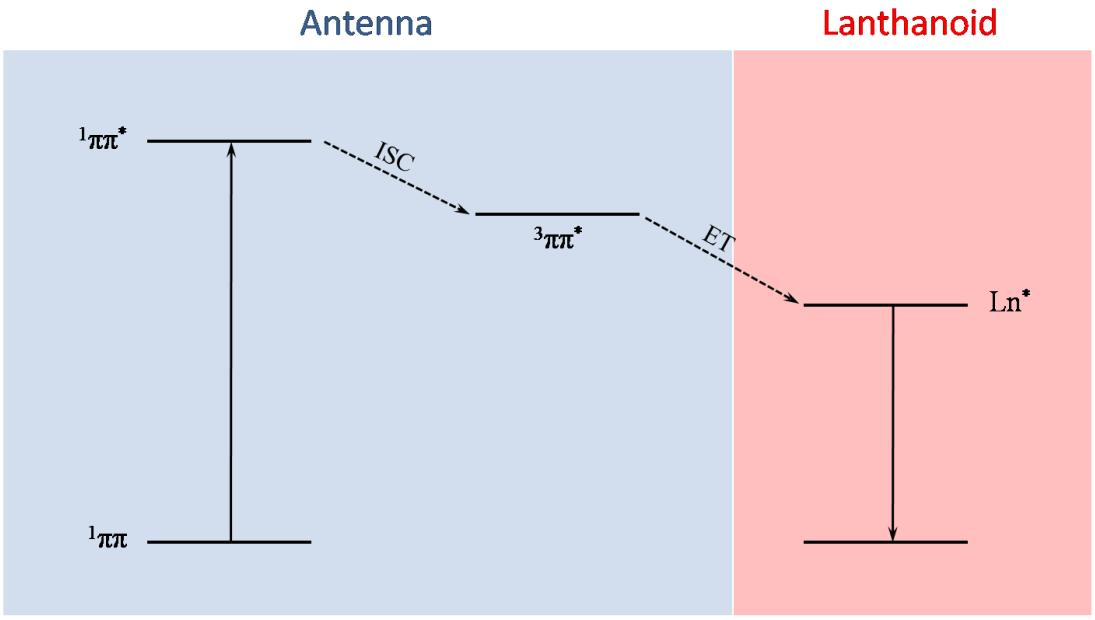

Figure 5.3: Jablonski diagram demonstrating the energy transfer mechanism of the antenna effect.

Literature has demonstrated the optimal energy gap between the singlet and triplet excited states of the ligand required for lanthanoid-enhanced intersystem crossing is 5000 cm^{-1}. The optimal energy gap between the ligands triplet excited state and the excited state of the lanthanoid has been reported between 2500-3000 cm^{-1}.[74,94,105]

Determination of the ligand triplet state is performed *via* two methods. The first method is the use of a 'ligand only' glassed solution at 77K. Glassing the solution reduces the amount of non-radiative vibrational relaxation occurring, increasing radiative emission from the triplet state. The second method uses gadolinium as the lanthanoid in solution. Gadolinium has a very high energy for its first excited state (~30,000 cm^{-1}) which is typically well above the energy of the ligand triplet state. Consequently, the energy within the ligand orbitals cannot undergo energy transfer processes to the lanthanoid. Instead to return to the ground state, both radiative and non-radiative relaxation from the

ligand occurs, of which the energy of the triplet state is estimated as the highest energy of the emitted phosphorescence light.[102,168]

5.2 Bottlebrush cluster solid state photophysics

The photophysics reported within this section will focus on the solid state bottlebrush samples isolated from the crystallisation solutions. Analysis of the bottlebrush cluster crystal structures shows the presence of a large number of OH functional groups within close proximity of the lanthanoid core. The lanthanoid-hydroxo lattice, of which the core consists, has the potential to be emissive dependent on the level of quenching involved within the system. Despite the hydroxyl groups being present within the core, the potential quenching of the lanthanoid emission is likely reduced due to the OH moieties all being involved in hydrogen bonding. Bünzli has previously demonstrated that this reduces the efficiency of the OH groups to quench the emission.[74,169]

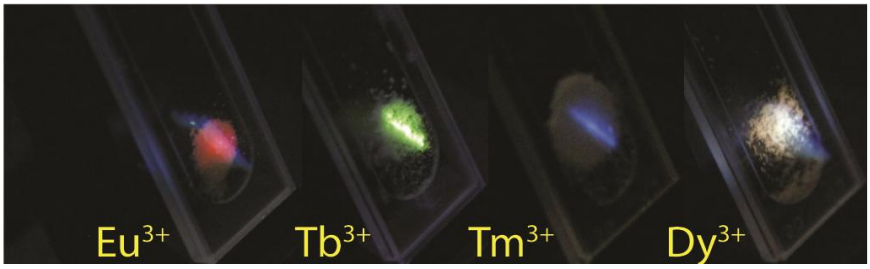

Figure 5.4: Emission from the solid state Ln_{19} bottlebrush samples.

Unfortunately, any attempt to redissolve the crystals in a wide range of both polar and non-polar solvents was unsuccessful. Considering the previously stated results (see Section 4.4.2) outlining the reproducibility of the bottlebrush clusters, solid state photophysics, Figure 5.4, was performed on the complexes formed with the lanthanoids ranging between samarium to ytterbium.

5.2.1 Triplet state of the ligand

Determining the ligands triplet state energy is pivotal in the understanding of key photophysical properties associated with the lanthanoid complexes. The triplet state of

the di-tetrazole calixarene **1** in solution was determined using both the 77K glass and gadolinium complex method as outlined in Section 5.1.4.

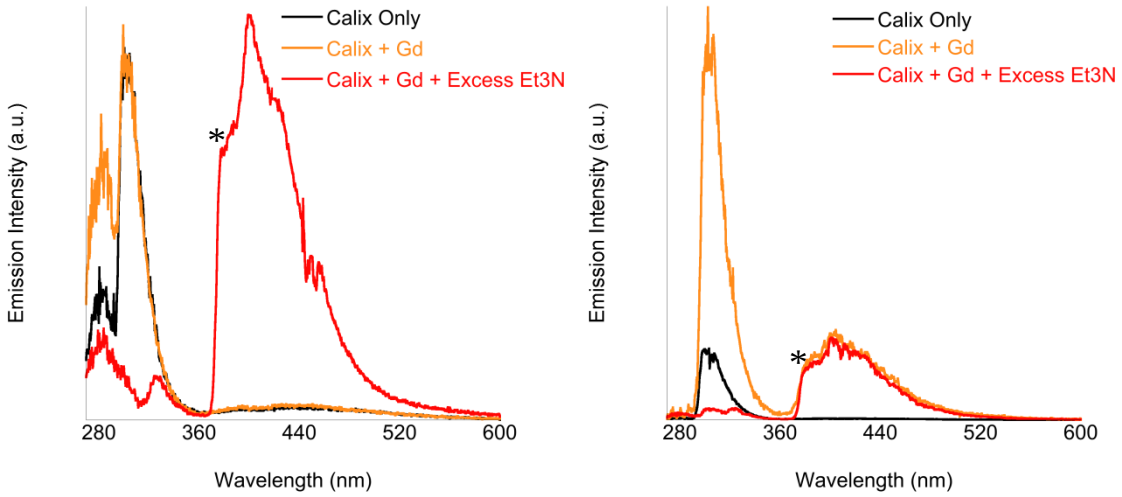

Figure 5.5: Emission spectra at 77K for the determination of the triplet state of di-tetrazole calixarene 1. Dichloromethane (left) and ethanol/ethyl acetate mixture (right). Asterix denotes 0-0 phonon transition.

Calculating the triplet energy level of the ligand from the 0-0 phonon transition, indicated by the asterix, showed that there was very little difference between the energy values obtained for the two solutions. The calculated value was 26,320 cm^{-1} which is very similar to the values reported within the literature for calixarenes.[53,102,105]

5.2.2 Visible emitters

Emission of the bottlebrush cluster in the visible region of the electromagnetic spectrum was observed for; samarium, europium, terbium, dysprosium and thulium. The emission from each species was typical for the respective lanthanoid, with the spectra being reported in Figure 5.6.

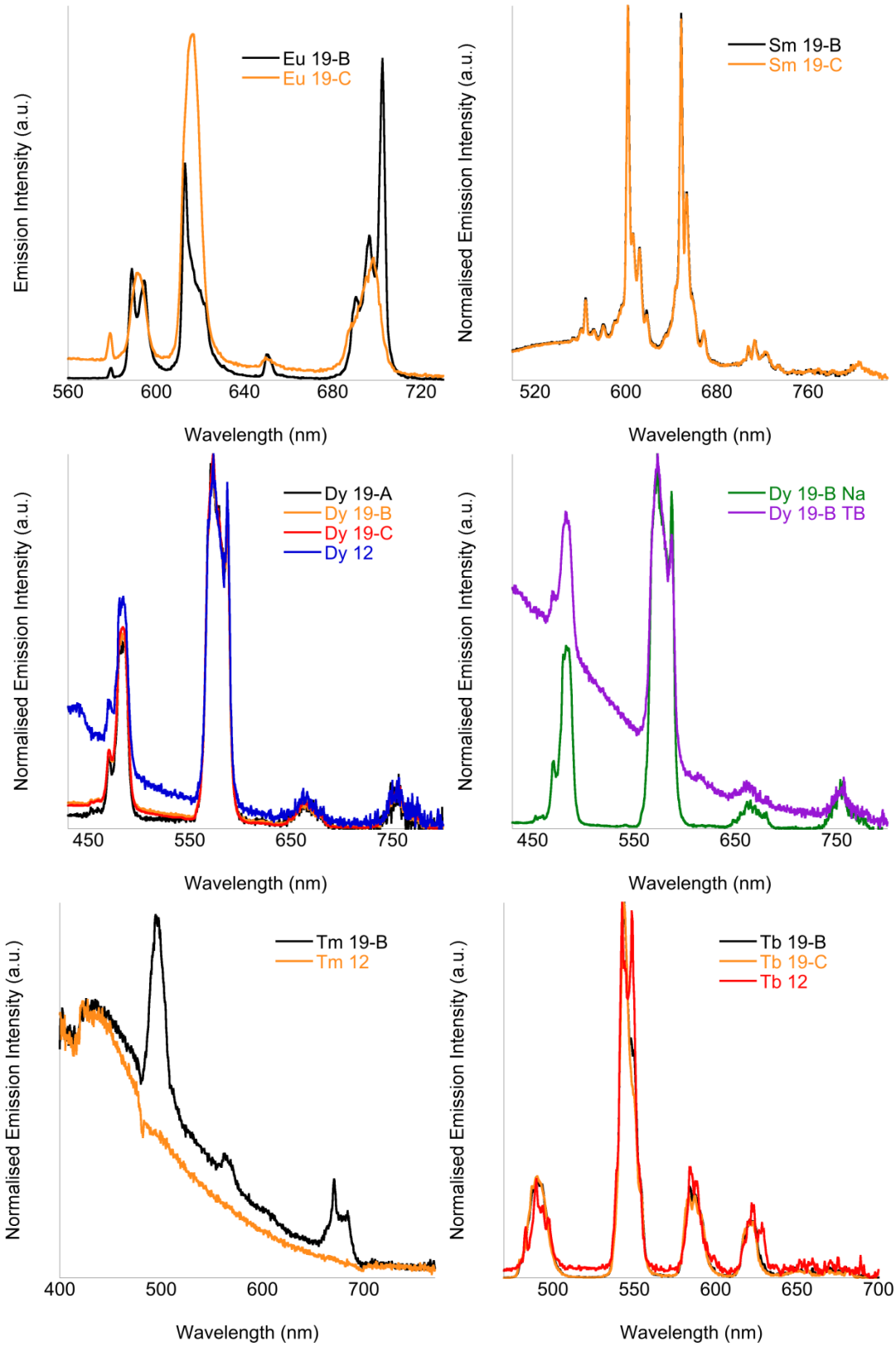

Figure 5.6: Normalised emission spectra of the solid state bottlebrush cluster crystals at room temperature.

Each of the spectra show typical emission of the particular lanthanoid with the specific transitions shown in the tables below.

Table 5.7: Samarium

Transition	Wavelength of highest intensity (nm)
$^4G_{5/2} \rightarrow {}^6H_{5/2}$	564
$^4G_{5/2} \rightarrow {}^6H_{7/2}$	602
$^4G_{5/2} \rightarrow {}^6H_{9/2}$	648
$^4G_{5/2} \rightarrow {}^6H_{11/2}$	714
$^4G_{5/2} \rightarrow {}^6H_{13/2}$	808

Table 5.8: Europium

Transition	Wavelength of highest intensity (nm)
$^5D_0 \rightarrow {}^7F_0$	579
$^5D_0 \rightarrow {}^7F_1$	591
$^5D_0 \rightarrow {}^7F_2$	618
$^5D_0 \rightarrow {}^7F_3$	650
$^5D_0 \rightarrow {}^7F_4$	698

Table 5.9: Terbium

Transition	Wavelength of highest intensity (nm)
$^5D_4 \rightarrow {}^7F_6$	490
$^5D_4 \rightarrow {}^7F_5$	544
$^5D_4 \rightarrow {}^7F_4$	584
$^5D_4 \rightarrow {}^7F_3$	621
$^5D_4 \rightarrow {}^7F_{0,1,2}$	-

Table 5.10: Dysprosium

Transition	Wavelength of highest intensity (nm)
$^4I_{15/2} \rightarrow {}^6H_{15/2}$	459
$^4F_{9/2} \rightarrow {}^6H_{15/2}$	486
$^4I_{15/2} \rightarrow {}^6H_{13/2}$	-
$^4F_{9/2} \rightarrow {}^6H_{13/2}$	572
$^4F_{9/2} \rightarrow {}^6H_{11/2}$	662
$^4F_{9/2} \rightarrow {}^6H_{9/2}$	-

Table 5.11: Thulium

Transition	Wavelength of highest intensity (nm)
$^1G_4 \rightarrow {}^3H_6$	476
$^1G_4 \rightarrow {}^3F_4$	651
$^1G_4 \rightarrow {}^3H_5$	-

Spectra of the three isolated species; 5 eq of ammonium acetate (Ln_{19}-B), 10 eq of ammonium acetate (Ln_{19}-C), and the ammonium benzoate (Ln_{12}) system were usually recorded. Unfortunately, the benzoate system for both europium and samarium could not be measured due to insufficient crystals. As each of the separate bottlebrush systems had identical cluster motifs, with similar metal environments, it is expected that the emission spectra would also be similar. This hypothesis is consistent for samarium, terbium and dysprosium. However, both europium and thulium show inconsistent results for the samples tested.

Triplet state emission can be observed in all of the less emissive species, originating from ligand species unable to undergo energy transfer processes. The broad emission begins at 370 nm and ends at approximately 700 nm, masking the line like emission of the lanthanoids. Emission from the ligand triplet state is constantly occurring in conjunction with lanthanoid emission, as generally, energy transfer to the excited state of a lanthanoid is not 100% efficient. Despite this, there are two independent scenarios which can maximise the ligands triplet state emission making it higher in intensity than the lanthanoid emission. Firstly, an energy gap between the ligand triplet state and the lanthanoid excited state that is too large to allow efficient energy transfer, or too small, resulting in increased energy back transfer. Emission from the thulium species shows only poor emission, which is attributed to the small energy gap between the two excited states (~2900 cm^{-1}) resulting in high amounts of energy back transfer to the ligand. The other scenario is the presence of free ligand within the crystal matrix which is not associated with a lanthanoid and hence not acting as an antenna. A possible example of this would be the dysprosium species which have variable emission intensity for the same lanthanoid and cluster motif. The only way that the emission intensity can be

reduced for the same lanthanoid is through lack of coordination of calixarene **1**, hence a reduction in the energy transferred to the excited state of the lanthanoid. This may also suggest an additional reason why any elemental analysis of the crystals has variability between samples (see Section 4.6).

For the bottlebrush clusters, europium was used to help confirm the lanthanoid coordination sphere while in the solid state. The emissive state of Eu^{3+} being the $^5D_0$ state allows individual transitions to be related to specific changes in the coordination sphere of the complex.[53,96] From X-ray crystal structure determination, there are three independent europium environments present within the cluster trigonal bipyramidal motif, Figure 5.12.

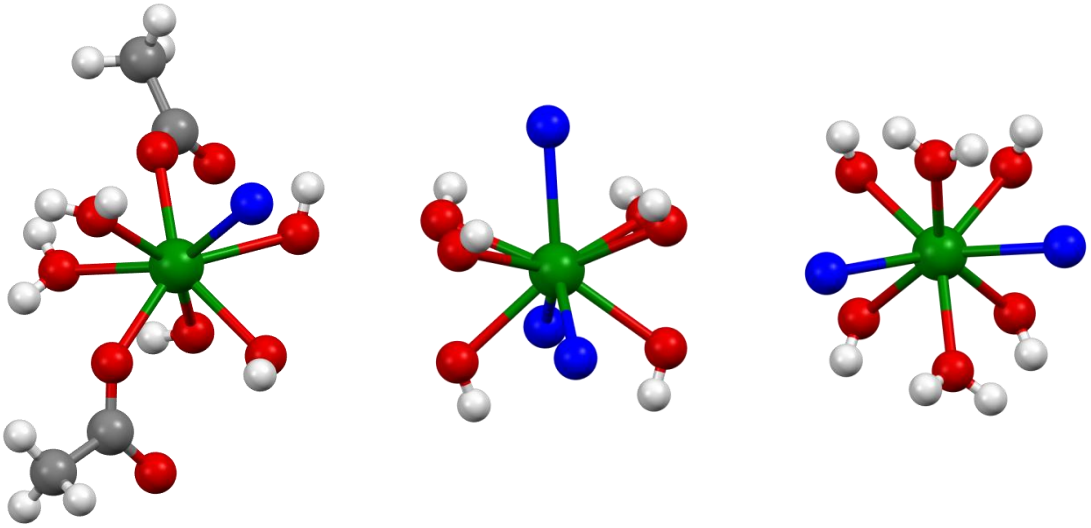

Figure 5.12: The three first-sphere coordination environments of the lanthanoids in the Ln_{19} trigonal bipyramidal cluster motif.

The emission profiles for both of the Eu_{19} species show a peak around 579 nm, corresponding to the $^5D_0 \rightarrow {}^7F_0$ transition. The existence of this peak confirms that the local europium environments shown above, have symmetries lower than D_3. This low symmetry environment is also the likely reason for the splitting of the $^5D_0 \rightarrow {}^7F_1$ transition in the Eu_{19}-B emission spectrum. The full width half maximum of the $^5D_0 \rightarrow {}^7F_0$ transition is 60 cm^{-1} which according to experimental evidence is consistent

with the presence of more than one unique europium metal centre in the cluster. The lifetime of the europium bottlebrush species, monitoring the 618 nm $^5D_0 \rightarrow {}^7F_2$ peak, was best fitted to a bi-exponential decay with values of 280 μs (31%) and 564 μs (69%). The bi-exponential nature of the decay again suggests that there are multiple unique europium environments which are emitting. Hence, all the photophysical data for the europium bottlebrush species is in agreement with the crystal structure determination, supporting the retention of the species upon isolation from solution.

The lifetimes of each terbium sample, outlined in Table 5.13, was also measured to allow a direct comparison between each of the different bottlebrush species. Monitoring the $^5D_4 \rightarrow {}^7F_5$ transition of the terbium species gave a lifetime best fitted to a bi-exponential decay in a similar fashion to the europium clusters. This provides further evidence supporting the results of the crystal structure determination, which show multiple independent coordination environments of the lanthanoid ions present within the cluster structure.

Table 5.13: Lifetime data of the Tb_{19} and Tb_{12} species.

	τ_1	τ_2
Tb_{19}-B	219 μs (10%)	745 μs (90%)
Tb_{19}-C	164 μs (30%)	492 μs (70%)
Tb_{12}	97 μs (7%)	661 μs (93%)

The inconsistency between the lifetimes of the Tb_{19}-B and Tb_{19}-C, which have identical structures, may be a result of the different packing of the clusters within the crystal lattice. The different packing of the crystals has already been reported in Section 4.4.1. The coordination of the central lanthanoid atoms is similar for all samples including the Tb_{12} species, which could explain the similarity in the longer component of the lifetime between Tb_{19}-B and Tb_{12}.

The emission of dysprosium was identical for the six variations of the bottlebrush cluster tested; Dy_{19}-A/B/C, Dy_{19}-sodium acetate and Dy_{19}-tetra-butyl ammonium acetate. While

some of the samples had higher signal to noise ratio, this was attributed to the purity of the sample as discussed previously. Both the emission spectra recorded for Dy_{19}-A and Dy_{19}-B show some small shoulders at 459 nm and 547 nm. These shoulders are actually independent transitions from a different excited state. Dysprosium has two main emissive states, the $^4I_{15/2}$ and $^4F_{9/2}$ energy levels. The emissive level with more intense emission is determined mainly by the triplet energy of the ligand. For each of the emission traces, it is evident that there is no difference in the fine structure or the position of the peaks. This is expected, as there should be very little difference in the coordination environment of the metal centres and there are no hypersensitive transitions for dysprosium which would allow for easy identification of any minor changes. Most importantly the lack of distinction between the Dy_{19} species with different cations as the salt of the acetate ion, support the X-ray crystallography which obtains a similar cell to that of the Dy_{19}-B system it was designed to replicate. Recording of the lifetime for the various dysprosium species was attempted, however it was too short to be measured by the equipment available.

5.2.3 Near-infrared (NIR) emitters

The only lanthanoids, within the bottlebrush series, having significant emission in the NIR region of the electromagnetic spectrum were samarium and ytterbium. Neodymium is also luminescent in the NIR, however this was known to only crystallise as the 1:1 complex, and hence was not compared to the bottlebrush cluster emission profiles. As was the case for the lanthanoids emitting in the visible region, the excitation spectra for the NIR emitting lanthanoids contained broad featureless peaks consistent with the excitation of the organic chromophore involved in the antenna effect.

As observed previously in Section 5.2.2, samarium has several visible emissions from the $^4G_{5/2}$ excited state. This is also the emissive energy level for the NIR transitions. The difference in energy of the transitions originates from the differing ground states,

$^6H_{5/2\text{-}13/2}$ for the visible transitions where as the NIR transitions have ground states $^6F_{3/2\text{-}9/2}$.

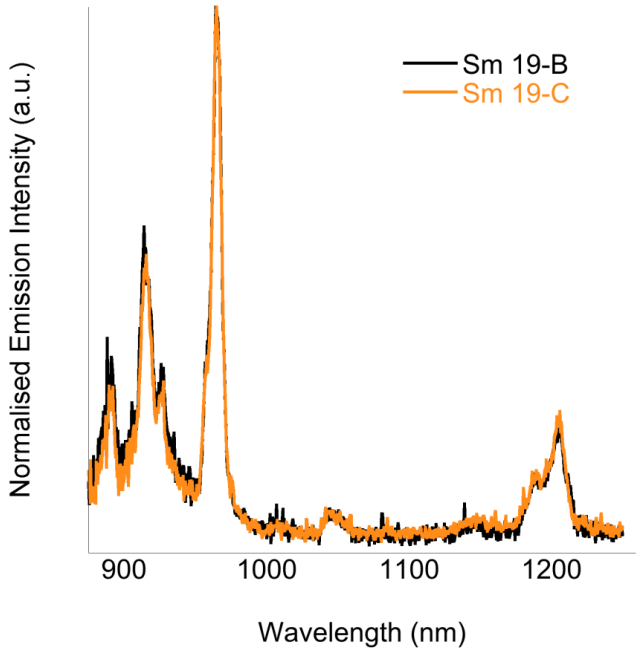

Figure 5.14: Normalised NIR emission spectra of the Sm_{19} species at room temperature in the solid state.

The samarium bottlebrush species displays typical emission in the NIR, and has identical emission profiles for both Sm_{19}-B and Sm_{19}-C. This is similar to the species emission in the visible region.

The other NIR emissive bottlebrush is the ytterbium containing cluster. Ytterbium is different from other lanthanoids in that it emits *via* fluorescence rather than phosphorescence. This means that the spin of the excited state ($^2F_{5/2}$) and the ground state ($^2F_{7/2}$) is identical. The excited state of ytterbium is well below the triplet energy level of the ligand, with a gap of approximately 12,000 cm^{-1}, which is far from the optimal energy difference for efficient sensitisation of the lanthanoid. However, as can be seen in Figure 5.15, despite the significant energy gap there is still observable emission from each of the ytterbium species. A possible explanation for emission despite the large energy gap is that the energy is passing from the triplet excited state of the ligand to an energy sub level of ytterbium associated with the reduced Yb^{2+} state. The

ligand to metal charge transfer state varies in exact energy depending on the ligands coordinated to the ytterbium metal centre, but is usually reported in the region of 19,000 cm^{-1}.[170] This results in a significantly lower energy gap to the triplet state of the ligand than directly to the Yb^{3+} excited state.

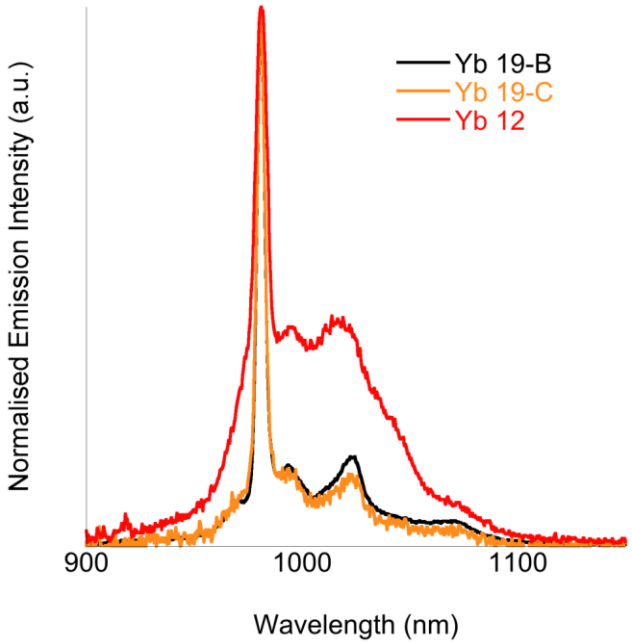

Figure 5.15: Normalised NIR emission spectra of the Yb_{19} species at room temperature in the solid state.

The highest intensity emission from the Yb^{3+} excited state ($^2F_{5/2}$) occurs at 980 nm. This peak corresponds to radiative decay to the lowest ground state ($^2F_{7/2}$). The peaks at higher wavelengths are a result of crystal field splitting which splits the J value of the ground state. The small shoulder at a lower wavelength than the main peak is actually emission from thermally accessible vibrational J sublevels of the $^2F_{5/2}$ state. These transitions are referred to as 'hot bands' in the literature.[171] Confirmation of their origin can be determined by measuring the emission spectrum at low temperature and comparing it to the room temperature measurement. This normalised spectral comparison, of the compound Yb_{19}-B, can be seen in Figure 5.16 and distinctly shows the loss of the hot band and increased emission of several of the crystal field splitting peaks of the $^2F_{5/2} \rightarrow {}^2F_{7/2}$ transition.

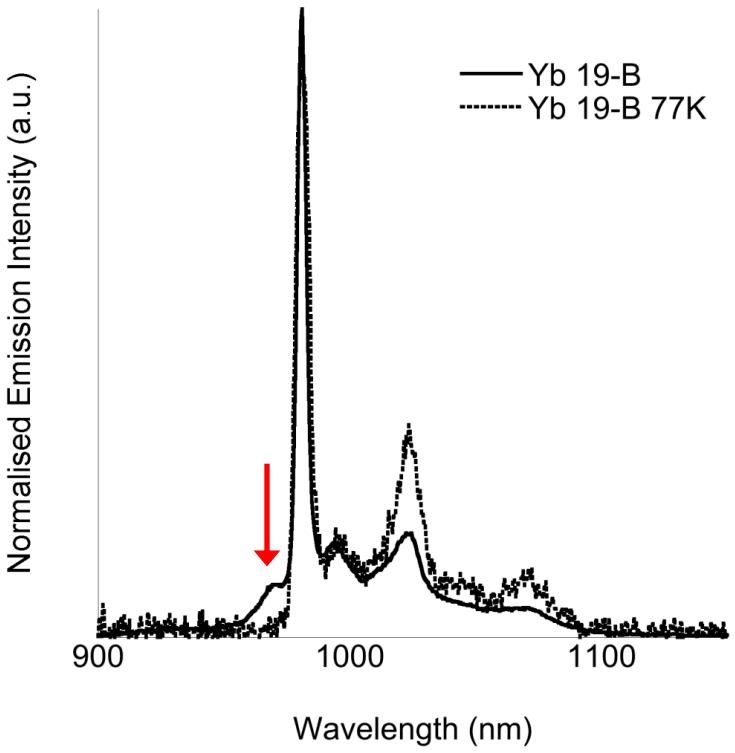

Figure 5.16: Normalised NIR emission spectra of the Yb_{19} species at room temperature *vs* 77K.

5.3 Conclusions

The preliminary photophysical investigation of the solid state bottlebrush samples demonstrated that the clusters are luminescent in both the visible and NIR range. More specifically; samarium, europium, terbium, dysprosium and thulium have typical visible emission, with the NIR emitters being samarium and ytterbium. Determination of the di-tetrazole calixarene ligands triplet state resulted in an energy of 26,320 cm^{-1} which is typical of calixarene complexes. The excitation spectra for the various clusters confirms the antenna effect, for both the visible and NIR emissions. Analysis of the europium spectra suggested the presence of multiple unique lanthanoid environments with a bi-exponential lifetime. This is consistent with the X-ray crystallography which shows two similar metal centres with a third being considerably different.

6 Conclusions and further work

Isolation and characterisation of three new tetrazolyl calixarene ligands was successful upon conversion of the lower rim nitrile substituents to tetrazole moieties. Significant optimisation of the reaction conditions used to form the nitrile derivatives was required, however, this resulted in the synthesis and characterisation of a new nitrile-calixarene molecule; the tri-nitrile calixarene **5**. Completing the series of calixarene substitutions with the synthesis of the mono-nitrile calixarene would not only complete the story, but would also be a useful comparison, in terms of coordination, once converted to the tetrazole moiety.

It was observed that at high temperatures the nitrile substituted calixarenes may not be conformationally stable, leading to conversion of the cone conformer. The percentage distribution of the conformations between the synthesis solutions and those prepared for rotation experiments was found to be dissimilar for most of the ligands. This

phenomenon was hypothesised to be a consequence of the metal templating effect where an alkali metal, sodium in this case, preferentially preorganises the calixarene in a particular conformation before addition of the nitrile functional groups. Determination of the activation energy of the nitrile rotation for the different substituents would allow for an examination of the effect of increased steric bulk on the percentage distribution of the different conformers.

Successful conversion of the nitrile substituents to tetrazole moieties resulted in the creation of three new ligands. These ligands were fully characterised and were all found to be in the desired cone conformation, ideal for coordination to metal ions. Due to the presence of acidic hydrogens on both the tetrazole and remaining calixarene phenols, crystallisation conditions employing a base to deprotonate the ligand were attempted. These yielded the mono-nuclear 1:1 complex with di-tetrazole calixarene ligand **1**. Unfortunately identical conditions used with the tri- and tetra-tetrazole calixarenes (**2** and **3**) failed to crystallise any metal complexes, only sodium adducts. It was hypothesised that the failure to form complexes with these two ligands was a mixture of both π stacking interactions, and the persistence of a strong intra-molecular hydrogen bond between the tetrazole N-H and the distal phenoxy oxygen. The current crystallisation conditions failed to disrupt both of these interactions as they were consistent features in all crystal structures determined. As a result, further work could include crystallisation conditions that involve the initial input of additional energy to try and interrupt one or both of these interactions, hopefully leading to the isolation of mono-nuclear 1:1 complexes with these higher dentate ligands.

Addition of a co-ligand, aqueous ammonium acetate, to the di-tetrazole calixarene crystallisations resulted in the characterisation of an unprecedented discrete linear lanthanoid hydroxo cluster. This cluster had the formulation of; $[Ln_{19}(\mathbf{1}\text{-}3H)(\mathbf{1}\text{-}2H)_{11}(CH_3CO_2)_6(OH)_{26}(H_2O)_{30}]$. Variation of numerous crystallisation conditions observed that the crystallisation of the Ln_{19} structure was remarkably

reproducible, with usually only changes occurring in the crystal packing of the large molecules. One variation, the change of the co-ligand, demonstrated that the cluster was specific to the species added. As upon addition of an aqueous ammonium benzoate solution to the crystallisation, a new discrete cluster was formed; $[Ln_{12}(\mathbf{1}\text{-}3H)_3(\mathbf{1}\text{-}2H)_3(PhCO_2)_6(OH)_{16}(H_2O)_{21}]$. This benzoate capped cluster had an identical trigonal bipyramidal lanthanoid hydroxo cluster motif, however, it was reduced in length. The ability to alter the length of these linear clusters with a simple substitution of the co-ligand implores for an investigation into the possible structure-activity relationship between the length of the lanthanoid hydroxo core and the species of co-ligand used.

An attempt at observing the formation/presence/indication of cluster sized species within solution was performed using dynamic light scattering (DLS), ^1H NMR and photophysical measurements. The results for all solution state methods were not quantitative, however, DLS measurements showed a trend towards a higher average size distribution along with an increase in peak width upon subsequent aliquots of ammonium acetate. This trend was also extended to the addition of ammonium benzoate under the same conditions. Hence, addition of different co-ligands in solution could further exploit the possible correlation between the DLS results and solid state characterisation. Photophysical measurements identified that a lifetime symptomatic of the 1:1 mono-nuclear complex was predominant in solution upon addition of triethylamine. When ammonium acetate was added, the lifetime was best fitted to a bi-exponential decay with a shorter lifetime attributed to the 1:1 complex, and components of a second longer lifetime inconsistent with the uncoordinated metal. These lifetime results were similar to those obtained for the Ln_{19} cluster in the solid state, suggesting a possible correlation of the presence of cluster type species in solution. Additional solution state photophysical studies on the tri/tetra-tetrazole calixarenes **2** and **3** could help further identify a trend in the emission/excitation/lifetime indicating cluster formation.

A detailed exploration of the cluster crystal structures showed extensive hydrogen bond networks in the second coordination sphere, suggesting that these interactions are stabilising the formation of the cluster core. The di-tetrazole calixarene **1** only coordinates to the lanthanoid core through one tetrazole moiety per calixarene. This tri-dentate mono-tetrazole coordination then leaves the other tetrazole to interact as a crucial component of the hydrogen bond network. Synthesis and subsequent crystallisation of the mono-tetrazole calixarene under identical conditions would allow for a systematic investigation into the extent of stabilisation that the second sphere interactions have on cluster formation and persistence. It would also be interesting to explore the possible formation of clusters with the addition of further tetrazole moieties on the calixarene scaffold, i.e. the tri/tetra-tetrazole calixarenes **2** and **3**.

Despite the interest in the formation of polynuclear metal clusters, there is currently insufficient knowledge to reliably predict a structure from a set of ligands.[111,122] Along with this lack of knowledge, there is also a limitation in the synthetic ability to control the formation of polynuclear species, restricting the characterised shapes and sizes to a narrow range.[117] This work not only introduces a new shape into the expanding library of lanthanoid hydroxo cluster morphologies, but by demonstrating that there is a possibility to adjust only one dimension of the structure, also gives additional insight into the possible structure activity relationship these structures possess. Better control of lanthanoid structural chemistry will ultimately underpin ongoing development of the application of these elements, which currently includes phosphors for lighting, bioimaging probes, amplifiers for fiber-optic communication, luminescent tags for biological molecules, and contrast agents for magnetic resonance imaging.[52,122,126,172]

7 Experimental

General Procedures

All reagents were purchased from Sigma Aldrich or Alfa Aesar and used as received, with no further purification. All procedures concerning synthesis of the ligands was carried out under a nitrogen atmosphere using standard Schlenk techniques. All crystallisations and metal salt synthesis were isolated and grown under atmospheric conditions in a standard climate controlled laboratory.

Nuclear magnetic resonance spectra (consisting of ^{1}H, ^{13}C, HMBC, HSQC and COSY experiments) were recorded using a Bruker Avance 400 spectrometer (400.1 MHz for ^{1}H, 100 MHz for ^{13}C) at room temperature, ^{1}H and ^{13}C chemical shifts were referenced

to residual solvent resonances. The assignment of peaks for the calixarene based compounds is based on the combination of HMBC, HSQC and COSY 2D spectra.

Infrared spectra were all recorded in the solid state using the Perkin Elmer Spectrum 100 FT-IR spectrometer with a diamond stage attenuated total reflectance attachment. Compounds were scanned from 650 - 4000 cm^{-1}. The intensities of the IR bands were reported as broad (b), strong (s), medium (m) or weak (w) as appropriate.

Elemental analyses were performed by Dr Thomas Rodemann at the Central Science Laboratory, University of Tasmania or by Robert Herman at the Department of Chemistry, Curtin University. All analyses were performed on samples that had not been dried under high vacuum to ensure uniform inclusion of solvent within the cavity of the calixarene.

Melting points were determined using a BI Barnsted Electrothermal 9100 apparatus and are uncorrected for temperature and pressure.

Absorption spectra were recorded at room temperature using the Perkin Elmer Lambda 35 UV/Vis spectrometer. Uncorrected steady state emission and excitation spectra were recorded on an Edinburgh FLSP980-S2S2-stm spectrometer equipped with: i) a temperature monitored cuvette holder; ii) 450 W Xenon arc lamp; iii) double excitation and emission monchromators; iv) a Peltier cooled Hamamatsu R928P photomultiplier tube for detection of visible radiation (spectral range 200-870 nm); v) and a Hamamatsu R5509-42 photomultiplier for detection of NIR radiation (spectral range 800-1400 nm). Emission and excitation spectra were corrected for source intensity (lamp and grating) and emission spectral response (detector and grating) by a calibration curve supplied with the instrument.

Emission lifetimes (τ) were determined using the time correlated single photon counting technique (TCSPC) with the same Edinburgh FLSP980-S2S2-stm spectrometer. The excitation source was a pulsed high energy xenon flashlamp (μF2) and the above-mentioned photomultiplier tube(s) as detector(s). The goodness of fit was assessed by minimising the reduced χ^2 function and by visual inspection of the weighted residuals.

All 77K luminescence spectra were recorded with samples placed in quartz tubes (2mm in diameter) and inserted into a quartz dewar filled with liquid nitrogen.

The solvent(s) used for the preparation of solutions intended for photophysical investigation were of analytical HPLC grade in the case of dichloromethane, while both the ethanol and ethyl acetate were reagent grade solvents.

Experimental uncertainties are estimated to be ±8% for lifetime determinations, ±2 nm and ±5 nm for absorption and excitation/emission peaks respectively.

All crystals were grown at Curtin University laboratories by the candidate and were then sent away for analysis to the Centre for Microscopy, Characterisation and Analysis (CMCA) where crystallographers; Associate Professor Brian Skelton and Dr. Alexandre Sobolev both performed data collection and refinement. Crystallographic data was collected on either an Oxford Diffraction Gemini diffractometer using Cu Kα radiation (λ = 1.54178 Å), or an Oxford Diffraction Xcalibur diffractometer using Mo Kα radiation (λ = 0.71073 Å). Following multi-scan or analytical absorption corrections and solution by direct methods, the structures were refined against F^2 with full-matrix least-squares using the programs SHELXL-97 or SHELX-2013. Final R indices are quoted for those reflections with $I > 2\sigma(I)$. CIF's containing the crystal data have been deposited with the Cambridge Crystallographic Data Centre. These data can be obtained free of charge *via* http://www.ccdc.cam.ac.uk/data_request/cif. Crystal data including more detailed refinement information are listed in appendix A.

Synthesis of $1^2,3^2,5^2,7^2$-tetrahydroxy-$1^5,3^5,5^5,7^5$-*tert*butylcalix[4]arene

p-tert-Butylphenol (65.28 g, 0.43 mol) was added to formaldehyde (32.60 g, 1.12 mol), sodium hydroxide (0.98 g, 0.02 mol) and water (1 mL). The solution was then heated at 100°C, until a yellow foam expanded. The foam was cooled to room temperature and diphenyl ether (600 mL) was added. The yellow/brown solution was heated at a state of reflux with a stream of nitrogen blowing over the mixture to remove water. After 30 minutes the nitrogen was replaced with a condenser and heated to reflux for a further 3 hours. After this time, the reaction was cooled and ethyl acetate (1 L) was added and stirred for 30 minutes. The solution was filtered and the beige crystals were washed sequentially with acetic acid (20 mL), water (100 mL) and acetone (10 mL). The resulting white crystals were recrystallised from toluene (250 mL). White platelet crystals resulted (23.29 g, 34%). MP = 340-342°C. ^{1}H NMR ($CDCl_3$, δ, ppm) 10.34 (s, 4H, Ar-O**H**), 7.05 (s, 8H, *m* Ar-**H**), 4.26 (broad s, 4H, Ar-C$\mathbf{H_2}$-Ar), 3.49 (broad s, 4H, Ar-C$\mathbf{H_2}$-Ar), 1.21 (s, 36H, C-C$\mathbf{H_3}$). IR (ATR): ν/cm^{-1} 3167 (b), 3058 (w), 2952 (s), 2868 (w), 1605 (w), 1480 (s), 1461 (m), 1361 (m), 1303 (w), 1200 (m), 1124 (w), 870 (w), 814 (w), 781 (m), 695 (w).

Synthesis of $1^2,5^2$-dicyanomethoxy-$3^2,7^2$-dihydroxy-$1^5,3^5,5^5,7^5$-*tert*butylcalix[4]arene

Potassium iodide (9.62 g, 57.90 mmol) was added to dry THF (150 mL) and allowed to stir for five minutes. To this, chloroacetonitrile (7.00 mL, 111.70 mmol) was added dropwise and stirred overnight. This resulted in a bright yellow solution with a white precipitate. The white solid was filtered off and *p*-tertbutyl-calix[4]arene (13.03 g, 20.10 mmol) along with potassium carbonate (10.04 g, 72.60 mmol) were added to the clear yellow solution. This was heated to reflux overnight producing a brown solution with a dark brown precipitate. The solution was allowed to cool and then filtered through celite. The celite was washed with DCM (3×50 mL) producing a brown filtrate which was dried over magnesium sulfate. The solvent was removed under reduced pressure and recrystallised from a minimum volume of chloroform which furnished the nitrile calixarene **4** as a white powder. (8.75 g, 79%)

MP = 312°C with decomposition. ^{1}H NMR ($CDCl_3$, δ, ppm) 7.12 (s, 4H, Ar-**H**), 6.73 (s, 4H, Ar-**H**), 5.54 (s, 2H, Ar-O**H**), 4.81 (s, 4H, Ar-O-C**H$_2$**), 4.23 (d, 4H, *axial* Ar-C**H**$_2$-Ar, J=13.4 Hz), 3.45 (d, 4H, *equatorial* Ar-C**H$_2$**-Ar, J=13.5 Hz), 1.33 (s, 18H, Ar-CC**H$_3$**), 0.88 (s, 18H, Ar-CC**H$_3$**). ^{13}C NMR ($CDCl_3$, δ, ppm) 150.0, 148.8, 148.6, 142.6, 131.9, 127.9, 126.3, 125.4, 115.2, 60.5, 34.1, 34.0, 32.1, 31.8. IR (ATR): ν/cm^{-1} 3502 (m), 2956 (s), 2905 (m), 2868 (m), 1598 (w), 1479 (s), 1430 (m), 1362 (m), 1190 (m), 1014 (m), 872 (w).

Synthesis of 1^2,5^2-ditetrazolyl-3^2,7^2-dihydroxy-1^5,3^5,5^5,7^5-*tert*butylcalix[4]arene

Toluene (65 mL) was placed into a round bottom flask immersed in an ice bath. To the cold solvent, triethylamine (5.00 mL, 35.82 mmol) and hydrochloric acid (2.50 mL, 25.01 mmol) was added and the flask stoppered immediately. A white gas was evolved but upon stirring the solution for ten minutes this dissolved into solution resulting in a white residue on the walls of the flask. Calixarene **4** (5.09 g, 7.00 mmol) was then added to the solution along with sodium azide (2.01 g, 30.92 mmol) and heated to reflux for 12 hours. The solution was cooled to room temperature and the solvent was removed under reduced pressure yielding a white solid. The residue was dissolved in ethyl acetate resulting in a cloudy white solution which was filtered and then washed with hydrochloric acid (1 M, 3×100 mL). The organic fraction was dried over magnesium sulfate and solvent removed by distillation under reduced pressure. The residue was recrystallised from DCM furnishing tetrazole calixarene **1** as a white crystalline solid (3.76 g, 66%) MP = 253°C with decomposition. ^{1}H NMR ($CDCl_3$, δ, ppm) 7.08 (s, 4H, Ar-**H**), 7.00 (s, 4H, Ar-**H**), 5.50 (s, 4H, Ar-O-C**H$_2$**), 4.10 (d, 4H, *axial* Ar-C**H**$_2$-Ar, J=13.4 Hz), 3.50 (d, 4H, *equatorial* Ar-C**H$_2$**-Ar, J=13.5 Hz), 1.23 (s, 18H, Ar-CC**H$_3$**), 1.08 (s, 18H, Ar-CC**H$_3$**). ^{13}C NMR ($CDCl_3$, δ, ppm) 149.3, 149.1, 149.0, 143.7, 132.5, 127.4, 126.6, 125.9, 68.5, 53.52, 34.4, 34.1, 32.5, 31.7, 31.1. IR (ATR): ν/cm^{-1} 3390 (m), 3135 (w), 3050 (w), 2951 (s), 2904 (m), 2869 (m), 1600 (w), 1558 (w), 1483 (s), 1361 (m), 1193 (s), 873 (m).

Synthesis of 1^2,3^2,5^2-tricyanomethoxy-7^2-hydroxy-1^5,3^5,5^5,7^5-*tert*butylcalix[4]arene

A barium hydroxide (0.17 g, 0.55 mmol), barium oxide (0.08 g, 0.55 mmol) mixture was added to dry DMF (25 mL) and allowed to stir for 45 minutes at room temperature under a nitrogen atmosphere. To this, calix[4]arene **4** (0.51 g, 0.70 mmol) was allowed to stir for a further 30 minutes. Bromoacetonitrile (0.14 mL, 2.06 mmol) was then added and the resulting beige solution was stirred overnight at room temperature. This resulted in a black, completely opaque solution. Hydrochloric acid (50 mL, 1 M) was slowly added causing a pale brown precipitate to evolve, which was filtered off and washed several times with water. The cream coloured solid is a mixture of both calixarene **5** and **6** with the tri-nitrile calixarene **5** component calculated as (0.37 g, 69%) MP = 254°C. ^{1}H NMR (DMSO, δ, ppm) 7.27 (s, 2H, Ar-**H**), 7.15 (s, 2H, Ar-**H**), 6.79 (d, 2H, Ar-**H**, J=2.4 Hz), 6.63 (d, 2H, Ar-**H**, J=2.4 Hz), 4.96 (d, 4H, Ar-O-C**H$_2$**, J=2.2 Hz), 4.83 (s, 2H, Ar-O-C**H$_2$**), 4.26 (d, 2H, *axial* Ar-C**H**$_2$-Ar, J=13.2 Hz), 4.05 (d, 2H, *axial* Ar-C**H**$_2$-Ar, J=13.3 Hz), 3.45 (d, 2H, *equatorial* Ar-C**H$_2$**-Ar, J=13.5 Hz), 3.35 (d, 2H, *equatorial* Ar-C**H**$_2$-Ar, J=13.2 Hz), 1.28 (s, 9H, Ar-CC**H$_3$**), 1.27 (s, 9H, Ar-CC**H$_3$**), 0.89 (s, 18H, Ar-CC**H$_3$**). ^{13}C NMR (DMSO, δ, ppm) 151.6, 150.7, 150.4, 147.6, 146.6, 135.3, 132.5, 132.3, 128.2, 126.6, 126.0, 125.6, 125.5, 118.4, 117.4, 60.15, 57.9, 34.5, 34.0, 33.9, 32.0, 31.9, 31.7, 31.1. IR (ATR): ν/cm^{-1} 3525 (m), 3135 (w), 2959 (s), 2905 (m), 2868 (m), 1600 (w), 1479 (s), 1362 (m), 1190 (s), 1024 (m), 873 (m).

Synthesis of 1^2,3^2,5^2-tritetrazolyl-7^2-hydroxy-1^5,3^5,5^5,7^5-*tert*butylcalix[4]arene

Toluene (20 mL) was placed into a round bottom flask immersed in an ice bath. To the cold solvent, triethylamine (0.43 mL, 4.97 mmol) and hydrochloric acid (0.29 mL, 4.97 mmol) was added and the flask stoppered immediately. A white gas was evolved but upon stirring the solution for five minutes this dissolved into solution resulting in a white residue on the walls of the flask. Calixarene **5** (0.47 g, 0.50 mmol) was then added to the solution along with sodium azide (0.25 g, 3.21 mmol) and heated at a state of reflux for 12 hours. The solution was cooled to

room temperature and the solvent was removed under reduced pressure yielding a white solid. The residue was dissolved in ethyl acetate resulting in a cloudy pale cream solution which was filtered and washed with hydrochloric acid (1 M, 3×50 mL). The organic fraction was dried over magnesium sulfate, filtered and solvent removed by reduced pressure evaporation. The residue was dissolved in a minimum amount of acetonitrile and purified via HPLC chromatography using a Waters prep HPLC column. An isocratic run was performed with 80% water 10% acetonitrile and 10% of a 1% trifluoroacetic acid aqueous solution. Retention time was 26.3 mins furnishing the tetrazole calixarene **2** as a white solid (0.39 g, 81%) MP = 263°C with decomposition. ^{1}H NMR (DMSO, δ, ppm) 7.32 (s, 2H, Ar-**H**), 7.14 (s, 2H, Ar-**H**), 6.64(5) (2, dH, Ar-**H**, J=1.64 Hz), 6.57 (d, 2H, Ar-**H**, J=1.64 Hz), 5.26 (s, 2H, Ar-O-C**H$_2$**), 5.02 (d, 2H, Ar-O-C**H$_2$**, J=12.6 Hz), 4.94 (d, 2H, Ar-O-C**H$_2$**, J=12.6 Hz), 4.06 (d, 2H, *axial* Ar-C**H**$_2$-Ar, J=12.9 Hz), 4.02 (d, 2H, *axial* Ar-C**H**$_2$-Ar, J=12.9 Hz), 3.21 (d, 2H, *equatorial* Ar-C**H$_2$**-Ar, J=13.6 Hz), 3.20 (d, 2H, *equatorial* Ar-C**H$_2$**-Ar, J=12.4 Hz), 1.30 (s, 9H, Ar-CC**H$_3$**), 1.27 (s, 9H, Ar-CC**H$_3$**), 0.80 (s, 18H, Ar-CC**H$_3$**). ^{13}C NMR (DMSO, δ, ppm) 151.3, 149.4, 146.9, 145.9, 141.47, 135.0, 131.9, 131.5, 127.6, 126.0, 125.2, 125.1, 125.0, 64.8, 63.6, 34.0, 33.6, 33.4, 31.5, 31.3, 30.6, 30.3, 30.0 N.B. Tetrazole carbon not observed. (m+1)/z = 895.442,

(m-1)/z = 893.486. IR (ATR): ν/cm^{-1} 3524 (w), 3209 (w), 2955 (s), 2868 (m), 1791 (w), 1585 (w) 1567 (w), 1481 (s), 1362 (m), 1301 (w), 1194 (s), 1119 (m), 1002 (m), 870 (m).

Synthesis of 1^2,3^2,5^2,7^2-tetracyanomethoxy-1^5,3^5,5^5,7^5-*tert*butylcalix[4]arene (cone)

Sodium hydride (1.06 g, 43.97 mmol) and calixarene **4** (2.13 g, 2.93 mmol) were added to dry DMF (100 mL) and allowed to stir for 20 minutes. To this, bromoacetonitrile (0.96 mL, 13.7 mmol) was added and stirred overnight at room temperature under a nitrogen atmosphere. This resulted in a black completely opaque solution. Water (150 mL) was slowly added causing a pale brown precipitate to occur, which was filtered off and washed several times with water. The solid,

consisting of conformational isomers **6** and **7**, was dissolved in a minimum amount of DCM and separated using a silica column with straight DCM as the eluent. The organic volatiles were evaporated leaving a white solid which upon characterisation proved to be tetra-nitrile calixarene **6** (1.62 g, 69%). ^{1}H NMR (DMSO, δ, ppm) 6.91 (s, 8H, Ar-**H**), 2.00 (s, 8H, Ar-O-C**H$_2$**), 4.28 (d, 4H, *axial* Ar-C**H**$_2$-Ar, J=13.2 Hz), 3.32 (d, 4H, *equatorial* Ar-C**H$_2$**-Ar, J=13.3 Hz), 1.05 (s, 36H, Ar-CC**H$_3$**). ^{13}C NMR (DMSO, δ, ppm) 151.5, 146.7, 133.8, 125.8, 118.0, 59.5, 34.2, 31.7, 31.4. IR (ATR): ν/cm^{-1} 2959 (s), 2868 (m), 1604 (w), 1473 (s), 1362 (m), 1190 (s), 1024 (s), 878 (w).

Synthesis of 1^2,3^2,5^2,7^2-tetracyanomethoxy-1^5,3^5,5^5,7^5-*tert*butylcalix[4]arene (partial cone)

Sodium hydride (0.10 g, 4.13 mmol) and calixarene **4** (0.50 g, 0.69 mmol) were added to dry THF (60 mL) and allowed to stir for 30 minutes. To this, bromoacetonitrile (0.19 mL, 2.75 mmol) was added and stirred overnight at room temperature under a nitrogen atmosphere. This resulted in a dark brown solution. The solvent was removed under reduced pressure, and the brown solid redissolved in dichloromethane. The organic was washed with water (3×50 mL) which had a dark brown semi solid within the water layer. The organics were removed leaving a slight brown solid. The solid was purified via column chromatography using dichloromethane, resulting in the product eluting as the first spot as a white solid which upon characterisation proves to be partial cone tetra-nitrile calixarene **7** (0.156 g, 28%) MP = 288°C. ^{1}H NMR (DMSO-d$_6$, δ, ppm) 7.37 (s, 2H, Ar-**H**), 7.23 (s, 2H, Ar-**H**), 7.01 (d, 2H, Ar-**H**, J=2.5 Hz), 6.60 (d, 2H, Ar-**H**, J=2.4 Hz), 4.81 (dd, 4H, Ar-O-C**H$_2$**, J=11.2 Hz), 4.53 (s, 2H, Ar-O-C**H$_2$**), 4.08 (d, 2H, Ar-C**H**$_2$-Ar, J=13.4 Hz), 3.86 (d, 2H, Ar-C**H$_2$**-Ar, J=14.4 Hz), 3.77 (d, 2H, Ar-C**H$_2$**-Ar, J=14.4 Hz), 3.25 (d, 2H, Ar-C**H$_2$**-Ar, J=13.6 Hz), 1.41 (s, 9H, Ar-CC**H$_3$**), 1.29 (s, 9H, Ar-CC**H$_3$**), 1.02 (s, 18H, Ar-CC**H$_3$**). ^{13}C NMR ($CDCl_3$, δ, ppm) 153.5, 152.0, 151.2, 147.5, 146.0, 145.2. 135.4, 133.1, 132.5, 131.9, 128.2, 126.6, 126.4, 125.8, 118.3, 117.9, 117.7, 58.7, 56.9, 56.7, 67.7, 34.5, 34.3, 34.0, 31.8, 31.7, 31.6, 31.4. IR (ATR): ν/cm^{-1} 2957 (s), 2868 (m), 1600 (w), 1474 (s), 1362 (m), 1188 (s), 1024 (s), 875 (m).

Synthesis of 1^2,3^2,5^2,7^2-tetratetrazolyl-1^5,3^5,5^5,7^5-*tert*butylcalix[4]arene (cone)

Toluene (30 mL) was placed into a round bottom flask immersed in an ice bath. To the cold solvent, triethylamine (0.69 mL, 4.97 mmol) and hydrochloric acid (0.48 mL, 4.97 mmol) was added and the flask stoppered immediately. A white gas was evolved but upon stirring the solution for five minutes this dissolved into solution resulting in a white residue on the walls of the flask. Calixarene **6** (0.40 g, 0.50 mmol) was then added to the solution along with sodium azide (0.21 g, 3.21 mmol) and heated to reflux for 12 hours. The solution was cooled to room temperature and the solvent was removed under reduced pressure yielding a white solid. The residue was dissolved in ethyl acetate resulting in a cloudy pale cream solution which was filtered and washed with hydrochloric acid (1 M, 3×50 mL). The organic fraction was dried over magnesium sulfate, filtered and solvent removed by reduced pressure evaporation. The residue was washed with small amounts of cold DCM to remove the coloured impurity, furnishing the tetrazole calixarene **3** as a white solid (0.39 g, 81%) MP = 246°C with decomposition. ^{1}H NMR (DMSO, δ, ppm) 6.81 (s, 8H, Ar-**H**), 5.21 (s, 8H, Ar-O-C**H$_2$**), 3.84 (d, 4H, *axial* Ar-C**H**$_2$-Ar, J=12.7 Hz), 2.95 (d, 4H, *equatorial* Ar-C**H$_2$**-Ar, J=12.8 Hz), 1.02 (s, 36H, Ar-CC**H$_3$**). ^{13}C NMR (DMSO, δ, ppm) 151.4, 145.1, 133.2, 125.1, 63.0, 33.6, 31.0, 30.7, 30.4 N.B. Tetrazole carbon not observed. (m+1)/z = 977.514 (m+Na)/z = 999.517. IR (ATR): ν/cm^{-1} 3279 (w), 2961 (s), 2904 (m), 2869 (m), 1780 (w) 1574 (w), 1479 (s), 1363 (m), 1302 (w), 1192 (s), 1124 (m), 1006 (m), 871 (m).

Synthesis of 1^2,5^2-diamide-3^2,7^2-dicyanomethoxy-1^5,3^5,5^5,7^5-*tert*butylcalix[4]arene

THF (50 mL) was placed into a round bottom flask containing calixarene **4** (0.44 g, 0.60 mmol) and sodium hydride (0.10 g, 2.52 mmol). This mixture was stirred for 30 minutes at room temperature. *N*,*N*-diethylchloroacetamide (0.33 mL, 2.40 mmol) and potassium iodide (0.46 g, 2.80 mmol) was added to the pale yellow cloudy solution. The reaction was heated at reflux for 12 hours. The brown solution was reduced to dryness leaving a brown solid which was redissolved in DCM. The organic fraction

was washed with hydrochloric acid (1 M, 3×50 mL). The organic layer was dried over magnesium sulphate and distilled under reduced pressure. The resulting solid was separated into its different components using column chromatography and a 5% methanol in DCM mixture. This resulted in three different fractions being collected. First fraction: *p*-tertbutyl-calix[4]arene, second fraction: di-amide di-nitrile partial cone **9** (0.38 g, 66%) and third fraction: di-amide di-nitrile cone **8** (0.13 g, 22%)

Partial Cone

MP = 256°C with decomposition. ^{1}H NMR (DMSO, δ, ppm) 7.36 (s, 2H, Ar-**H**), 7.18 (s, 2H, Ar-**H**), 6.95 (d, 2H, Ar-**H,** J=2.5 Hz), 6.50 (d, 2H, Ar-**H,** J=2.5 Hz), 4.69 (s, 2H, Ar-O-C**H$_2$**CN), 4.63 (d, 2H, Ar-O-C**H$_2$**CON, J=13.6 Hz), 4.52 (s, 2H, Ar-O-C**H$_2$**CN), 4.27 (d, 2H, Ar-O-C**H$_2$**CON, J=13.6 Hz), 4.15 (d, 2H, Ar-C**H**$_2$-Ar, J=13.3 Hz), 3.94 (d, 2H, Ar-C**H**$_2$-Ar, J=13.8 Hz), 3.67 (d, 2H, Ar-C**H**$_2$-Ar, J=13.8 Hz), 3.45-3.23 (broad m, 4H, N-C**H$_2$**-CH$_3$), 3.17 (d, 2H, Ar-C**H$_2$**-Ar, J=13.4 Hz), 1.31 (s, 9H, Ar-CC**H$_3$**), 1.30 (s, 9H, Ar-CC**H$_3$**), 1.18-1.03 (t, 12H, N-CH$_2$-C**H$_3$**, J=7.0 Hz), 1.01 (s, 18H, Ar-CC**H$_3$**). ^{13}C NMR ($CDCl_3$, δ, ppm) 167.1, 154.4, 153.6, 151.2, 146.8, 144.6, 144.5, 136.2, 132.9, 131.9, 128.7, 126.2, 125.7, 12.54, 118.6, 118.1, 71.3, 56.9, 56.5, 36.8, 34.4, 34.2, 33.9, 31.8, 31.6, 19.0, 14.9, 13.5. IR (ATR): ν/cm^{-1} 2954 (s), 2905 (m), 2870 (m), 1655 (s), 1480 (s), 1361 (m), 1197 (s), 1124 (m), 1029 (m), 870 (w).

Cone

MP = 257°C. ^{1}H NMR (DMSO, δ, ppm) 7.25 (s, 4H, Ar-**H**), 6.45 (s, 4H, Ar-**H**), 5.55 (s, 4H, Ar-O-C**H$_2$**CON), 4.47 (s, 4H, Ar-O-C**H$_2$**CN), 4.27 (d, 4H, *axial* Ar-C**H**$_2$-Ar, J=13.0 Hz), 3.40-3.30 (broad m, 4H, N-C**H$_2$**-CH$_3$), 3.28-3.10 (broad m, 4H, N-C**H$_2$**-CH$_3$ and 4H, *equatorial* Ar-C**H$_2$**-Ar), 1.31 (s, 18H, Ar-CC**H$_3$**), 1.16-1.04 (m, 12H, N-CH$_2$-C**H$_3$**), 0.77 (s, 18H, Ar-CC**H$_3$**). ^{13}C NMR ($CDCl_3$, δ, ppm) 167.2, 152.2, 152.1, 147.0, 144.7, 136.2, 131.9, 126.0, 124.8, 118.5, 77.4, 58.8, 34.5, 33.7, 31.8, 31.1, 14.6, 13.5. IR (ATR): ν/cm^{-1} 2957 (s), 2868 (m), 1600 (w), 1474 (s), 1362 (m), 1188 (s), 1024 (s), 875 (m).

Synthesis of 1^2-amide-3^2,5^2,7^2-tricyanomethoxy-1^5,3^5,5^5,7^5-*tert*butylcalix[4]arene

THF (50 mL) was placed into a round bottom flask containing tri-nitrile calixarene **5** (0.53 g, 0.69 mmol) and sodium hydride (0.06 g, 2.63 mmol). This mixture was stirred for 30 minutes at room temperature. A solution of *N*,*N*-diethylchloroacetamide (0.36 mL, 2.63 mmol) and potassium iodide (0.33 g, 1.97 mmol) in THF was added dropwise to the cloudy solution. The reaction was then heated at a state of reflux for 12 hours. The yellow solution was reduced to dryness leaving a yellow oil which was redissolved in DCM. The organic fraction was washed with hydrochloric acid (1 M, 3×50 mL), dried over magnesium sulphate and distilled under reduced pressure. The resulting solid was purified by column chromatography, using a 70/30 petroleum spirit/ethyl acetate mixture. Product eluted as the first spot, which upon characterisation proved to be pure mono-amide tri-nitrile calixarene **10** (0.39 g, 65%) MP = 248°C with decomposition. ^{1}H NMR (DMSO, δ, ppm) 7.28 (d, 2H, Ar-**H**, J=2.5 Hz), 7.26 (d, 2H, Ar-**H**, J=2.5 Hz), 6.53 (s, 2H, Ar-**H**), 6.49 (s, 2H, Ar-**H**), 5.58 (d, 2H, Ar-O-C**H$_2$**CN, J=16.8 Hz), 5.07 (d, 2H, Ar-O-C**H$_2$**CN, J=16.8 Hz), 4.91 (s, 2H, Ar-O-C**H$_2$**CON), 4.47 (s, 2H, Ar-O-C**H$_2$**CN), 4.39 (d, 2H, Ar-C**H**$_2$-Ar, J=12.8 Hz), 4.19 (d, 2H, Ar-C**H**$_2$-Ar, J=12.9 Hz), 3.46-3.38 (m, 4H, N-C**H$_2$**-CH_3,), 3.34-3.18 (m, 4H, Ar-C**H$_2$**-Ar), 1.31 (s, 18H, Ar-CC**H$_3$**), 1.14-1.08 (m, 6H, N-CH_2-C**H$_3$**), 0.80 (s, 9H, Ar-CC**H$_3$**), 0.79 (s, 9H, Ar-CC**H$_3$**). ^{13}C NMR ($CDCl_3$, δ, ppm) 167.3, 152.6, 151.9, 150.5, 147.2, 145.8, 144.9, 135.8, 135.7, 132.3, 131.8, 126.4, 126.0, 125.1, 125.0, 118.7, 117.5, 70.5, 60.3, 58.5, 56.5, 34.5, 33.8, 33.7, 31.8, 31.4, 31.1, 19.0, 14.5, 13.5. IR (ATR): ν/cm^{-1} 2961 (s), 2908 (m), 2868 (m), 1648 (m), 1480 (s), 1362 (w), 1196 (s), 1030 (m), 871 (w).

Synthesis of 1^2-benzoyl-3^2,5^2,7^2-trihydroxy-1^5,3^5,5^5,7^5-*tert*butylcalix[4]arene

To a round bottom containing DMF (60 mL), both *p*-tertbutyl-calix[4]arene (0.52 g, 0.79 mmol) and caesium fluoride (0.53 g, 3.85 mmol) were added and stirred for 30 minutes at room temperature. Benzoyl chloride (0.11 mL, 0.93 mmol) was added to the clear solution. The reaction was stirred at room temperature for 2 days. After this

time hydrochloric acid (1 M, 100 mL) was added causing a white precipitate to form. DCM (50 mL) was added and washed with water (3×50 mL), the organic fraction was dried over magnesium sulphate and distilled under reduced pressure. The resulting solid was purified via column chromatography using a 1:1 petroleum spirits:DCM mixture. A white solid was isolated which proved to be the desired product mono-benzoyl calixarene (0.23 g, 38%) MP = 303°C. ^{1}H NMR (DMSO, δ, ppm) 7.37 (s, 2H, Ar-**H**), 7.20 (s, 2H, Ar-**H**), 7.09 (t, 1H, Ar-**H** *benzoyl*), 6.85 (d, 2H, Ar-**H**, J=12.6 Hz), 6.63 (m, 4H, Ar-**H** *benzoyl*), 6.55 (d, 2H, Ar-**H**, J=12.6 Hz), 4.12 (d, 2H, *axial* Ar-C**H**$_2$-Ar, J=12.6 Hz), 3.95 (dd, 4H, Ar-C**H**$_2$-Ar, J=12.6 Hz), 3.53 (d, 2H, *equatorial* Ar-C**H$_2$**-Ar, J=12.7 Hz), 1.40 (s, 9H, Ar-CC**H$_3$**), 1.37 (s, 9H, Ar-CC**H$_3$**), 0.74 (s, 18H, Ar-CC**H$_3$**). IR (ATR): ν/cm^{-1} 3462 (m), 3343 (m), 2958 (s), 2908 (m), 2869 (m), 1751 (m), 1729 (m), 1602 (w), 1482 (s), 1452 (m), 1362 (m), 1258 (s), 1170 (s), 872 (m), 702 (m).

Synthesis of 1^2-benzoyl-5^2-cyanomethoxy-3^2,7^2-dihydroxy-1^5,3^5,5^5,7^5-*tert*butylcalix[4]arene

To a round bottom containing DMF (30 mL), mono-benzoyl calixarene (0.15 g, 0.20 mmol) and calcium hydride (0.11 g, 2.61 mmol) were added and stirred for 30 minutes at room temperature. Bromoacetonitrile (0.09 mL, 1.20 mmol) was added to the clear solution. The reaction was stirred at room temperature for 3 days. After this time hydrochloric acid (1 M, 100 mL) was added causing a white precipitate to form. DCM (50 mL) was added and washed with water (3×50 mL), the organic fraction was dried over magnesium sulphate and distilled under reduced pressure. The resulting solid was purified by column chromatography with a 1:1 petroleum spirits:DCM mixture as the eluent. A white solid was isolated which proved to be mono-benzoyl mono-nitrile calixarene (0.12 g, 74%) MP = 168°C with decomposition. ^{1}H NMR (DMSO, δ, ppm) 8.29 (d, 2H, Ar-**H** *benzoyl*, J=9.7 Hz), 7.58 (m, 3H, Ar-**H** *benzoyl*), 7.11 (d, 2H, Ar-**H**), 7.01 (d, 2H, Ar-**H**), 6.87 (s, 2H, Ar-**H**), 6.86 (s, 2H, Ar-**H**), 4.77 (s, 2H, Ar-O-C**H$_2$**), 4.13 (d, 2H, *axial* Ar-C**H**$_2$-Ar, J=12.6 Hz), 3.95 (d, 2H, *axial* Ar-C**H**$_2$-Ar, J=12.6 Hz), 3.55 (d, 2H, *equatorial* Ar-

C**H$_2$**-Ar, J=12.7 Hz), 3.43 (d, 2H, *equatorial* Ar-C**H$_2$**-Ar, J=12.7 Hz), 1.25 (s, 18H, Ar-CC**H$_3$**), 0.98 (s, 9H, Ar-CC**H$_3$**), 0.97 (s, 9H, Ar-CC**H$_3$**). IR (ATR): ν/cm^{-1} 3583 (w), 3134 (w), 2961 (s), 2904 (m), 2868 (m), 1604 (w), 1478 (s), 1361 (m), 1300 (w), 1192 (s), 871 (m).

Synthesis of 1^2-benzoyl-5^2-amide-3^2,7^2-dihydroxy-1^5,3^5,5^5,7^5-*tert*butylcalix[4]arene

To a round bottom stirring under a nitrogen atmosphere, DMF (100 mL), mono-benzoyl calixarene (0.50 g, 0.66 mmol), calcium hydride (0.17 g, 4.00 mmol) and potassium iodide (0.55 g, 3.33 mmol) were added and stirred for 30 minutes at room temperature. *N*,*N*-diethylchloroacetamide (0.45 mL, 3.27 mmol) was added to the clear solution. The reaction was stirred at room temperature for 3 days. After this time hydrochloric acid (1 M, 70 mL) was added causing a white precipitate to form. The white solid was filtered *via* vacuum filtration and dried in a dessicator. The isolated product was analysed as mono-benzoyl mono-amide calixarene (0.41 g, 72%) MP = 284°C. ^{1}H NMR ($CDCl_3$, δ, ppm) 8.57 (d, 2H, Ar-**H** *benzoyl*, J=9.6 Hz), 7.58 (m, 3H, Ar-**H** *benzoyl*), 7.05 (d, 2H, Ar-**H** *free phenol*, J=11.9 Hz), 7.03 (d, 2H, Ar-**H** *free phenol*, J=12.0 Hz), 6.89 (s, 2H, Ar-**H** *benzoyl substituted*), 6.76 (s, 2H, Ar-**H** *amide substituted*), 4.74 (s, 2H, Ar-O-C**H$_2$**), 4.12 (m, 4H, Ar-C**H**$_2$-Ar), 3.40 (m, 4H, Ar-C**H**$_2$-Ar), 1.26 (s, 18H, Ar-CC**H$_3$**), 1.24 (q, 4H, N-C**H$_2$**-CH_3, J=6.3 Hz), 1.15 (t, 6H, N-CH_2-C**H$_3$**, J=6.4 Hz), 1.01 (s, 9H, Ar-CC**H$_3$**), 0.88 (s, 9H, Ar-CC**H$_3$**). IR (ATR): ν/cm^{-1} 3393 (s), 2958 (s), 2904 (m), 2869 (m), 1723 (m), 1652 (s), 1482 (s), 1450 (s), 1361 (w), 1268 (s), 1174 (m), 872 (w).

Crystallisation Experiments

The di-tetrazole ligand **1** was crystallised by slow evaporation of DCM or acetonitrile resulting in clear rhombohedral crystals. Anal. Calculated for $C_{48}H_{60}O_4N_8.0.4CH_2Cl_2$: C, 68.63; H, 7.24; N, 13.23. Found C, 68.45; H, 7.14; N, 13.27.

The tri-tetrazole ligand **2** was crystallised by slow evaporation of DCM or acetonitrile resulting in clear rhombohedral crystals. Anal. Calculated for $C_{50}H_{62}O_4N_{12}.2H_2O$: C, 64.49; H, 7.145; N, 18.05, Found C, 64.25; H, 6.77; N, 17.76.

The tetra-tetrazole ligand **3** was crystallised by slow evaporation of ethanol resulting in clear rhombohedral crystals. Anal. Calculated for $C_{52}H_{64}O_4N_{16}.H_2O$: C, 62.75; H, 6.685; N, 22.52, Found C, 62.57; H, 6.45; N, 22.42.

The tri-nitrile calixarene **5** was crystallised by slow evaporation of a 1:1 chloroform:ethanol solvent mixture. Anal. Calculated for $C_{50}H_{59}O_4N_3$: C, 78.40; H, 7.76; N, 5.49, Found C, 78.40; H, 7.99; N, 5.35.

The tetra-nitrile calixarene **7** in the partial cone conformation, was crystallised by slow evaporation of a 1:1 chloroform:ethanol solvent mixture. Anal. Calculated for $C_{52}H_{60}O_4N_4$: C, 77.58; H, 7.51; N, 6.96, Found C, 77.86; H, 7.62; N, 7.01.

The di-amide di-nitrile calixarene **8** in the cone conformation was crystallised by slow evaporation of a 1:1 chloroform:ethanol solvent mixture. Anal. Calculated for $C_{60}H_{80}O_6N_4.[C_2H_6O]$: C, 74.51; H, 8.67; N, 5.61, Found C, 74.20; H, 8.42; N, 5.63.

The di-amide di-nitrile calixarene **9** in the partial cone conformation was crystallised by slow evaporation of a 1:1 chloroform:ethanol solvent mixture. Anal. Calculated for $C_{60}H_{80}O_6N_4.2[C_2H_6O]$: C, 73.53; H, 8.87; N, 5.36, Found C, 73.91; H, 8.43; N, 5.84.

The mono-amide tri-nitrile calixarene **10** in the cone conformation was crystallised by slow evaporation of a 1:1 chloroform:ethanol solvent mixture. Anal. Calculated for $C_{56}H_{70}O_5N_4.[C_2H_6O]$: C, 75.29; H, 8.28; N, 6.06, Found C, 75.40; H, 8.67; N, 5.71.

The mono-amide mono-benzoyl calixarene in the cone conformation was crystallised by slow evaporation of a 1:1 DCM:ethanol solvent mixture. Anal. Calculated for $C_{52}H_{70}O_5N_4.2[C_2H_6O]$: C, 76.45; H, 8.73; N, 1.46, Found C, 76.25; H, 8.85; N, 1.61.

The europium complex of the di-tetrazole ligand **1**: (1-Eu) was crystallised by the slow evaporation of a 1:1 methanol/acetonitrile solution (5 mL) of ligand (40.00 mg, 0.05 mmol) and $Eu(NO_3)_3(DMSO)_4$ (34.00 mg, 0.06 mmol) along with eight equivalents of triethylamine (65 μL, 0.40 mmol). Yellow/orange needle crystals suitable for single crystal X-ray structure determination were deposited. Anal. Calculated for $C_{48}H_{60}O_4N_8Eu.H_2O$: C, 56.74; H, 6.25; N, 11.02. Found C, 56.93; H, 6.74; N, 11.20. IR (ATR): ν/cm^{-1} 3198 (b), 2954 (s), 1601 (w), 1477 (s), 1324 (s), 1123 (w), 1015 (m), 876 (m), 777 (w).

The neodymium complex of the di-tetrazole ligand **1**: (1-Nd) was crystallised by the slow diffusion of ether into a DMSO (2 mL) solution of ligand (40.00 mg, 0.05 mmol) and $Nd(NO_3)_3(DMSO)_4$ (34.00 mg, 0.06 mmol) along with four equivalents of triethylamine (65 μL, 0.20 mmol). Purple rhombic platelet crystals suitable for single crystal X-ray structure determination were deposited. Anal. Calculated for $C_{56}H_{82}O_6N_9Nd.(DMSO)(H_2O)_3$: C; 52.86, H; 7.19, N; 9.57, S; 7.30. Found C; 52.72, H; 7.37, N; 9.37, S; 7.42. IR (ATR): ν/cm^{-1} 3412 (b), 2956 (s), 2910 (m), 1600 (w), 1479 (s), 1324 (s), 1186 (w), 1011 (s), 830 (w).

The triethylammonium salt of the di-tetrazole ligand **1**: (1-NEt_3) was crystallised by the slow evaporation of toluene (10 mL) from a solution of free ligand (30.00 mg, 0.04 mmol) and $Dy(NO_3)_3(DMSO)_4$ (24.00 mg, 0.04 mmol) along with

four equivalents of triethylamine (21 μL, 0.16 mmol). White needle like crystals were evolved which were characterised by single crystal X-ray structure determination. Unfortunately due to the likely inclusion of the metal salt within the crystal matrix, attempts at performing elemental analysis resulted in meaningless values. IR (ATR): ν/cm^{-1} 3418 (s), 3363 (b), 2954 (s), 1645 (w), 1482 (s), 1361 (w), 1191 (m), 1123 (w), 871 (w).

The lanthanum complex with the di-tetrazole calixarene **1**: (1-La) was crystallised by the slow evaporation of methanol (20 mL) from a solution of free ligand (30.00 mg, 0.04 mmol) and $La(NO_3)_3(DMSO)_4$ (21.00 mg, 0.04 mmol) along with five equivalents of aqueous ammonium acetate (1 M, 186 μL). White star shaped crystals evolved upon slow evaporation of the solvent which were characterised by single crystal X-ray structure determination. Unfortunately due to the multiple species within the unit cell for this complex elemental analysis was not attempted. IR (ATR): ν/cm^{-1} 3245 (b), 2952 (s), 1649 (w), 1481 (s), 1455 (s), 1360 (w), 1119 (w), 991 (m), 869 (w).

The praseodymium complex with the tri-tetrazole calixarene **2**: (2-Pr) was crystallised by the slow evaporation of a 50:50 ethanol:ethyl acetate solvent mixture (20 mL) from a solution of free ligand (30.00 mg, 0.03 mmol) and $Pr(NO_3)_3(DMSO)_4$ (18.00 mg, 0.03 mmol) along with five equivalents of aqueous ammonium acetate (1 M, 167 μL). Pale green needle like crystals were evolved which were characterised by single crystal X-ray structure determination. Unfortunately due to the nature of the complex attempts at performing elemental analysis resulted in meaningless values. IR (ATR): ν/cm^{-1} 3245 (b), 2952 (s), 1649 (w), 1481 (s), 1455 (s), 1360 (w), 1119 (w), 991 (m), 869 (w).

The triethylammonium and sodium salt of the tetra-tetrazole ligand **4**: (4-Na/NEt_3) was crystallised by the slow evaporation of ethanol/ethyl acetate (50/50, 10 mL) from a solution of free ligand (30.00 mg, 0.04 mmol) and $Tb(NO_3)_3(DMSO)_4$ (21.41 mg, 0.04 mmol) along with ten equivalents of triethylamine (51 μL). Clear

needle like crystals evolved which were characterised by single crystal X-ray structure determination. Unfortunately due to the likely incorporation of the metal salt within the crystal, elemental analysis resulted in meaningless values. IR (ATR): ν/cm^{-1} 3422 (s), 3356 (b), 2952 (s), 2863 (m), 1733 (m), 1642 (w), 1484 (s), 1358 (w), 1191 (m), 1123 (w), 933 (w), 871 (w).

The sodium salt of the tri-tetrazole ligand **2**: (2-Na) was crystallised by the slow evaporation of ethanol/ethyl acetate (50/50, 10 mL) from a solution of free ligand (30.00 mg, 0.03 mmol) and $Y(ClO_4)_3(DMSO)_4$ (14.00 mg, 0.03 mmol) along with five equivalents of aqueous ammonium acetate (1 M, 167 μL). Clear cubic crystals evolved which were characterised by single crystal X-ray structure determination. Unfortunately due to the likely incorporation of the metal salt within the crystal, elemental analysis resulted in meaningless values. IR (ATR): ν/cm^{-1} 3366 (b), 2954 (s), 2872 (m), 1728 (b), 1718 (m), 1642 (w), 1482 (s), 1360 (w), 1202 (m), 1124 (w), 875 (w).

Generic procedure for crystallisation of bottlebrush clusters:

Ln_{19}-B

The needled shaped bottlebrush crystals were crystallised by the slow evaporation of a 50:50 mixture of ethanol and ethyl acetate (20 mL) containing di-tetrazole ligand **1** (30.00 mg, 0.04 mmol), $Ln(NO_3)_3(DMSO)_4$ (0.04 mmol) along with five equivalents of aqueous ammonium acetate (1 M, 186 μL). Clear or coloured needle shaped crystals evolved after approximately 2 weeks of slow evaporation of solvent. These needles were characterised by single crystal X-ray structure determination. IR (ATR): ν/cm^{-1} 3344 (b), 2959 (s), 2871 (m), 1737 (m), 1568 (b), 1484 (s), 1458 (m), 1362 (m), 1241 (m), 1202 (m), 1046 (w), 995 (w), 871 (w).

Ln_{19}-A

In a similar fashion to the Ln_{19}-B species, the platelet crystals were crystallised by slow evaporation of an ethanol only solution (20 mL) containing di-tetrazole

ligand **1** (30.00 mg, 0.04 mmol), $Ln(NO_3)_3(DMSO)_4$ (0.04 mmol) along with five equivalents of aqueous ammonium acetate (1 M, 186 μL). Clear platelet crystals evolved after approximately 3 weeks of slow evaporation of solvent. These crystals were then characterised by single crystal X-ray structure determination. IR (ATR): ν/cm^{-1} 3394 (b), 2957 (s),2868 (m), 1648 (b), 1481 (s), 1459 (m), 1362 (w), 1191 (m), 1122 (w), 1007 (w), 872 (w).

Ln_{19}-C

In a similar fashion to the Ln_{19}-B species, the cubic block shaped crystals were crystallised by slow evaporation of a 50:50 mixture of ethanol and ethyl acetate (20 mL) containing di-tetrazole ligand **1** (30.00 mg, 0.04 mmol), $Ln(NO_3)_3(DMSO)_4$ (0.04 mmol) along with ten equivalents of aqueous ammonium acetate (1 M, 372 μL). Clear or coloured cubic blocks evolved after approximately 2 weeks of slow evaporation of the solvent. These crystals were then characterised by single crystal X-ray structure determination. IR (ATR): ν/cm^{-1} 3346 (b), 2958 (s), 2874 (m), 1568 (b), 1482 (s), 1458 (m), 1363 (m), 1242 (s), 1046 (w), 995 (w), 873 (w).

Ln_{12}

In a similar fashion to the Ln_{19}-C species, the cubic block shaped crystals were crystallised by slow evaporation of a 50:50 mixture of ethanol and ethyl acetate (20 mL) containing di-tetrazole ligand **1** (30.00 mg, 0.04 mmol), $Ln(NO_3)_3(DMSO)_4$ (0.04 mmol) along with five **or** ten equivalents of aqueous ammonium benzoate (1 M, 186 μL). Clear or coloured cubic blocks evolved after approximately 2 weeks of slow evaporation of the solvent. These crystals were then characterised by single crystal X-ray structure determination. IR (ATR): ν/cm^{-1} 3341 (b), 2957 (s), 1735 (m), 1600 (m), 1556 (m), 1484 (s), 1412 (s), 1361 (w), 1240 (m), 1192 (m), 1043 (w), 992 (w), 870 (w), 718 (w).

8 References

(1) Gutsche, D. *Acc. Chem. Res.* **1983**, *16* (5), 161–170.

(2) Gutsche, C. D. In *Calixarenes Revisited*; Gutsche, C. D., Ed.; The Royal Society of Chemistry, 1989; pp 1–9.

(3) Kappe, T. *J. Incl. Phenom. Mol. Recognit. Chem.* **1994**, *19* (1), 3–15.

(4) Gutsche, C. D.; Muthukrishnan, R. *J. Org. Chem.* **1978**, *43* (25), 4905–4906.

(5) Gutsche, C. D.; Pagoria, P. F. *J. Org. Chem.* **1985**, *123* (4), 5795–5802.

(6) Collins, E.; McKervey, A.; Harris, S. J.; Owens, M.; Ferguson, G.; Moran, M. *J. Chem. Soc. Perkin Trans. 1* **1991**, *3* (7), 3137–3142.

(7) Bois, J.; Espinas, J.; Darbost, U.; Felix, C.; Duchamp, C.; Bouchu, D.; Taoufik, M.; Bonnamour, I. *J. Org. Chem.* **2010**, *75* (22), 7550–7558.

(8) Gutsche, C. D. *Calixarenes: An Introduction*, 2nd ed.; RSC Publishing: Cambridge, 2008.

(9) Gutsche, C. D.; Dhawan, B.; Hyun No, K.; Muthukrishnan, R. *J. Am. Chem. Soc.* **1981**, *103* (13), 3782–3792.

(10) Favre, H. A.; Hellwinkel, D.; Powell, W. H.; Smith, H. A. *Pure Appl. Chem.* **2002**, *74* (5), 809–834.

(11) Powell, W. H.; Panico, R.; Traynham, J. G.; Coordinator, W. *Pure Appl. Chem.* **1998**, *70* (8), 1513–1545.

(12) Panico, R.; Powell, W. H.; Richer, J. *A Guide to IUPAC Nomenclature of Organic Compounds Recommendations 1993*; Blackwell Scientific Publications: Melbourne, 1993.

(13) Shinkai, S. *Tetrahedron* **1993**, *49* (40), 8933–8968.

(14) Perez-Jimenez, C.; Harris, S. J.; Diamond, D. *Chem. Commun.* **1993**, *93* (5), 480–483.

(15) Iwamoto, K.; Araki, K.; Shinkai, S. *J. Org. Chem.* **1991**, *29* (26), 4955–4962.

(16) Ogden, M. I.; Skelton, B. W.; White, A. H. *Dalt. Trans.* **2001**, *1* (20), 3073–3077.

(17) Dondoni, A.; Marra, A. *Tetrahedron* **2007**, *63* (27), 6339–6345.

(18) Mogck, O.; Pons, M.; Bohmer, V.; Vogt, W. *J. Am. Chem. Soc.* **1997**, *119* (24), 5706–5712.

(19) Gutsche, D.; Levine, J. *J. Am. Chem. Soc.* **1982**, *104* (9), 2652–2653.

(20) Blixt, J.; Detellier, C. *J. Am. Chem. Soc.* **1994**, *116* (26), 11957–11960.

(21) Danila, C.; Böhmer, V.; Bolte, M. *Org. Biomol. Chem.* **2005**, *3* (19), 3508–3513.

(22) Iwamoto, K.; Fujimoto, K.; Matsuda, T.; Shinkai, S. *Tetrahedron Lett.* **1990**, *31* (49), 7169–7172.

(23) Cornforth, J. W.; Hart, P. D.; Nicholls, G. a.; Rees, R. J. W.; Stock, J. a. *Br. J. Pharmacol. Chemother.* **1955**, *10* (1), 73–86.

(24) Gutsche, C. D. *Calixarenes*; Royal Society of Chemistry: Cambridge, 1989.

(25) Gutsche, C. D.; Dhawan, B.; Levine, J.; No, K. H.; Bauer, L. *Tetrahedron* **1983**, *39* (3), 409–426.

(26) Kammerer, H.; Happel, G.; Mathiasch, W. B. *Die Makromol. Chemie* **1981**, *182* (6), 1685–1694.

(27) Butler, R. N.; Garvin, V. C. *J. Chem. Soc. Perkin Trans. 1* **1981**, *1* (10), 390–393.

(28) Butler, R. N.; Garvin, V. C.; Lumbroso, H.; Liegeois, C. *J. Chem. Soc. Perkin Trans. 2* **1984**, *3* (4), 721–725.

(29) Bauer, M.; Harris, R. K.; Rao, R. C.; Apperley, D. C.; Rodger, C. a. *J. Chem. Soc. Perkin Trans. 2* **1998**, *16* (3), 475–481.

(30) Rao, K.; Dandala, R.; Handa, V.; Rao, I.; Rani, A.; Shivashankar, S.; Naidu, A. *Synlett* **2007**, *2007* (8), 1289–1293.

(31) Duncia, J.; Pierce, M.; Santella, J. *J. Org. Chem.* **1991**, *56* (7), 2395–2400.

(32) El-Ahl, A.-A. S.; Elmorsy, S. S.; Elbeheery, A. H.; Amer, F. a. *Tetrahedron Lett.* **1997**, *38* (7), 1257–1260.

(33) Satoh, Y.; Lombaert, S. De; Marcopulos, N.; Molitemi, J.; Moskal, M.; Tan, J.; Wallace, E. *Tetrahedron Lett.* **1998**, *39* (21), 3367–3370.

(34) El-Ahl, A.; Elmorsy, S.; Soliman, H.; Amer, F. A. *Tetrahedron Lett.* **1995**, *36* (40), 7337–7340.

(35) Himo, F.; Demko, Z. P.; Noodleman, L.; Sharpless, K. B. *J. Am. Chem. Soc.* **2002**, *124* (41), 12210–12216.

(36) Herr, R. J. *Bioorg. Med. Chem.* **2002**, *10* (11), 3379–3393.

(37) Von Braun, J.; Keller, W. *Berichte der Dtsch. Chem. Gesellschaft* **1932**, *65* (10), 1677–1680.

(38) Herbst, R. M.; Froberger, C. F. *J. Org. Chem.* **1967**, *22* (9), 1050–1053.

(39) Behringer, H.; Kohl, K. *Die Synth.* **1956**, *89* (11), 2648–2653.

(40) Finnegan, W. G.; Henry, R. A.; Lofquist, R. *J. Am. Chem. Soc.* **1958**, *80* (4), 3908–3911.

(41) Demko, Z. P.; Sharpless, K. B. *J. Org. Chem.* **2001**, *66* (24), 7945–7950.

(42) Wittenberger, S. J. *Org. Prep. Proced. Int.* **1994**, *26* (5), 499–531.

(43) Koguro, K.; Oga, T.; Mitsui, S.; Orita, R. *Synthesis (Stuttg).* **1997**, *06* (1), 910–914.

(44) Mohite, P. B.; Bhaskar, V. H. *Int. J. Pharm. Technol.* **2011**, *3* (3), 1557–1566.

(45) Roh, J.; Vávrová, K.; Hrabálek, A. *European J. Org. Chem.* **2012**, *2012* (31), 6101–6118.

(46) Kraus, J. *Pharmalogical Res. Commun.* **1983**, *15* (2), 183–189.

(47) Benson, F. R. *Chem. Rev.* **1947**, *41* (1), 1–61.

(48) Holland, G.; Pereira, J. *J. Med. Chem.* **1967**, *10* (2), 149–154.

(49) Pinter, T.; Jana, S.; Courtemanche, R. J. M.; Hof, F. *J. Org. Chem.* **2011**, *76* (10), 3733–3741.

(50) Boyko, V.; Rodik, R.; Danylyuk, O.; Tsymbal, L.; Lampeka, Y.; Suwinska, K.; Lipkowski, J.; Kalchenko, V. *Tetrahedron* **2005**, *61* (52), 12282–12287.

(51) Chen, Y.-J.; Chung, W.-S. *European J. Org. Chem.* **2009**, *2009* (28), 4770–4776.

(52) D'Alessio, D.; Sobolev, A. N.; Skelton, B. W.; Fuller, R. O.; Woodward, R. C.; Lengkeek, N. a; Fraser, B. H.; Massi, M.; Ogden, M. I. *J. Am. Chem. Soc.* **2014**, *136* (43), 15122–15125.

(53) D'Alessio, D.; Muzzioli, S.; Skelton, B. W.; Stagni, S.; Massi, M.; Ogden, M. I. *Dalt. Trans.* **2012**, *41* (16), 4736–4739.

(54) Jeong, S.; Song, X.; Jeong, S.; Oh, M.; Liu, X.; Kim, D.; Moon, D.; Lah, M. S. *Inorg. Chem.* **2011**, *50* (23), 12133–12140.

(55) Wright, P. J.; Muzzioli, S.; Werrett, M. V.; Raiteri, P.; Skelton, B. W.; Silvester, D. S.; Stagni, S.; Massi, M. *Organometallics* **2012**, *31* (21), 7566–7578.

(56) Liang, L.; Peng, G.; Sun, L.; Deng, H.; Li, H.; Li, W. *Cryst. Growth Des.* **2012**, *12* (3), 1151–1158.

(57) D'Alessio, D.; Karagiannidis, A. L. E.; Skelton, B. B. W.; Massi, M.; A, M. I. O. *Aust. J. Chem.* **2012**, *65* (7), 3–6.

(58) Liu, Y.; Gao, L.; Lv, X.; Liu, J.; Hu, T. *Inorg. Chem. Commun.* **2012**, *19* (5), 15–18.

(59) Shavaleev, N. M.; Eliseeva, S. V; Scopelliti, R.; Bünzli, J.-C. G. *Inorg. Chem.* **2014**, *53* (10), 5171–5178.

(60) Wu, M.-F.; Wang, M.-S.; Guo, S.-P.; Zheng, F.-K.; Chen, H.-F.; Jiang, X.-M.; Liu, G.-N.; Guo, G.-C.; Huang, J.-S. *Cryst. Growth Des.* **2011**, *11* (2), 372–381.

(61) Liu, N.; Yue, Q.; Wang, Y.-Q.; Cheng, A.-L.; Gao, E.-Q. *Dalt. Trans.* **2008**, *3* (34), 4621.

(62) Ouellette, W.; Darling, K.; Zubieta, J. *Inorganica Chim. Acta* **2012**, *391* (8), 36–43.

(63) Yu, Z.; Xie, Y.; Wang, S.; Yong, G.; Wang, Z. *Inorg. Chem. Commun.* **2008**, *11* (4), 372–376.

(64) Castor, S. B.; Hedrick, J. B. *Rare Earth Elements*, 7th ed.; Society for Mining, Metallurgy and Exploration: Littleton, Colorado, 2006.

(65) Cotton, S. In *Encyclopedia of inorganic chemistry*; King, R., Ed.; John Wiley & Sons, Ltd, 1994; p 3595.

(66) Sabbatini, N.; Guardigli, M.; Lehn, J.-M. *Coord. Chem. Rev.* **1993**, *123* (1-2), 201–228.

(67) Cotton, S. *Scandium, yttrium and the lanthanides*, 2nd ed.; McCleverty, J., Meyer, T., Eds.; Elsevier, 2004.

(68) Cotton, S. *Lanthanide and Actinide Chemistry*; John Wiley & Sons, Ltd: Chichester, UK, 2006.

(69) Connelley, N. In *The Red Book*; RSC Publishing: Cambridge, 1985; p 45.

(70) Cotton, F.; Wilkinson, G. *Advanced Inorganic Chemistry*, 4th ed.; Wiley & Sons, 1980.

(71) Friedmon, H. G.; Choppin, G. R.; Feuerbocherz, D. G. *J. Chem. Educ.* **1964**, *41* (7), 354–358.

(72) Bettencourt-dias, A. De. In *Encyclopedia of Inorganic and Bioinorganic Chemistry*; John Wiley & Sons, Ltd, 2012; pp 1–8.

(73) Becker, C. *J. Chem. Educ.* **1964**, *41* (7), 358–360.

(74) Bunzli, J. G.; Eliseeva, S. V. In *Lanthanide Luminescence*; Hanninen, P., Harma, H., Eds.; Springer-Verlag: Berlin, 2011; pp 1–45.

(75) Leonard, J. P.; Nolan, C. B.; Stomeo, F. *Top. Curr. Chem.* **2007**, *281* (1), 1–43.

(76) Andrews, P. C.; Gee, W. J.; Junk, P. C.; Massi, M. *New J. Chem.* **2013**, *37* (1), 35.

(77) Luzon, J.; Sessoli, R. *Dalt. Trans.* **2012**, *41* (44), 13556–13567.

(78) Huang, C.; Bian, Z. In *Rare Earth Coordination Chemistry: Fundamentals and Applications*; Huang, C., Ed.; John Wiley & Sons, Ltd: Singapore, 2010; pp 1–40.

(79) Liang, L.; Li, G.; Sun, L.; Lan, G.; Zhang, L.; Yang, C.; Ma, Y.; Deng, H. *Inorg. Chem. Commun.* **2012**, *20* (6), 295–298.

(80) Zhang, X.; Yu, B. Q.; Bian, A. H.; Yan, A. S.; Liao, D.; Gu, B. W.; A, H. L. *Aust. J. Chem.* **2008**, *61* (4), 303–309.

(81) Steinhauser, G.; Giester, G.; Leopold, N.; Wagner, C. *Helv. Chim. Acta* **2009**, *92* (10), 2038–2051.

(82) He, M.-H.; Ji, C.; Shen, Z.-D.; Li, Q.-Y.; Yang, G.-W.; Shen, W.; Qiou, Q.-G.; Shen, X.-F. *J. Coord. Chem.* **2013**, *66* (9), 1538–1548.

(83) Pietraszkiewicz, M.; Mal, S.; Pietraszkiewicz, O. *Opt. Mater. (Amst).* **2012**, *34* (9), 1507–1512.

(84) Wartenberg, N.; Raccurt, O.; Bourgeat-Lami, E.; Imbert, D.; Mazzanti, M. *Chem. A Eur. J.* **2013**, *19* (10), 3477–3482.

(85) Bozoklu, G.; Marchal, C.; Pécaut, J.; Imbert, D.; Mazzanti, M. *Dalt. Trans.* **2010**, *39* (38), 9112–9122.

(86) Andrews, P. C.; Beck, T.; Fraser, B. H.; Junk, P. C.; Massi, M. *Polyhedron* **2007**, *26* (18), 5406–5413.

(87) Kratsch, J.; Beele, B. B.; Koke, C.; Denecke, M. A.; Geist, A.; Panak, P. J.; Roesky, P. W. *Inorg. Chem.* **2014**, *35* (1), 8949–8958.

(88) Andreiadis, E. S.; Demadrille, R.; Imbert, D.; Pécaut, J.; Mazzanti, M. *Chem. A Eur. J.* **2009**, *15* (37), 9458–9476.

(89) Andreiadis, E. S.; Imbert, D.; Pécaut, J.; Demadrille, R.; Mazzanti, M. *Dalt. Trans.* **2012**, *41* (4), 1268–1277.

(90) Giraud, M.; Andreiadis, E. S.; Fisyuk, A. S.; Demadrille, R.; Pecaut, J.; Imbert, D.; Mazzanti, M. *Inorg. Chem.* **2008**, *47* (10), 3952–3954.

(91) Eulgem, P. J.; Klein, A.; Maggiarosa, N.; Naumann, D.; Pohl, R. W. H. *Chem. A Eur. J.* **2008**, *14* (12), 3727–3736.

(92) Pierpont, G.; Buchanan, M. *Coord. Chem. Rev.* **1981**, *38* (1), 45–87.

(93) Freeman, G. E.; Raymond, K. N. *Inorg. Chem.* **1985**, *24* (9), 1410–1417.

(94) Latva, M.; Takalo, H.; Mukkala, V.; Matachescu, C.; Rodriguez-ubis, J. C.; Kankare, J. *J. Lumin.* **1997**, *75* (2), 149–169.

(95) Bünzli, J.-C. G.; Piguet, C. *Chem. Rev.* **2002**, *102* (6), 1897–1928.

(96) Bünzli, J.-C. G.; Piguet, C. *Chem. Soc. Rev.* **2005**, *34* (12), 1048–1077.

(97) Georgiev, E. M.; Roundhill, D. M. *Inorganica Chim. Acta* **1997**, *258* (1), 93–96.

(98) Marcos, P.; Ascenso, J.; Segurado, M.; Cragg, P.; Michel, S.; Hubscher-Bruder, V.; Arnaud-Neu, F. *Supramol. Chem.* **2011**, *23* (1), 93–101.

(99) Ogden, M. I.; Skelton, B. W.; White, A. H. *Comptes Rendus Chim.* **2005**, *8* (2), 181–187.

(100) Baldini, L.; Sansone, F.; Casnati, A. In *Supramolecular Chemistry: From Molecules to Nanomaterials*; John Wiley and Sons, Ltd.: Hoboken, USA, 2012; pp 1–31.

(101) Furphy, B. M.; Harrowfield, J. M.; Kepert, D. L.; Skelton, B. W.; White, A. H.; Wilner, F. R. *J. Am. Chem. Soc.* **1987**, *26* (25), 4231–4236.

(102) Sabbatini, N.; Guardigli, M.; Mecati, A.; Balzani, V.; Ungaro, R.; Ghidini, E.; Csanati, A.; Pochini, A. *Chem. Commun.* **1990**, *1990* (12), 878–879.

(103) Bunzli, J. G.; Froidevaux, P.; Harrowfield, J. M. *Inorg. Chem.* **1993**, *32* (15), 3306–3311.

(104) Sherry, A.; C.F, G. *Lanthanide Probes in Life, Chemical and Earth Sciences, Theory and Practice*; Bunzli, J. G., Choppin, G. R., Eds.; Elsevier Science Publishers, 1989.

(105) Steemers, F. J.; Verboom, W.; Reinhoudt, D. N.; Tal, E. B. Van Der; Verhoeven, J. W. *J. Am. Chem. Soc.* **1995**, *117* (14), 9408–9414.

(106) Steemers, F. J.; Meuris, H. G.; Verboom, W.; Reinhoudt, D. N.; van Der Tol, E. B.; Verhoeven, J. W. *J. Org. Chem.* **1997**, *62* (13), 4229–4235.

(107) Kajiwara, T.; Iki, N.; Yamashita, M. *Coord. Chem. Rev.* **2007**, *251* (13-14), 1734–1746.

(108) Georgiev, E. M.; Mcpherson, G. L.; Roundhill, D. M.; Clymire, J. *Inorganica Chim. Acta* **1994**, *227* (2), 293–296.

(109) Arnaud-neu, Ó.; Barboso, S.; Casnati, A.; Pinalli, A.; Cedex, S. *New J. Chem.* **2000**, *24* (12), 967–972.

(110) Arnaud-neu, F.; Schwing-Weill, M. J.; Ziat, K.; Cremin, S.; Harris, S.; McKervey, M. *New J. Chem.* **1991**, *15* (1), 33–37.

(111) Argent, S. P.; Greenaway, A.; Gimenez-Lopez, M. D. C.; Lewis, W.; Nowell, H.; Khlobystov, A. N.; Blake, A. J.; Champness, N. R.; Schröder, M. *J. Am. Chem. Soc.* **2012**, *134* (1), 55–58.

(112) Andrews, P. C.; Brown, D. H.; Fraser, B. H.; Gorham, N. T.; Junk, P. C.; Massi, M.; St Pierre, T. G.; Skelton, B. W.; Woodward, R. C. *Dalt. Trans.* **2010**, *39* (46), 11227–11234.

(113) Andrews, P. C.; Forsyth, C. M.; Fraser, B. H.; Junk, P. C.; Massi, M.; Silberstein, M. *CrystEngComm* **2007**, *9* (4), 282–285.

(114) Andrews, P. C.; Gee, W. J.; Junk, P. C.; Maclellan, J. G. *Inorg. Chem.* **2010**, *49* (11), 5016–5024.

(115) Baraniak, E.; Bruce, R. S.; Freeman, H.; Hair, N.; James, J. *Inorg. Chem.* **1976**, *15* (9), 2226–2230.

(116) Andrews, P. C.; Beck, T.; Forsyth, C. M.; Fraser, B. H.; Junk, P. C.; Massi, M.; Roesky, P. W. *Dalton Trans.* **2007**, *9226* (48), 5651–5654.

(117) Zheng, Z. *Chem. Commun.* **2001**, *2001* (24), 2521–2529.

(118) Wang, R.; Carducci, M. D.; Zheng, Z. *Inorg. Chem.* **2000**, *39* (9), 1836–1837.

(119) Chen, L.; Guo, J.-Y.; Xu, X.; Ju, W.-W.; Zhang, D.; Zhu, D.-R.; Xu, Y. *Chem. Commun.* **2013**, *49* (84), 9728–9730.

(120) Petit, S.; Baril-Robert, F.; Pilet, G.; Reber, C.; Luneau, D. *Dalt. Trans.* **2009**, *9* (34), 6809–6815.

(121) Kong, X.-J.; Long, L.-S.; Zheng, L.-S.; Wang, R.; Zheng, Z. *Inorg. Chem.* **2009**, *48* (7), 3268–3273.

(122) Chen, X.-Y.; Yang, X.; Holliday, B. J. *Inorg. Chem.* **2010**, *49* (6), 2583–2585.

(123) Pasquale, S.; Sattin, S.; Escudero-Adán, E. C.; Martínez-Belmonte, M.; de Mendoza, J. *Nat. Commun.* **2012**, *3* (785), 1–7.

(124) Whitehead, G. F. S.; Moro, F.; Timco, G. a; Wernsdorfer, W.; Teat, S. J.; Winpenny, R. E. P. *Angew. Chemie* **2013**, *52* (38), 9932–9935.

(125) Aromí, G.; Barrios, L. a.; Roubeau, O.; Gamez, P. *Coord. Chem. Rev.* **2011**, *255* (5), 485–546.

(126) Romanelli, M.; Kumar, G. A.; Emge, T. J.; Riman, R. E.; Brennan, J. G. *Angew. Chemie* **2008**, *47* (32), 6049–6051.

(127) He, F.; Tong, M.-L.; Yu, X.-L.; Chen, X.-M. *Inorg. Chem.* **2005**, *44* (3), 559–565.

(128) Zhao, H.; Qu, Z.-R.; Ye, H.-Y.; Xiong, R.-G. *Chem. Soc. Rev.* **2008**, *37* (1), 84–100.

(129) Giester, G.; Leopold, N.; Wagner, C.; Villa, M.; Musilek, A.; Seaborg, G. T. *Helv. Chim. Acta* **2010**, *93* (2), 183–202.

(130) Asfari, Z.; Harrowfield, Ja.; Ogden, M.; Vicens, J.; White, A. H. *Angew. Chem. Int. Ed. Engl.* **1991**, *30* (7), 854–856.

(131) Bi, Y.; Wang, X.-T.; Liao, W.; Wang, X.; Deng, R.; Zhang, H.; Gao, S. *Inorg. Chem.* **2009**, *48* (24), 11743–11747.

(132) Taylor, S. M.; Sanz, S.; McIntosh, R. D.; Beavers, C. M.; Teat, S. J.; Brechin, E. K.; Dalgarno, S. J. *Chem. A Eur. J.* **2012**, *18* (50), 16014–16022.

(133) Liu, C.; Zhang, D.; Hao, X.; Zhu, D. *Cryst. Growth Des.* **2012**, *12* (4), 2948–2954.

(134) Sanz, S.; McIntosh, R. D.; Beavers, C. M.; Teat, S. J.; Evangelisti, M.; Brechin, E. K.; Dalgarno, S. J. *Chem. Commun.* **2012**, *48* (10), 1449–1451.

(135) Fairbairn, R. E.; McLellan, R.; McIntosh, R. D.; Taylor, S. M.; Brechin, E. K.; Dalgarno, S. J. *Chem. Commun.* **2012**, *48* (68), 8493–8495.

(136) Sanz, S.; Ferreira, K.; McIntosh, R. D.; Dalgarno, S. J.; Brechin, E. K. *Chem. Commun.* **2011**, *47* (32), 9042–9044.

(137) Groenen, L. C.; Ruel, B. H. M.; Casnati, A.; Verboom, W.; Pochini, A.; Ungaro, R.; Reinhoudf, D. N. *Tetrahedron* **1991**, *47* (39), 8379–8384.

(138) Shinkai, S.; Araki, K.; Kubota, M.; Arimura, T.; Matsuda, T. *J. Org. Chem.* **1991**, *56* (1), 295–300.

(139) Arnaud-neu, F.; Collins, E. M.; Deasy, I. M.; Ferguson, G.; Harris, S. J.; Kaitner, I. B.; Lough, A. J.; Mckervey, M. A.; Marques, E.; Ruhl, B. L.; Schwing-weill, M. J.; Sewardt, E. M. *J. Am. Chem. Soc.* **1989**, *111* (9), 8681–8691.

(140) Casnati, A.; Verboom, W.; Pochini, O. A.; Ungaro, R.; Reinhoudf, D. N. *Tetrahedron* **1991**, *47* (39), 8379–8384.

(141) Iwamoto, K.; Araki, K.; Shinkai, S. *Tetrahedron* **1991**, *47* (25), 4325–4342.

(142) Iwamoto, K.; Shinkai, S. *J. Org. Chem.* **1992**, *57* (15), 7066–7073.

(143) Mokhtari, B.; Pourabdollah, K.; Dallali, N. *J. Radioanal. Nucl. Chem.* **2011**, *287* (3), 921–934.

(144) Scheerder, J.; Fochi, M.; Engbersen, J. F. J.; Reinhoudt, D. N. *J. Org. Chem.* **1994**, *59* (25), 7815–7820.

(145) Hal, H.; Dumazet, I.; Perrin, M.; Lamartine, R. *J. Org. Chem.* **2004**, *69* (20), 6521–6527.

(146) Kim, J. M.; Chun, J. C.; Nam, K. C. *Bull. Korean Chem. Soc.* **1997**, *18* (4), 409–415.

(147) Nam, K. C.; Kang, S. O.; Ki, Y. J. *Supramol. Chem.* **2002**, *14* (6), 503–509.

(148) Joseph, R.; Chinta, J. P.; Rao, C. P. *Inorg. Chem.* **2011**, *50* (15), 7050–7058.

(149) Ikeda, A.; Nagasaki, T.; Araki, K.; Shinkai, S. *Tetrahedron* **1992**, *48* (6), 1059–1070.

(150) Hoorn, W. P. Van; Morshuis, M. G. H.; Veggel, F. C. J. M. Van; Reinhoudt, D. N. *J. Phys. Chem. A* **1998**, *102* (7), 1130–1138.

(151) Creaven, B. S.; Donlon, D. F.; McGinley, J. *Coord. Chem. Rev.* **2009**, *253* (7), 893–962.

(152) Martinez, C. R.; Iverson, B. L. *Chem. Sci.* **2012**, *3* (7), 2191.

(153) García, F.; Korevaar, P. a; Verlee, A.; Meijer, E. W.; Palmans, A. R. a; Sánchez, L. *Chem. Commun.* **2013**, *49* (77), 8674–8676.

(154) Marino, N.; Vortherms, A. R.; Hoffman, A. E.; Doyle, R. P. *Inorg. Chem.* **2010**, *49* (15), 6790–6792.

(155) Beckmann, J.; Duthie, A.; Gesing, T. M.; Koehne, T.; Lork, E. *Organometallics* **2012**, *31* (8), 3451–3454.

(156) Peng, J.-B.; Kong, X.-J.; Ren, Y.-P.; Long, L.-S.; Huang, R.-B.; Zheng, L.-S. *Inorg. Chem.* **2012**, *51* (4), 2186–2190.

(157) Rodríguez-Diéguez, A.; Mota, A. J.; Seco, J. M.; Palacios, M. a; Romerosa, A.; Colacio, E. *Dalt. Trans.* **2009**, *2* (43), 9578–9586.

(158) In *Zetasizer Nano Series*; 2004.

(159) An, Y.; Schramm, G. E.; Berry, M. T. *J. Lumin.* **2002**, *97* (1), 7–12.

(160) Shuvaev, S.; Utochnikova, V.; Marciniak, L.; Freidzon, A.; Sinev, I.; Van Deun, R.; Freire, R. O.; Zubavichus, Y.; Grünert, W.; Kuzmina, N. *Dalt. Trans.* **2014**, *43* (8), 3121–3136.

(161) Chesman, A. S. R.; Turner, D. R.; Moubaraki, B.; Murray, K. S.; Deacon, G. B.; Batten, S. R. *Dalt. Trans.* **2012**, *41* (36), 10903–10909.

(162) Bunzli, J.-C.; Eliseeva, S. *Chem. Sci.* **2013**, *4* (5), 1939–1949.

(163) Hofstraat, J. W.; Wolbers, M. P. O.; Veggel, F. C. J. M. Van; Reinhoudt, D. N.; Werts, M. H. V; Verhoeven, J. W. *J. Fluoresc.* **1998**, *8* (4), 301–308.

(164) Klink, S. I. Synthesis and Photphysics of Light-Converting Lanthanide Complexes, 2000.

(165) Weissman, S. I. *J. Chem. Phys.* **1942**, *10* (4), 214.

(166) Dexter, D. L. *J. Chem. Phys.* **1953**, *21* (5), 836.

(167) Forster, T. *Discuss. Faraday Soc.* **1959**, *2* (27), 7–17.

(168) Sato, S.; Wada, M. *Bull. Chem. Soc. Jpn.* **1970**, *43* (7), 1955–1962.

(169) Eliseeva, S. V; Bünzli, J.-C. G. *Chem. Soc. Rev.* **2010**, *39* (1), 189–227.

(170) Liu, G. K.; Jensen, M. P.; Almond, P. M. *J. Phys. Chem. A* **2006**, *110* (6), 2081–2088.

(171) Asano-Someda, M.; Kaizu, Y. *J. Photochem. Photobiol. A Chem.* **2001**, *139* (2-3), 161–165.

(172) Thielemann, D. T.; Wagner, A. T.; Rösch, E.; Kölmel, D. K.; Heck, J. G.; Rudat, B.; Neumaier, M.; Feldmann, C.; Schepers, U.; Bräse, S.; Roesky, P. W. *J. Am. Chem. Soc.* **2013**, *135* (20), 7454–7457.

9 Appendix

Appendix A - Crystal data

A.1 X-ray crystal data for compound 1

Empirical formula $C_{52}H_{66}N_{10}O_4$; formula weight 895.15; crystal system: monoclinic; space group *C*2/*c*; unit cell a = 23.526(5) Å, b = 11.962(2) Å, c = 37.255(6) Å, β= 110.96(2)°; volume 9790(3) Å^3; Z = 8; density (calculated) 1.215 Mg/m^3; absorption coefficient 0.079 mm^{-1}; crystal size 0.25 x 0.20 x 0.06 mm^3; θ range for data collection 2.77 to 25.00°; reflections collected 71629; independent reflections 8627 [R(int) = 0.135]; completeness to θ = 25.00° 99.8%; data/restraints/parameters 8627/0/600 goodness-of-fit on F^2 1.031; final R indices [$I>2\sigma(I)$] R_1 = 0.0890, wR_2 = 0.1961; R indices (all data) R_1 = 0.1435, wR_2 = 0.2289.

A.2 X-ray crystal data for compound 2

Empirical formula $C_{101}H_{133}N_{25}O_{10}$; formula weight 1857.32; crystal system: monoclinic; space group $P2_1$; unit cell a = 12.1728(7) Å, b = 46.6720(18) Å, c = 9.9406(4) Å, β= 111.066(6)°; volume 5720.1(4) Å^3; Z = 2; density (calculated) 1.170 Mg/m^3; absorption coefficient 0.627 mm^{-1}; crystal size 0.28 x 0.17 x 0.07 mm^3; θ range for data collection 2.86 to 25.00°; reflections collected 41171; independent reflections 16642 [R(int) = 0.0712]; completeness to θ = 25.00° 99.9%; data/restraints/parameters 16642/185/620 goodness-of-fit on F^2 1.023; final R indices [$I>2\sigma(I)$] R_1 = 0.0954, wR_2 = 0.2440; R indices (all data) R_1 = 0.1655, wR_2 = 0.2387.

A.3 X-ray crystal data for compound 3

Empirical formula $C_{54}H_{72}N_{16}O_6$; formula weight 1041.28; crystal system: monoclinic; space group *Cc*; unit cell a = 11.5045(7) Å, b = 41.964(2) Å, c = 12.3762(6) Å, β= 108.656(6)°; volume 5661.0(5) Å^3; Z = 4; density (calculated) 1.222 Mg/m^3; absorption coefficient 0.083 mm^{-1}; crystal size 0.47 x 0.23 x 0.10 mm^3; θ range for data collection 3.61 to 30.75°; reflections collected 37551; independent reflections 8252 [R(int) = 0.0837]; completeness to θ = 29.00° 99.5%; data/restraints/parameters 8252/4/708

goodness-of-fit on F^2 0.904; final R indices [$I>2\sigma(I)$] R_1 = 0.0636, wR_2 = 0.1323; R indices (all data) R_1 = 0.1192, wR_2 = 0.1483.

A.4 X-ray crystal data for compound 5

Empirical formula $C_{50}H_{59}N_3O_4$; formula weight 766.00; crystal system: triclinic; space group $P\bar{1}$; unit cell dimensions a = 11.2306(5) Å, b = 12.9547(5) Å, c = 16.8293(7) Å, α = 78.456(3)°, β = 71.355(4)°, γ = 75.486(4)°; volume 2226.64(16) Å^3; Z = 2; density (calculated) 1.143 Mg/m^3; absorption coefficient 0.072 mm^{-1}; crystal size 0.34 x 0.30 x 0.14 mm^3; θ range for data collection 2.81 to 29.00°; reflections collected 20351; independent reflections 11503 [R(int) = 0.0300]; completeness to θ = 29.00° 99.4%; data/restraints/parameters 11503/9/588 goodness-of-fit on F^2 1.023; final R indices [$I>2\sigma(I)$] R_1 = 0.0641, wR_2 = 0.1368; R indices (all data) R_1 = 0.0910, wR_2 = 0.1496.

A.5 X-ray crystal data for compound 7

Empirical formula $C_{52}H_{60}N_4O_4$; formula weight 805.04; crystal system: monoclinic; space group $C2/c$; unit cell dimensions a = 14.6327(2), b = 167338(2), c = 37.5113(4) Å, β = 938360(10) °; volume 9164.46(19) Å^3; Z = 8; density (calculated) 1.167 Mg/m^3; absorption coefficient 0.074 mm^{-1}; crystal size 0.51 x 0.37 x 0.32 mm^3; θ range for data collection 3.70 to 38.00°; reflections collected 95516; independent reflections 24922 [R(int) = 0.0341]; completeness to θ = 38.00° 99.9%; data/restraints/parameters 24922/6/569 goodness-of-fit on F^2 0.985; final R indices [$I>2\sigma(I)$] R_1 = 0.0504, wR_2 = 0.1410; R indices (all data) R_1 = 0.0774, wR_2 = 0.1488.

A.6 X-ray crystal data for compound 8

Empirical formula $C_{60}H_{80}N_4O_6$; formula weight 953.28; crystal system: monoclinic; space group $P2_1/n$; unit cell dimensions a = 21.0623(5), b = 21.8364(3), c = 25.8796(5) Å, β = 109.896(2) °; volume 11192.2(4) Å^3; Z = 8; density (calculated) 1.131 Mg/m^3; absorption coefficient 0.072 mm^{-1}; crystal size 0.37 x 0.28 x 0.26 mm^3; θ range for data

collection 2.81 to 32.00°; reflections collected 141567; independent reflections 38570 [R(int) = 0.0439]; completeness to θ = 32.00° 99.2%; data/restraints/parameters 38570/76/1432 goodness-of-fit on F^2 1.102; final R indices [$I>2\sigma(I)$] R_1 = 0.0700, wR_2 = 0.1463; R indices (all data) R_1 = 0.0950, wR_2 = 0.1582.

A.7 X-ray crystal data for compound 9

Empirical formula $C_{62}H_{86}N_4O_7$; formula weight 999.35; crystal system: triclinic; space group $P\bar{1}$; unit cell dimensions a = 11.3151(8), b = 15.0871(7), c = 17.7550(12) Å, α = 86.040(5), β = 80.157(6), γ = 76.643(5)°; volume 2904.2(3) $Å^3$; Z = 2; density (calculated) 1.143 Mg/m^3; absorption coefficient 0.074 mm^{-1}; crystal size 0.57 x 0.24 x 0.17 mm^3; θ range for data collection 3.54 to 29.00°; reflections collected 29154; independent reflections 15430 [R(int) = 0.0626]; completeness to θ = 29.00° 99.8%; data/restraints/parameters 15430/1/676 goodness-of-fit on F^2 1.014; final R indices [$I>2\sigma(I)$] R_1 = 0.0638, wR_2 = 0.1408; R indices (all data) R_1 = 0.1040, wR_2 = 0.1626.

A.8 X-ray crystal data for compound 10

Empirical formula $C_{58}H_{76}N_4O_6$; formula weight 925.23; crystal system: triclinic; space group $P\bar{1}$; unit cell dimensions a = 10.6671(5), b = 12.4238(5), c = 21.0581(9) Å, α = 81.960(4), β = 79.731(4), γ = 84.962(4)°; volume 2713.4(2) $Å^3$; Z = 2; density (calculated) 1.132 Mg/m^3; absorption coefficient 0.073 mm^{-1}; crystal size 0.39 x 0.27 x 0.06 mm^3; θ range for data collection 2.81 to 29.00°; reflections collected 32902; independent reflections 14427 [R(int) = 0.0342]; completeness to θ = 29.00° 99.9%; data/restraints/parameters 14427/21/689 goodness-of-fit on F^2 1.088; final R indices [$I>2\sigma(I)$] R_1 = 0.0856, wR_2 = 0.1905; R indices (all data) R_1 = 0.1144, wR_2 = 0.2064.

A.9 X-ray crystal data for compound 1-Eu

Empirical formula $C_{48}H_{61}N_8O_6Eu$; formula weight 998.01; crystal system: Monoclinic; space group *C*2/*m*; unit cell dimensions *a* = 20.852(3) Å, *b* = 12.9596(12) Å, *c* = 24.4175(19) Å, β = 103.649(11)°; volume 6412.2(11) $Å^3$; Z = 4; density (calculated) 1.034 Mg/m^3; absorption coefficient 1.019 mm^{-1}; crystal size 0.59 x 0.48 x 0.21 mm^3; θ range for data collection 2.94 to 27.50°; reflections collected 31105; independent reflections 7685 [R(int) = 0.0435]; completeness to θ = 27.50° 99.8%; data/restraints/parameters 7685/120/388 goodness-of-fit on F^2 1.121; final R indices [$I>2\sigma(I)$] R_1 = 0.0838, wR_2 = 0.2084; R indices (all data) R_1 = 0.0884, wR_2 = 0.2109.

A.10 X-ray crystal data for compound 1-Nd

Empirical formula $C_{62}H_{97.65}N_9O_{8.83}S_4Nd$; formula weight 1382.90; crystal system: Triclinic; space group $P\bar{1}$; unit cell dimensions *a* = 15.2461(1) Å, *b* = 17.2142(1) Å, *c* = 27.0057(2) Å, α = 89.904(1)°, β = 87.299(1)°, γ = 81.458(1)°; volume 7001.12(8) $Å^3$; Z = 4; density (calculated) 1.312 Mg/m^3; absorption coefficient 0.918 mm^{-1}; crystal size 0.49 x 0.42 x 0.29 mm^3; θ range for data collection 3.59 to 32.00°; reflections collected 92173; independent reflections 48557 [R(int) = 0.0294]; completeness to θ = 32.00° 99.8%; data/restraints/parameters 48557/4/1632 goodness-of-fit on F^2 0.991; final R indices [$I>2\sigma(I)$] R_1 = 0.0419, wR_2 = 0.1039; R indices (all data) R_1 = 0.0649, wR_2 = 0.1094.

A.11 X-ray crystal data for compound 1-NEt_3

Empirical formula $C_{54}H_{75}N_9O_4$; formula weight 914.23; crystal system: Triclinic; space group $P\bar{1}$; unit cell dimensions *a* = 10.4839(2) Å, *b* = 13.0830(4) Å, *c* = 21.5006(6) Å, α = 97.165(2)°, β = 100.403(2)°, γ = 109.891(2)°; volume 2671.70(12) $Å^3$; Z = 2; density (calculated) 1.136 Mg/m^3; absorption coefficient 0.073 mm^{-1}; crystal size 0.42 x 0.23 x 0.16 mm^3; θ range for data collection 2.81 to 30.00°; reflections collected 32555; independent reflections 15567 [R(int) = 0.0279]; completeness to θ = 30.00° 99.9%;

data/restraints/parameters 15567/271/1043 goodness-of-fit on F^2 1.023; final R indices [$I>2\sigma(I)$] R_1 = 0.0911, wR_2 = 0.2375; R indices (all data) R_1 = 0.1261, wR_2 = 0.2628.

A.12 X-ray crystal data for compound 1-La

Empirical formula $C_{196.50}H_{287}N_{32}O_{38.50}La_2$; formula weight 3991.40; crystal system: Triclinic; space group $P\bar{1}$; unit cell dimensions a = 21.7530(6) Å, b = 24.0255(6) Å, c = 24.3524(7) Å, α = 105.150(2)°, β = 100.459(3)°, γ = 90.175(2)°; volume 12063.7(6) Å^3; Z = 2; density (calculated) 1.099 Mg/m^3; absorption coefficient 0.416 mm^{-1}; crystal size 0.47 x 0.16 x 0.09 mm^3; θ range for data collection 2.71 to 26.00°; reflections collected 87365; independent reflections 46899 [R(int) = 0.0378]; completeness to θ = 26.00° 98.9%; data/restraints/parameters 46899/252/2518 goodness-of-fit on F^2 1.340; final R indices [$I>2\sigma(I)$] R_1 = 0.1374, wR_2 = 0.3679; R indices (all data) R_1 = 0.1842, wR_2 = 0.3974.

A.13 X-ray crystal data for compound 2-Pr

Empirical formula $C_{56}H_{89.74}N_{12}O_{15.63}S_{0.37}Pr$; formula weight 1333.99; crystal system: Monoclinic; space group $P2_1/c$; unit cell dimensions a = 11.7117(3) Å, b = 58.5616(11) Å, c = 10.0077(3) Å, β = 108.281(3)°, volume 6517.4(3) Å^3; Z = 4; density (calculated) 1.360 Mg/m^3; absorption coefficient 0.831 mm^{-1}; crystal size 0.54 x 0.18 x 0.06 mm^3; θ range for data collection 2.78 to 30.00°; reflections collected 73929; independent reflections 18972 [R(int) = 0.0669]; completeness to θ = 30.00° 99.9%; data/restraints/parameters 18972/42/907 goodness-of-fit on F^2 1.372; final R indices [$I>2\sigma(I)$] R_1 = 0.0813, wR_2 = 0.1431; R indices (all data) R_1 = 0.0921, wR_2 = 0.1465.

A.14 X-ray crystal data for compound 2-Na

Empirical formula $C_{54}H_{86}N_{12}O_{15}Na_2$; formula weight 1189.33; crystal system: Triclinic; space group $P\bar{1}$; unit cell dimensions a = 10.9110(3) Å, b = 12.8389(3) Å, c = 25.5081(6) Å, α = 77.424(2)°, β = 87.776(2)°, γ = 66.624(2)°; volume 3196.80(14) Å^3;

Z = 2; density (calculated) 1.236 Mg/m^3; absorption coefficient 0.865 mm^{-1}; crystal size 0.34 x 0.17 x 0.07 mm^3; θ range for data collection 3.56 to 67.35°; reflections collected 29000; independent reflections 11313 [R(int) = 0.0255]; completeness to θ = 67.00° 99.1%; data/restraints/parameters 11313/33/854 goodness-of-fit on F^2 1.033; final R indices [I>2σ(I)] R_1 = 0.0589, wR_2 = 0.1683; R indices (all data) R_1 = 0.0642, wR_2 = 0.1755.

A.15 X-ray crystal data for compound 3-Na/NEt$_3$

Empirical formula $C_{116}H_{169}N_{34}O_{14}Na$; formula weight 2286.84; crystal system: Monoclinic; space group $P2_1/c$; unit cell dimensions a = 11.5310(4) Å, b = 46.1981(12) Å, c = 12.1227(3) Å, β = 106.787(3)°, volume 6182.7(3) Å^3; Z = 2; density (calculated) 1.228 Mg/m^3; absorption coefficient 0.087 mm^{-1}; crystal size 0.43 x 0.12 x 0.10 mm^3; θ range for data collection 3.46 to 26.75°; reflections collected 32504; independent reflections 12953 [R(int) = 0.0443]; completeness to θ = 26.75° 98.5%; data/restraints/parameters 12953/157/867 goodness-of-fit on F^2 1.026; final R indices [I>2σ(I)] R_1 = 0.0649, wR_2 = 0.1434; R indices (all data) R_1 = 0.0998, wR_2 = 0.1581.

A.16 X-ray crystal data for compound Dy$_{19}$-A

Empirical formula $C_{586}H_{801}N_{96}O_{116}Dy_{19}$, $C_{48}H_{58}N_8O_4$, 27(C_2H_6O), 43(H_2O): $C_{688}H_{1107}N_{104}O_{190}Dy_{19}$; formula weight 16963.21; crystal system: Monoclinic; space group $P2_1/n$; unit cell dimensions a = 27.1914(2) Å, b = 64.5676(6) Å, c = 59.3556(12) Å, β = 92.701(1)°, volume 104094(2) Å^3; Z = 4; density (calculated) 1.082 Mg/m^3; absorption coefficient 7.665 mm^{-1}; crystal size 0.35 x 0.21 x 0.09 mm^3; T = 100(2) K; $2\theta_{max}$= 136.1°; reflections collected 430483; independent reflections 186689 [R(int) = 0.0910]; data/restraints/parameters 430483/2790/8702; goodness-of-fit on F^2 1.002; final R indices [I>2σ(I)] R_1 = 0.1061, wR_2 = 0.3052.

Several tertiary butyl groups were modelled as being disordered over two sets of sites and were refined with geometries restrained to ideal values. Site occupancies were constrained after trial refinement. Solvent molecules were refined as either ethanol or

water molecules with the some of the water molecules refined with partial occupancy factors. The atoms of some of the disordered tertiary butyl group and solvent molecules were refined with isotropic or common displacement parameters. Solvent water molecule hydrogen atoms were not located. A number of further constraints and restraints were employed during refinement to keep chemical integrity of the compound.

Gd_{19}-A, P 21/n, a = 27.19, b = 64.57, c = 59.36 Å, β = 92.70˚

A.17 X-ray crystal data for compound Dy_{19}-B

Empirical formula $C_{588}H_{799}N_{96}O_{116}Dy_{19}$, $12(C_4H_8O_2)$, $8(C_2H_6O)$, $24(H_2O)$: $C_{652}H_{959}N_{96}O_{172}Dy_{19}$; formula weight 15981.65; crystal system: Monoclinic; space group $C2/c$; unit cell dimensions a = 52.1542(10) Å, b = 44.1877(10) Å, c = 50.9434(8) Å, β = 112.332(2)°, volume 108597(4) $Å^3$; Z = 4; density (calculated) 0.977 Mg/m^3; absorption coefficient 7.309 mm^{-1}; crystal size 0.74 x 0.07 x 0.07 mm^3; T = 100(2) K; $2\theta_{max}$= 100.9°; reflections collected 252791; independent reflections 56875 [R(int) = 0.1261]; data/restraints/parameters 252791/911/3969; goodness-of-fit on F^2 1.012; final R indices [$I>2\sigma(I)$] R_1 = 0.0773, wR_2 = 0.2112.

Many tertiary butyl groups were modelled as being disordered over two sets of sites and were refined with geometries restrained to ideal values. Most of the ethyl acetate solvent molecules were also modelled as being disordered or were refined with geometries restrained to ideal values, some with partial occupancies and isotropic or common displacement parameters. Other peaks in later difference maps were modelled as solvent water molecules and were refined with partial occupancies after trial refinement. Solvent water molecule hydrogen atoms were not located. Several further restraints were employed during refinement to keep the chemical integrity of the compound. Residual

electron density in the crystal which could not be interpreted as chemically reasonable moieties was effectively removed by use of the program Squeeze.

Gd_{19}-B, C2/c, a = 52.34, b = 44.87, c = 50.98 Å, β = 112.328˚

Eu_{19}-B, C2/c, a = 52.42, b = 45.10, c = 51.00 Å, β = 112.49˚

Y_{19}-B, C2/c, a = 52.09, b = 44.62, c = 50.96 Å, β = 112.236˚

Er_{19}-B, C2/c, a = 52.09, b = 45.08, c = 51.09 Å, β = 112.445˚

Ho_{19}-B, C2/c, a = 52.01, b = 45.14, c = 50.95 Å, β = 112.14˚

Tm_{19}-B, C2/c, a = 51.99, b = 44.3, c = 50.87 Å, β = 112.4˚

Yb_{19}-B, C2/c, a = 51.65, b = 43.82, c = 51.00 Å, β = 112.176˚

Lu_{19}-B, C2/c, a = 51.79, b = 44.47, c = 50.99 Å, β = 112.331˚

A.18 X-ray crystal data for compound Dy_{19}-C

Empirical formula $C_{588}H_{799}N_{96}O_{116}Dy_{19}$, $12(C_4H_8O_2)$, $12(C_2H_6O)$, $10.5(H_2O)$: $C_{660}H_{988}N_{96}O_{162.50}Dy_{19}$; formula weight 15954.96; crystal system: Trigonal; space group *R3c*; unit cell dimensions a = 45.6636(6) Å, c = 151.631(3) Å, volume 273816(7) $Å^3$; Z = 12; density (calculated) 1.161 g/cm^3; absorption coefficient 8.687 mm^{-1}; crystal size 0.38 x 0.31 x 0.15 mm^3; T = 100(2) K; $2\theta_{max}$= 100.9°; reflections collected 429015; independent reflections 31871 [R(int) = 0.1134]; data/restraints/parameters 429015/980/2515; goodness-of-fit on F^2 1.268; final R indices [$I>2\sigma(I)$] R_1 = 0.1043, wR_2 = 0.2847.

Many tertiary butyl groups were modelled as being disordered over two sets of sites and were refined with geometries restrained to ideal values. Solvent molecules were refined

as either ethyl acetate, ethanol or water molecules with some of the water molecules refined with partial occupancy factors. The atoms of the disordered tertiary butyl groups and of some of the solvent molecules were refined with isotropic or common displacement parameters. Solvent water molecule hydrogen atoms were not located. A number of further constraints and restraints were employed during refinement to keep chemical integrity of the compound. Residual electron density in the crystal which could not be interpreted as chemically reasonable moieties was effectively removed by use of the program Squeeze.

Sm_{19}-C, R3c, a = 45.47, c = 154.96 Å

Eu_{19}-C, R3c, a = 45.3, c = 161.5 Å

Tb_{19}-C, R3c, a = 45.52, c = 150.71 Å

Er_{19}-C, R3c, a = 45.49, c = 150.12 Å

Tm_{19}-C, R3c, a = 45.52, c = 149.4 Å

Yb_{19}-C, R3c, a = 45.55, c = 152.3 Å

Lu_{19}-C, R3c, a = 45.37, c = 154.61 Å

A.19 X-ray crystal data for compound Dy_{12}

Empirical formula $C_{323}H_{425}N_{48}O_{71}Dy_{12}$, $3(C_4H_8O_2)$, $6(C_2H_6O)$: $C_{347}H_{485}N_{48}O_{83}Dy_{12}$; formula weight 8606.83; crystal system: Trigonal; space group *R3*; unit cell dimensions a = 39.2443(11) Å, c = 26.2023(8) Å, volume 34948.1(17) $Å^3$; Z = 3; density (calculated) 1.227 g/cm^3; absorption coefficient 1.963 mm^{-1}; crystal size 0.27 x 0.21 x 0.09 mm^3; T = 100(2) K; $2\theta_{max}$= 58°; reflections collected 108531; independent reflections 36330 [R(int) = 0.0496]; data/restraints/parameters 108531/502/1606; goodness-of-fit on F^2 1.030; final R indices [$I>2\sigma(I)$] R_1 = 0.0642, wR_2 = 0.1674.

Six of the eight tertiary butyl groups and the terminal benzoate groups were modelled as being disordered over two sets of sites. Occupancies were constrained to 0.5 after trial refinement except for those on C14n, where the site occupancy was refined to 0.67(2) and its complement and the benzoate groups (60) and (70) which were each refined with site occupancies of 1/3 after trial refinement. The ligands occupying the remaining 1/3 of the coordination sites were not identified but assumed to be water as included in the formula. Geometries were restrained to ideal values. Charge balance can be achieved by assuming deprotonation of the tetrazole units with the OH groups on one of the crystallographically independent calixarenes also being deprotonated. The ethanol molecules in the calices were also refined with restrained geometries and assigned full occupancy after trial refinement. Large residual peaks were modelled as disordered Dy atoms resulting from rotational disorder of the entire molecule. Site occupancies of the two sets of Dy atoms refined to 0.795(1) and its complement. The calices and some of the coordinated water molecules associated with the minor component of the Dy atoms appeared to be superimposed on that of the major component which were therefore refined with full occupancy. The bridging hydroxyl groups and the remaining coordinated water molecules of the minor component of the disorder were not located. The solvent ethylacetate molecule was refined with full occupancy after trial refinement. Phenolic and water molecule hydrogen atoms were not located. All remaining hydrogen atoms were added at calculated positions and refined by use of riding models with isotropic displacement parameters based on those of the parent atoms. Anisotropic displacement parameters were employed throughout for the non-hydrogen atoms. Residual electron density in the crystal which could not be interpreted as chemically reasonable moieties was effectively removed by use of the program Squeeze.

Tb_{12}, R3, a = 39.31, c = 26.10 Å

Er_{12}, R3, a = 39.20, c = 25.96 Å

Ho_{12}, R3, a = 39.07, c = 26.06Å

Tm_{12}, R3, a = 39.08, c = 25.94 Å

Yb_{12}, R3, a = 39.11, c = 25.99 Å

Appendix B – Ln_{12} Crystals

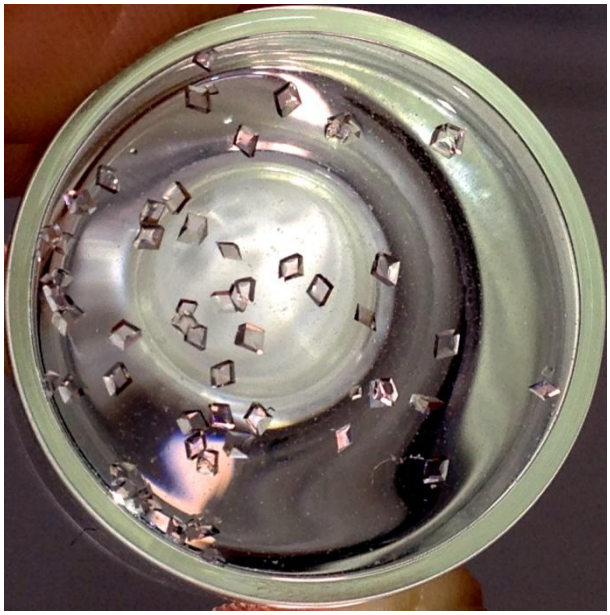

Regular crystals of the Ln_{12} bottlebrush species with ammonium benzoate.

Appendix C – Crystal structure of compound 10

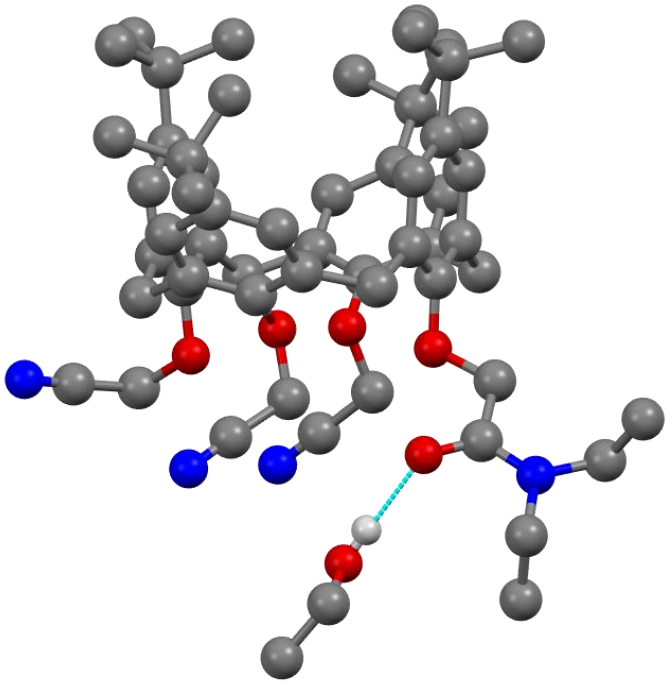

Hydrogen bond from the OH of the residual ethanol molecule to the amide oxygen of the mono-amide tri-nitrile calixarene **10**.

Appendix D – Elemental calculations

D.1 Calculations for compound Dy_{19}-B

$C_{588}H_{799}N_{96}O_{116}Dy_{19}$, $(C_4H_8O_2)_{12}$ $(C_2H_6O)_8$ $(H_2O)_{24}$

$C_{652}H_{991}N_{96}O_{172}Dy_{19}$ = 16078.648 $gmol^{-1}$

C = 7895.72 = 49.11%

H = 998.928 = 6.21%

N = 1344.672 = 8.36%

O = 2751.828 = 17.11%

Dy = 3087.50 = 19.20%

D.2 Calculations for compound Yb_{19}-B

$C_{588}H_{799}N_{96}O_{116}Yb_{19}$, $(C_4H_8O_2)_{12}$ $(C_2H_6O)_8$ $(H_2O)_{24}$

$C_{652}H_{991}N_{96}O_{172}Yb_{19}$ = 16279.174 $gmol^{-1}$

C = 7895.72 = 48.50%

H = 998.928 = 6.14%

N = 1344.672 = 8.26%

O = 2751.828 = 16.90%

Yb = 3288.026 = 20.198%

D.3 Calculations for compound Er_{19}-B

$C_{588}H_{799}N_{96}O_{116}Er_{19}$, $(C_4H_8O_2)_{12}$ $(C_2H_6O)_8$ $(H_2O)_{24}$

$C_{652}H_{991}N_{96}O_{172}Er_{19}$ = 16169.069 $gmol^{-1}$

C = 7895.72 = 48.83%

H = 998.928 = 6.18%

N = 1344.672 = 8.32%

O = 2751.828 = 17.02%

Er = 3177.921 = 19.65%

D.4 Calculations for compound Dy_{12}

$C_{323}H_{425}N_{48}O_{71}Dy_{12}$, $(C_4H_8O_2)_3$ $(C_2H_6O)_6$

$C_{347}H_{485}N_{48}O_{83}Dy_{12}$ = 8606.87 $gmol^{-1}$

C = 4167.817 = 48.42%

H = 488.88 = 5.68%

N = 672.336 = 7.81%

O = 1327.917 = 15.43%

Dy = 1950.00 = 22.66%

D.5 Calculations for compound Er_{12}

$C_{323}H_{425}N_{48}O_{71}Er_{12}$, $(C_4H_8O_2)_3$ $(C_2H_6O)_6$

$C_{347}H_{485}N_{48}O_{83}Er_{12}$ = 8664.058 $gmol^{-1}$

C = 4167.817 = 48.10%

H = 488.88 = 5.64%

N = 672.336 = 7.76%

O = 1327.917 = 15.33%

Er = 2007.108 = 23.17%

Appendix E – Total metal content calculations

E.1 Calculations for compound Dy_{19}-B (de-solvated)

$C_{588}H_{799}N_{96}O_{116}Dy_{19}$ = 14155.916 $gmol^{-1}$

C = 7062.468 = 49.89%

H = 805.392 = 5.69%

N = 1344.672 = 9.50%

O = 1855.884 = 13.11%

Dy = 3087.50 = 21.81%

E.2 Calculations for compound Dy_{12} (de-solvated)

$C_{323}H_{425}N_{48}O_{71}Dy_{12}$ = 8066.218 $gmol^{-1}$

C = 3879.553 = 48.10%

H = 428.40 = 5.31%

N = 672.336 = 8.33%

O = 1135.929 = 14.08%

Dy = 1950.00 = 24.17%

Appendix F – TGA calculations

F.1 Calculations for compound Dy_{19}-B

$C_{652}H_{991}N_{96}O_{172}Dy_{19}$ = 16078.648 $gmol^{-1}$

Di-tetrazole calixarenes = $C_{48}H_{53}N_8O_4 + (C_{48}H_{54}N_8O_4)_{11}$

= $C_{576}H_{647}N_{96}O_{48}$ = 9683.136 $gmol^{-1}$

= 60.22%

Acetate capping ligands = $(C_2H_3O_2)_6$

= $C_{12}H_{18}O_{12}$ = 354.264 $gmol^{-1}$

= 2.20%

Solvents = $(C_4H_8O_2)_{12} + (C_2H_6O)_8 + (H_2O)_{24}$

= $C_{64}H_{192}O_{56}$ = 1858.184 $gmol^{-1}$

= 11.55%

Solvents + Acetate caps = $C_{64}H_{192}O_{56} + C_{12}H_{18}O_{12}$

= $C_{82}H_{210}O_{68}$ = 2212.448 $gmol^{-1}$

= 13.76%

Calixarene + External H_2O = $C_{576}H_{647}N_{96}O_{48} + (H_2O)_{30}$

= $C_{576}H_{707}N_{96}O_{78}$ = 10223.616 $gmol^{-1}$

= 63.60%

Dysprosium + Internal OH = $Dy_{19} + (HO)_{26}$

= 3529.682 $gmol^{-1}$

= 21.95%

F.2 Calculations for compound Dy_{12}

$C_{347}H_{485}N_{48}O_{83}Dy_{12}$ = 8606.87 $gmol^{-1}$

Di-tetrazole calixarenes = $(C_{48}H_{53}N_8O_4)_3 + (C_{48}H_{54}N_8O_4)_3$

= $C_{288}H_{321}N_{48}O_{24}$ = 4839.048 $gmol^{-1}$

= 56.22%

Benzoate capping ligands = $(C_7H_5O_2)_6$

= $C_{42}H_{30}O_{12}$ = 726.69 $gmol^{-1}$

= 8.44%

Solvents = $(C_4H_8O_2)_3 + (C_2H_6O)_6$

= $C_{24}H_{60}O_{12}$ = 540.732 $gmol^{-1}$

= 6.28%

Solvents + Acetate caps = $C_{24}H_{60}O_{12} + C_{42}H_{30}O_{12}$

= $C_{68}H_{90}O_{24}$ = 1267.422 $gmol^{-1}$

= 14.72%

Calixarene + External H_2O = $C_{288}H_{321}N_{48}O_{24} + (H_2O)_{19}$

= $C_{288}H_{359}N_{96}O_{43}$ = 5181.352 $gmol^{-1}$

= 60.20%

Dysprosium + Internal OH = $Dy_{12} + (HO)_{16}$

= 2222.12 $gmol^{-1}$

= 25.82%